UNIVERSITY OF ALBERTA

Microfluidic Systems for Immunoassays

By

Nghia Hung Chiem

©

A thesis submitted to
The Faculty of Graduate Studies and Research
in partial fufillment of the requirements for the degree of

Doctor of Philosophy

Department of Chemistry

Edmonton, Alberta
Fall, 1997

National Library of Canada
Acquisitions and Bibliographic Services
395 Wellington Street
Ottawa ON K1A 0N4
Canada

Bibliothèque nationale du Canada
Acquisitions et services bibliographiques
395, rue Wellington
Ottawa ON K1A 0N4
Canada

Your file Votre référence

Our file Notre référence

The author has granted a non-exclusive licence allowing the National Library of Canada to reproduce, loan, distribute or sell copies of this thesis in microform, paper or electronic formats.

The author retains ownership of the copyright in this thesis. Neither the thesis nor substantial extracts from it may be printed or otherwise reproduced without the author's permission.

L'auteur a accordé une licence non exclusive permettant à la Bibliothèque nationale du Canada de reproduire, prêter, distribuer ou vendre des copies de cette thèse sous la forme de microfiche/film, de reproduction sur papier ou sur format électronique.

L'auteur conserve la propriété du droit d'auteur qui protège cette thèse. Ni la thèse ni des extraits substantiels de celle-ci ne doivent être imprimés ou autrement reproduits sans son autorisation.

0-612-22966-1

Canada

UNIVERSITY OF ALBERTA

LIBRARY RELEASE FORM

NAME OF AUTHOR: **Nghia Hung Chiem**

TITLE OF THESIS: **Microfluidic Systems for Immunoassays**

DEGREE: **Doctor of Philosophy**

YEAR THIS DEGREE GRANTED: **1997**

Permission is hereby granted to the University of Alberta Library to reproduce single copies of this thesis and to lend or sell such copies for private, scholarly or scientific research purpose only.

The author reserves all other publication and other rights in association with the copyright in the thesis, and except as hereinbefore provided, neither the thesis nor any substantial portion thereof may be printed or otherwise reproduced in any meterial form whatever without the author's prior written permission.

AUTHOR'S SIGNATURE: _____

PERMANENT ADDRESS: 7281-11th Avenue
Burnaby, B.C.
Canada V3M 2N9

Date: September 11, 1997

UNIVERSITY OF ALBERTA

FACULTY OF GRADUATE STUDIES AND RESEARCH

The undersigned certify that they have read, and recommend to the Faculty of Graduate Studies and Research for acceptance, a thesis entitled **Microfluidic Systems for Immunoassays** submitted by **Nghia Hung Chiem** in partial fulfillment of the requirements for the degree of **Doctor of Philosophy**.

Supervisor:

Dr. D. Jed. Harrison

Dr. Norman J. Dovichi

Dr. Mark McDermott

Dr. Monica Palcic

Dr. Mavanur R. Suresh

External Examiner:

Dr. Vassili Karanassios

To My Parents
Sister and Brothers

Abstract

The development of miniaturized, microfabricated devices for chemical analysis is a new and exciting application of micromachining technology. The research presented in this work demonstrates the feasibility of developing microfluidic systems for immunoassay, a technique which is increasingly used in clinical diagnostics and environmental monitoring.

Microfabrication has provided a means of fabricating a miniaturized, three dimensional network of channels in a small device (chip) capable of consuming only nano- to picoliters of sample and reagent and generating very little waste. Computers, relays and high voltage were used to control fluid flow within the valveless microchannels. Solution delivery and fluid manipulation were facilitated by electroosmosis, while efficient separation was achieved by electrophoresis in the glass microchannels. Separation efficiencies with submicron plate heights were achieved on-chip. Capillary electrophoresis allowed the separation of reagents and reaction products to take place in solution and led to rapid on-chip separation, typically within less than one minute. The laser induced fluorescence system used with these microdevices gave picomolar detection limits satisfactory for many immunoassays.

Integration of reagent mixing with diluted serum samples, immunological reaction and separation on-chip was also achieved. The ability to integrate these sample processing steps with separation on one monolithic device showed that the entire group of laboratory steps used in immunoassays can be integrated. No sacrifice is made through integration as the assay performance of the device is comparable to conventional instrumentation. Successful integration demonstrates the level of automation that can be achieved within such microdevices implying more rapid analysis times and a potential reduction in cost.

Acknowledgements

The multidisciplinary nature of this work required the involvement of many people. Their support and assistance is greatly appreciated.

Special gratitude to my research advisor, Professor D. Jed Harrison. He introduced me to this exciting and challenging field and has provided me with valuable guidance and support throughout the course of this research. Thanks to all the members of the Harrison's group especially to Thompson Tang for help in the lab. Thanks to Laura MacDougall, Dr. Christa Coyler and Dr. Hossein Salimi-Moosavi for reading and making comments on some sections of this publication.

My appreciation is also extended to the technical support staff in this chemistry department especially to those of the glass, electronic and machine shops. Thanks to Professors Norm J. Dovichi, Mavanur R. Surresh and Monica Palcic for many valuable discussions and suggestions for this research. Thanks is also extended to Dr. Gordon Alton and Dr. Joanna Sadowska for technical help in working with antibodies. I would like to also acknowledge the assistance of Dr. Randy Whittal who obtained the mass spectra of bovine serum albumin presented in chapter 2.

Thanks to the staff at the Alberta Microelectronic Centre (AMC) for their help with the chip fabrication, especially to Glen Fitzpatrick and Tran Tran. Thanks to Graham McKinnon for his support and guidance. The scholarships from AMC and from the University of Alberta are acknowleged and greatly appreciated.

Thanks to Clara Hernandez and Mesfin Bekele for being good friends. Finally, to my parents, sister and brothers for being there throughout the good and the bad times.

TABLE OF CONTENTS

CHAPTER 1: INTRODUCTION **1**

1.1 INTRODUCTION TO IMMUNOASSAY 1

1.1.1 Nomenclature of Immunoassays Methods *2*

1.1.2 Antibodies *4*

1.1.2.1 Polyclonal Antibodies 4

1.1.2.2 Monoclonal Antibodies 5

1.1.3 Immunoassay Classification *7*

1.1.4 Detection *8*

1.1.4.1 Direct Detection 8

1.1.4.1.1 Immunoprecipitation 8

1.1.4.1.2 Immunosensors 8

1.1.4.2 Indirect Detection with Labels 9

1.1.4.2.1 Radioisotopes Labels 11

1.1.4.2.2 Enzyme Labels 11

1.1.4.2.3 Fluorescent Labels 13

1.1.4.2.4 Chemiluminescent Labels 14

1.1.4.2.5 Particle Labels 14

1.1.4.2.6 Ligand Labels 15

1.1.5 Quantitation *15*

1.1.5.1 Separation-Free Assays 15

1.1.5.2 Assays with Separations 16

1.2 AUTOMATED ANALYZERS 16

1.2.1 Total Analysis Systems *16*

1.2.2 Immunoassay Systems *17*

1.3 MINIATURIZED SYSTEMS 18

1.3.1 Miniaturization Techniques *18*

1.3.2 Pumping and Separation with Capillary Electrophoresis *19*

1.3.3 CE-based Microfabricated Immunoassay Systems *21*

1.4 SCOPE OF PRESENT WORK 23

1.5 REFERENCES 25

CHAPTER 2: OPTIMIZATION OF SEPARATION AND DETECTION.....28

2.1 INTRODUCTION.....28
2.2 THEORY.....28
2.2.1 Electroosmosis and Electrophoresis.....28
2.2.2 Diffusion Effects on Separation Efficiencies.....30
2.2.3 Off-Column Effects Contribution to Separation Efficiencies.....31
2.2.4 Separation Resolution.....32
2.3 EXPERIMENTAL.....33
2.3.1 Materials and Reagents.....33
2.3.2 Procedures.....34
2.3.2.1 Amino Acid Labeling.....34
2.3.2.2 Labeling of H-IgG.....34
2.3.2.3 Mass Spectrometry of Bovine Serum Albumin.....34
2.3.3 Device Fabrication.....34
2.3.3.1 Microlithography and Etching.....35
2.3.3.2 Bonding.....35
2.3.3.2.1 Room Temperature Bonding.....35
2.3.3.2.2 High Temperature Bonding.....37
2.3.4 Chip Layout.....37
2.3.5 Instrumentation.....39
2.3.6 Chip Operation.....42
2.3.6.1 Electrokinetic Injection.....42
2.3.6.2 Vacuum Injection.....42
2.3.7 Coatings.....44
2.3.8 Vial IgG Adsorption Test.....45
2.4 RESULTS AND DISCUSSIONS.....45
2.4.1 Conditions to Reduce Antibody Adsorption On-Chip.....45
2.4.1.1 IgG Adsorption Test on Glass Vials.....47
2.4.1.2 Adsorption Testing On-Chip.....51
2.4.2 Evaluation of Chip Design and Optimization of Separation Efficiency.....54
2.4.2.1 Flow Evaluation.....54
2.4.2.2 Separation Efficiency.....55
2.4.2.3 Resolution of Amino Acids.....60
2.4.3 Optimization of Detection Limit.....66
2.4.3.1 Sensitivity Optimization.....66
2.4.3.2 Limiting Noise and its Origin.....68

2.4.3.3 Detection Limit 71
2.4.3.3.1 Detection Limit of Fluorescein 71
2.4.3.3.2 Detection limit of Amino Acids and Proteins 73
2.5 CONCLUSION 75
2.6 REFERENCES 76

CHAPTER 3: EVALUATION OF ROOM TEMPERATURE BONDED GLASS DEVICES 78

3.1 INTRODUCTION 78
3.2 EXPERIMENTAL SECTION 79
3.2.1 Chip Characterization 79
3.2.2 Instrumentation and Chip Operation 81
3.3 RESULTS AND DISCUSSION 81
3.3.1 Conditions for Absence of Interference Fringes 81
3.3.2 Leakage Testing 84
3.3.3 Separation Performance 88
3.4 CONCLUSION 88
3.5 REFERENCES 90

CHAPTER 4 : EVALUATION OF ANTIBODY BINDING AFFINITY AND COMPLEXES 92

4.1 INTRODUCTION 92
4.2 THEORY 93
4.3 EXPERIMENTAL SECTION 94
4.3.1 Materials And Reagents: 94
4.3.2 Procedures 94
4.4 RESULTS AND DISCUSSION 95
4.4.1 Equilibrium Distribution Of The Antigen, Antibody And Complexes 95
4.4.2 Binding Constants And Complex Speciations 98
4.5 CONCLUSION 102
4.6 REFERENCES 103

CHAPTER 5: SEPARATION AND QUANTITATION IN IMMUNOASSAYS ON-CHIP 104

5.1 INTRODUCTION 104
5.2 EXPERIMENTAL 105
5.2.1 Materials and Reagents 105
5.2.2 Device Fabrication, Instrumentation and Chip Operation 106

5.2.3 Labeling of H-IgG *106*
5.2.4 Direct Assay for Anti-BSA *108*
5.2.5 Direct Anti-Theophylline Assay *108*
5.2.6 Competitive Theophylline Assay *108*
5.3 RESULTS AND DISCUSSION 109
5.3.1 Buffer Composition *109*
5.3.2 Protein Assays *111*
5.3.3 Hapten Assays *114*
5.4 CONCLUSIONS 119
5.5 REFERENCES 120

CHAPTER 6: INTEGRATION OF SAMPLE PROCESSING, SEPARATION AND DETECTION ON-CHIP 122

6.1 INTRODUCTION 122
6.2 EXPERIMENTAL 123
6.2.1 Materials and Reagents *123*
6.2.2 Device Fabrication *123*
6.2.3 Instrumentation *126*
6.2.4 Competitive Immunoassay and Chip Operation *126*
6.3 RESULTS AND DISCUSSION 129
6.3.1 Mixing Dilution Ratio. *130*
6.3.2 Diffusional Mixing Design Issues *132*
6.3.2.1 Residence Time 132
6.3.2.2 Diffusional Dispersion 133
6.3.3 Immunoreactions On-Chip *137*
6.3.4 Competitive Theophylline Assays On-Chip *140*
6.3.4.1 Calibration 140
6.3.4.1 Accuracy and Precision 140
6.3.4.3 Detection Limit of Theophylline 142
6.4 CONCLUSION 142
6.5 REFERENCES 143

CHAPTER 7: CONCLUSIONS 145

7.1 SUMMARY 145
7.2 FUTURE DIRECTIONS 146

List of Tables

Table		Page
1.1	Some common immunoassay types	2
1.2	Some common labeling substances and measurement methods	10
2.1	PDMS coating conditions and fluorescence results from vial adsorption tests	48
2.2	Other coating conditions and fluorescence results from vial adsorption tests	50
2.3	Comparison of electrokinetic mobilities of seven amino acids in the 10 mM low ionic strength and the 50 mM high ionic strength tricine buffers	63
3.1	Combinations of glass type tested with room temperature bonding	82
3.2	Comparison of channel length and channel resistance ratios in room temperature bonded devices	86
6.1	Dimensions of channels of the chip layout in Figure 6.1	125

List of Figures

Figure		Page
1.1	Basic structure of an antibody molecule	3
1.2	Competitive versus immunometric assays	6
1.3	The use of an enzyme to label immunological reagents	12
1.4	Simplistic view of electroosmotic flow and electrophoretic flow	20
1.5	Schematic diagram of a microdevice for immunoassays	22
2.1	The sequence of device fabrication	36
2.2	A simple chip-layout showing channels with dimensions	38
2.3	Schematic diagram of the instrumental setup	40
2.4	Schematic diagram of the laser excitation (A) and fluorescence detection (B) setup on an optical bread board	41
2.5	Schematic diagram of electrokinetic sample loading, injection and separation steps	43
2.6	Electropherogram of fluorescein-labeled anti human-IgG (70 μg/mL) obtained with a PDMS coated chip	52
2.7	Electropherogram of fluorescein-labeled human-IgG and fluorescein-labeled BSA obtained with an uncoated chip	53
2.8	Plot of migration rate versus electric field for 10 μM fluorescein-labeled phenylalanine	56
2.9	Plot of theoretical plate number versus electric field for fluorescein-labeled phenylalanine	57
2.10	Plot of height equivalent to theoretical plate (HETP) versus migration time for fluorescein-labeled phenylalanine	58
2.11	Electropherogram of a mixture of 3.2 nM, fluorescein-labeled goat anti H-IgG and 15 nM, fluorescein-labeled BSA obtained with an uncoated, Borosilicate glass device	61

2.12 Electropherogram of a mixture of seven fluorescein-labeled amino acids with 10 mM, pH 8, low ionic strength tricine buffer.....62

2.13 Electropherogram of a mixture of seven fluorescein-labeled amino acids with 50 mM, pH 8, high ionic strength tricine buffer.....64

2.14 Plot of theoretical plate number versus electrokinetic mobilities for fluorescein-labeled amino acids.....65

2.15 Fluorescein signal versus concentration detected from 2 cm plug sample in devices made from three different types of glass.....67

2.16 Background fluorescence of devices made from three different types of glass: Borosilicate (Pyrex), zinc titania (0211) and soda lime (photomask).....69

2.17 Background noise of Pyrex, 0211 and photomask glass devices described in Figure 2.16.....70

2.18 Noise vs. square root of background fluorescence of Pyrex, 0211 and photomask glass devices described in Figure 2.16.....72

2.19 Electropherogram of 0.5 nM fluorescein-labeled amino acids obtained with a Borosilicate glass device.....74

3.1 Schematic layout of the channels for room temperature bonded glass devices.....80

3.2 Current-voltage curves for potentials applied between the solution reservoirs of a room temperature bonded glass device.....85

3.3 Current voltage curve for the highest resistance channel of a room temperature bonded glass device.....87

3.4 Electropherogram of fluorescein-labeled amino acids obtained from a room temperature bonded glass device.....89

4.1 Series of electropherograms obtained from mixtures of 361 nM anti-BSA* and increasing concentrations of BSA*.....96

4.2 Electropherogram of 301 nM fluorescein-labeled BSA.....97

4.3 Binding isotherm of antibody-bound BSA* versus free BSA for mixtures of increasing BSA* concentration with 361 nM anti-BSA*. 99

4.4 Scatchard plot of bound/free versus bound BSA* for the series of electropherograms shown in 4.1 100

5.1 Schematic of chip layout showing voltages applied for sample loading and voltages applied during separation 107

5.2 Separation of a mixture of fluorescein-labeled Human IgG and bovine serum albumin (BSA) on a chip. 110

5.3 On-chip electropherograms of 50 μg/mL of FITC labeled BSA, and of a mixture containing 50 μg/mL labeled BSA and 67 μg/mL of monoclonal anti-BSA in diluted mouse ascites fluid 112

5.4 Calibration curve for anti-BSA in diluted mouse ascites fluid. 113

5.5 Series of on-chip electropherograms for 10 μL of labeled theophylline with added antibody solution, showing titration of Th* with the antibody 115

5.6 Series of on-chip electropherograms for a competitive theophylline assay using 10 μL of labeled theophylline, 1.5 μL of stock anti-theophylline and increasing amounts of unlabeled theophylline. 117

5.7 Calibration curve of normalized peak area versus concentration of theophylline in serum standards. 118

6.1 Device layout for competitive immunoassay with integrated sample mixing, reaction and separation 124

6.2 Instrument setup showing relays and voltage connections to the chip reservoirs. 127

6.3 Schematic diagram showing on-chip mixing, reaction and separation 128

6.4 Electropherograms showing on-chip dilution of fluorescein-labeled theophylline. 131

6.5a Plot of normalized concentration of IgG as it diffuses across a 52 μm wide channel. 135

6.5b Plot of normalized concentration of theophylline as it diffuses across a 52 μm wide channel. 136

6.6 Electropherograms of the competitive theophylline assay with on-chip mixing of reagents. 138

6.7 Stop-flow study of the effect of mixing time on the amount of free, unreacted Th* in the presence of antibody and the indicated amounts of unlabeled Th. 139

6.8 Calibration curve of normalized peak area for free Th* and Ab-Th* complex vs concentration of Th in 50x diluted serum standards. 141

Chapter 1

Introduction

Immunoassays have become popular methods for a wide variety of environmental, clinical and biochemical analyses. The primary drawback of common immunoassay formats is that they tend to be slow, manually intensive procedures. When high throughput is necessary, immunoassays are performed in batches in large central labs; however, this is not desirable when rapid feedback is necessary. This research is focused on the development of small automated immunoassay systems using microfabrication technology and capillary electrophoresis separation techniques. Potential advantages of this system include simplicity of design for system automation and integration, rapid analysis, minute consumption of reagents, little generation of waste and use as portable monitors for environmental or industrial testing or point-of-care clinical diagnosis.

1.1 Introduction to Immunoassay

Rosalyn Yalow and Solomon Berson introduced immunoassays to the scientific community in 1959.[1] This important publication aroused considerable interest and excitement. However, who could have predicted that this early application of what would later become known as "biotechnology" would have so profound an impact in medicine and lead to an enormous and competitive industry?

The reasons for the continuing interest in immunoassays stem from three important characteristics: specificity, sensitivity and universal application. While the selectivity is derived from the natural binding characteristics of the antibody, the sensitivity is from antibody affinity and the choice of labels. The first assays used radioisotopes as labels and many assays still use this approach today. However, the advent of fluorescent, luminescent, light-scattering, and particularly enzyme labels has led to an explosion in the techniques available.[2-4] The use of labels has facilitated the extension of the analytical range of assays by virtue of lower detection limits. Universal application of immunoassays is derived from the capability of producing different specific antibodies to a wide range of different substances of different size and chemical composition.

Assay name (IA)	Acronym	Label used
RadioIA	RIA	Radioisotopes
Immunoradiometric assay	IRMA	
EnzymoIA	EIA	Enzymes
Enzyme linked immunosorbent assay	ELISA	
FluoroIA	FIA	Fluorescent compounds
Immunofluorometric assay	IFMA	
Fluorescent polarization IA	FPIA	
Fluorescent Quenching IA	FQIA	
Chemiluminescent IA	CLIA	Chemiluminescent compounds
Immunochemiluminometric assay	ICLMA	
Particle counting IA	PACIA	Particles

Table 1.1: Some common immunoassay types

Although immunoassays have been with us for nearly 40 years, the technology refuses to stand still. Today, immunoassays enjoy an almost unprecedented popularity as the method of choice for quantitation of chemical or biological substances. They have permeated many branches and disciplines of scientific investigation, especially in biologically related subjects. Not only has the use of immunoassays proliferated, but also the variety and type. There are numerous innovations and refinements every year. Many different methods are used; each has advantages and disadvantages and no one technique predominates.[5] Perhaps this diversity of approach is evidence of a some what immature technology. Certainly there are many further opportunities for improvement and growth.

1.1.1 Nomenclature of Immunoassays Methods

The nomenclature of immunoassay systems is confusing to anyone wishing to understand the similarities between different assays as well as the diversity of their designs. Further confusion is the widespread practice of using acronyms. Much of the variety in immunoassay names comes from the numerous labeling substances that have been exploited in the development of immunoassays.[6] These substances include (with common forms in parentheses) radioisotopes (radio), enzymes (enzymo or enzyme),

fluorescent (fluoro), chemi-, and bio-luminescent compounds. In general, all assay names contain "immuno," the combining form of the adjective "immune," and another combining word indicating the type of label used, along with the word "assay": e.g., radioimmunoassay (RIA). To distinguish reagent excess from reagent limited (competitive) assays, the common practice for reagent excess assays is to reverse the order of the combining forms, as in immunoradiometric assay (IRMA), immunofluorometric assay (IFMA), or immunoenzymometric assay. Some of the common methods used and their acronyms are given in Table 1.1. These rules are generally used as guidelines for naming the variety of immunoassay methods, but are frequently ignored. For example, the acronym ELISA is generally used for reagent excess assays but is also sometimes used interchangeably with enzyme immunoassay (enzymoimmunoassay).

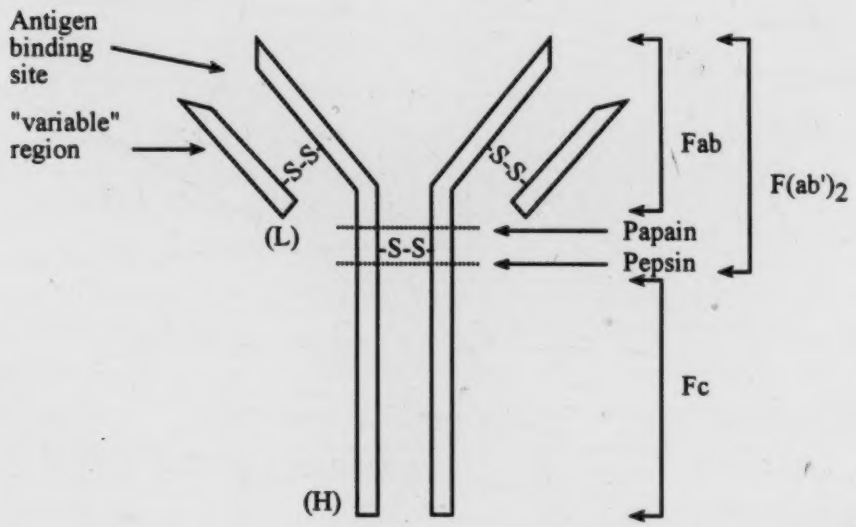

Figure 1.1: Basic structure of an antibody molecule. The molecule consists of two long or heavy (H) chains and two short or light (L) chains. Cleavage by the proteolytic enzymes, pepsin or papain, yields $F(ab')_2$ or Fab and Fc fragments. The "variable" region contains the antigen-binding site.

1.1.2 Antibodies

The critical component of an immunoassay is an antibody.[7] The antibodies present in antisera are large molecules with molecular weights usually ≥ 150,000 Daltons. They are proteins belonging to the immunoglobulin (Ig) class, which is divided into a number of sub-classes distinguishable by letters; for example, IgG, IgA, IgM, IgD and IgE. These antibodies share key structural and functional features. Functionally, they can be characterized by the ability to bind both to antigens and to specialized cells or proteins of the immune system. Structurally, antibodies are composed of one or more copies of a characteristic unit of IgG.

IgG has a basic molecular structure that can be visualized as forming a Y shape as illustrated in Figure 1.1 As indicated in this figure, the binding site for an antigen is located in the variable region of each arm of the Y. Each arm contains a site that can bind to an antigen, making IgG molecules bivalent. The terms "constant region" and "variable region" refer to constancy or variability of the amino acid sequence with a class of immunoglobulins. Variation in amino acid sequence give rise to the variety of different antigen binding sites. It has been calculated that these variations in structure can potentially give rise to 10^{10} different antigen binding sites.

A specific amino acid sequence and the tertiary structure of the variable region, determine the given specificity of the antigen binding site. It should be emphasized that "specificity" describes the uniqueness of the binding site on an antibody for an antigen with a unique molecular structure and discriminate against others. It is this discrimination that make immunoassays a powerful technique for trace analysis of analyte in complex samples. The antibody, as the specific reagent in immunoassay, is crucial to performance. An antiserum with high specificity and a high affinity constant will give the characteristics of good specificity and sensitivity with any assay in which it is used.

1.1.2.1 Polyclonal Antibodies

The production of antibodies is a specific event in the more general phenomenon known as the immune response.[7,8] The immune response is basically a series of related events in a living animal occurring in response to the presence of a substance considered to be alien or foreign. The end product of this response is the production of large numbers of antibody molecules that bind specifically to the antigen, following

immunization or stimulation of the immune response with an immunogen (an immunogen is that which will stimulate the immune system). In the animal, antibodies are synthesized primarily by plasma cells, a type of terminally differentiated B lymphocytes. Antibodies produced by the B lymphocytes will circulate in the blood system and may well be present for periods of time from weeks to months.

Every specific antibody produced by the immune system in response to any given immunogen will come from a lymphocyte line derived from an original single lymphocyte. Each lymphocyte line will have its own intrinsic and independent capacity to produce a particular antibody genetically determined by its original precursor cell. Because of the multiplicity of antigenic sites on any single immunogen, or because of impurities in the immunogen, or the presence of a number of chemically related substances derived by metabolism once injected into the animal, a large number of different and distinct lymphocytes may be stimulated following immunization. As a consequence, serum taken from blood of an immunized animal contains many different types of antibodies that are specific for many different antigens. Antibodies raised by this nature are referred as "polyclonal antibodies".

1.1.2.2 Monoclonal Antibodies

A polyclonal antibody is a heterogeneous mixture of different antibodies of varying specificity and affinity. The use of these mixed populations of antibodies creates a variety of different problems in immunochemical techniques. Therefore, the preparation of homogeneous antibodies with a defined specificity was a long-standing goal of immunochemical research. This goal was achieved with the development of the technology for hybridoma production.[8, 9] In this technique, an antibody-secreting cell, isolated from an immunized animal, is fused with a myeloma cell, a type of B-cell tumor. These hybrid cells or hybridomas can be maintained *in vitro* and will continue to secrete antibodies with a defined specificity. Antibodies that are produced by hybridomas are known as monoclonal antibodies.

The advance of monoclonal antibodies production offer improved continuity of antibody supply, better-defined specificity, and greatly increased opportunities for methodological advancement. Antibodies with special properties may be obtained that would have been impossible before the advent of hybridoma technology, e.g., bispecific monoclonal antibodies, which are produced after the fusion of two antibody-producing hybridoma lines;[10, 11] and inter-species chimeric antibodies.[12]

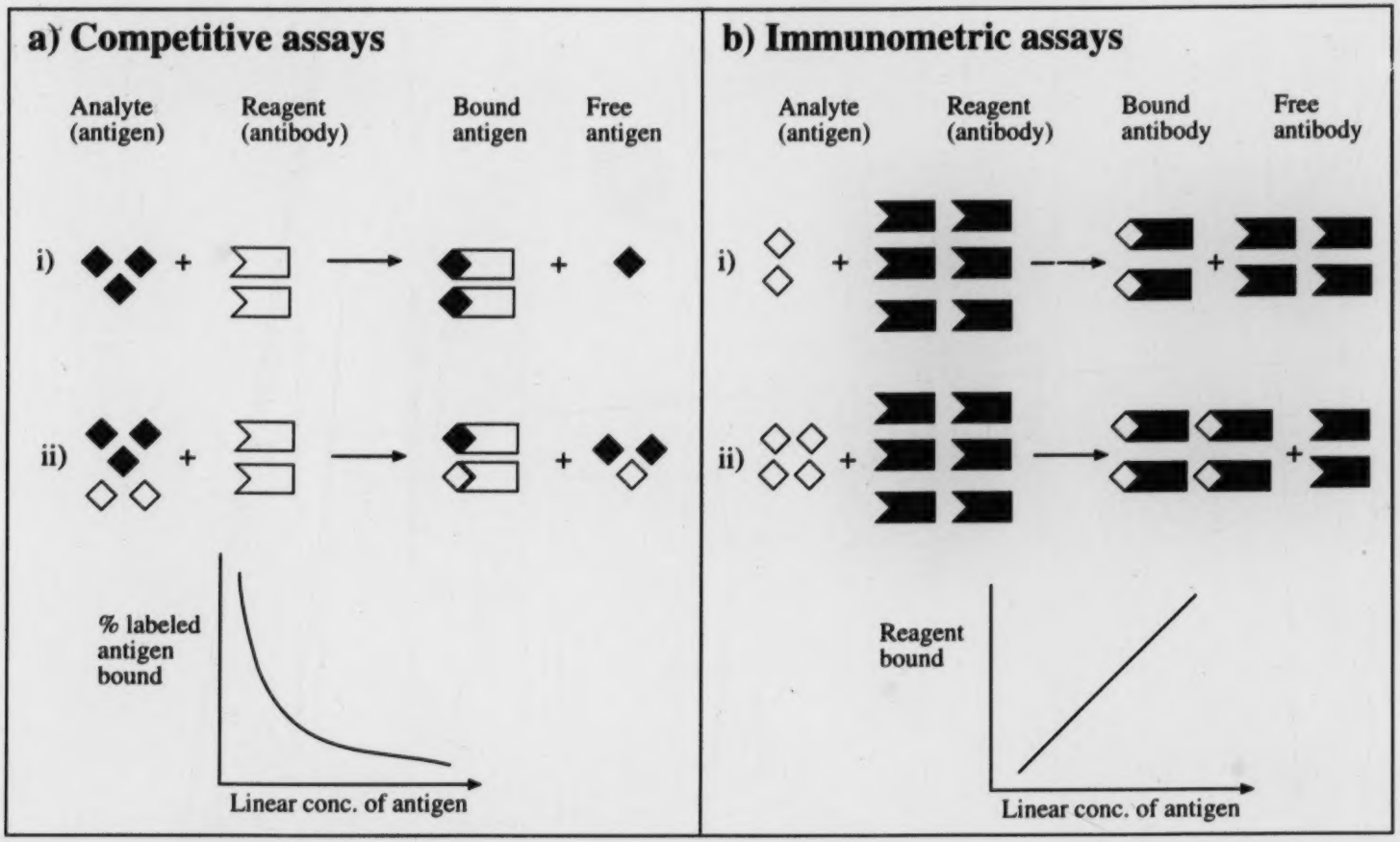

Figure 1.2: Competitive and immunometric assays. Solid symbols indicates labeled species.

1.1.3 Immunoassay Classification

An immunoassay is essentially the measurement of a substance (antigen (Ag) or antibody (Ab)) using the binding reaction

$$Ab + Ag \Leftrightarrow Ab\text{-}Ag$$

where Ab-Ag is the complex product. This reaction is reversible and the distribution of the products and reactants at equilibrium is determined by the association constant of the reaction. This constant is a measure of strength of the binding between the antibody and antigen in the complex and generally is referred to as antibody affinity. For many antibodies the affinity for the antigen is very high, and the reaction strongly favors the formation of the complex. Both antibodies and antigens can be determined using the specific chemistry of the antibody. The term "analyte" will be used to refer to a compound of interest to be determined and the term "reagent" will refer to its complimentary species.

An assay is simply an attempt to answer the question "how much of what?". Antibodies generally have very high specificity and thus are ideally suitable for defining the "what" of the question. They are also versatile because they can be raised against any nontoxic antigenic substance,[8] even weakly antigenic or nonantigenic compounds of molecular mass > 150 Da., by means of immunogens in which the weak antigen or hapten is conjugated to a carrier protein. In defining the "how much" of the question, assays using antibodies can be classified based on whether the reagent (antibody) is used at a limited concentration (competitive assay), or whether the reagent is used in excess (immunometric assay).

In competitive assays, varying concentrations of antigen (analyte) are allowed to compete with labeled antigen to react with a constant and limited amount of antibody (Figure 1.2a). The term limited is used to imply that the molar concentration of reagent (antibody) is much lower than the analyte. Given a high affinity between the antibody and the antigens, at equilibrium most of the antigens are bound to the antibody. The two states of the antigen are commonly referred to as bound (to the antibody) and free (not bound) fraction. By measuring the proportion of the labeled antigen distributed between the bound and free fractions, one arrives at a relationship where, for example, the amount bound, expressed as a percentage, varies inversely to the concentration of the analyte as shown in Figure 1.2a

In immunometric assays, varying concentrations of antigen are allowed to react with a constant and "an excess" amount of antibody. "Excess" is defined as a much

higher molar concentration of antibody than the molar concentration of antigen. At equilibrium, as before, given a high affinity between antibody and antigen, an increasing proportion of the antibody concentration will have reacted with the antigen. In immunometric assay, it is the distribution of antibody between the free and bound fractions that is measured, and not the antigen, as in competitive assay. The resulting relationship between bound antibody and concentration of antigen is linear (Figure 1.2b). This classification has been used in general and most immunoassays can be shown to belong either to one of the two classes; however, other variations are also found. The term "immunoassays" is used in a generic sense to mean assays of all variations.

The factors that have a bearing on the choice of immunoassay procedure include: the nature of the analyte (antigen or antibody), size of the analytes (large or small antigen (hapten)), concentration of analyte (picomolar vs. micromolar); chemical nature of analyte (particles, complex proteins or simple drug molecules); type of sample (in complex serum, or simple aqueous solution); type of test (quantitative or semi-quantitative); availability and quality of reagents (polyclonal vs. monoclonal antibody). Consideration of these factors often prejudice the choice to such an extent that only one, or possibly two, of the methods are really appropriate. It then becomes more apparent that methods have been developed for specific applications and not as alternative procedures to be followed on the basis of arbitrary choice.

1.1.4 Detection

1.1.4.1 Direct Detection

1.1.4.1.1 Immunoprecipitation

The first immunoassays were precipitation assays involving the direct detection of insoluble immune complexes and characterized by the lack of any labeled reagent. The antibody-antigen complex precipitates can be determined qualitatively by eye or quantitatively by weighing, nephelometric[13] or turbimetric techniques.[14] The major limitations of immunoprecipitation detection are their general unsuitability for the quantification of haptens, their limited ranges, and the requirement for controls and checks to guard against underestimation caused by antigen (analyte) excess.

1.1.4.1.2 Immunosensors

Another direct detection technique is by immunosensor technology.[15] An immunosensor is a device comprising an antigen or antibody species coupled to a signal transducer, which detects the binding of the complimentary species directly. The transducer detects the binding by a change in potential difference, current, resistance, mass, heat, or optical properties. An extensive range of analytes can be detected and measured without the need of labels. The most sensitive immunosensor offers detection limits of the order of 2×10^{-13} mol/L,[16] which compare well with many conventional labeling techniques.

1.1.4.2 Indirect Detection with Labels

Most immunoassays use indirect detection[2] through the use of labeled reagents. Labeling techniques in immunoassays can also be divided into two groups-the direct and indirect labeling methods. In the direct labeling method, the antigen-specific antibody is purified, labeled and used to bind directly to the antigen. In the indirect method, the antigen-specific antibody is unlabeled and need not be purified. Its complex with the antigen is detected by a secondary reagent, such as labeled anti-immunoglogulin antibodies or labeled protein A. An important variation that uses aspects of both the direct and indirect methods is to modify the primary antibody by coupling to it a small chemical group such as biotin. The modified primary antibody can then be detected by labeled reagents such as biotin-binding proteins (avidin or streptavidin) or hapten-specific antibodies.

The choice of the direct or indirect labeling method depends on the circumstances of the experiment . The use of directly labeled antibodies involves fewer steps, is less prone to background problems, but is less sensitive than indirect methods. It also requires a new labeling step for every antibody to be studied or for each labeling method being investigated. In contrast, indirect methods offer the advantages of widely available labeled reagents. The same reagents can be used to detect a large range of antigens and are available commercially. Also, the primary antibody is not modified so the loss of activity is avoided.

Regardless of whether the direct or indirect method will be used, the most crucial decision is the choice of label. Table 1.2 lists some of the most commonly used labels and their detection methods. The principal factor determining the suitability of a labeling substance include specific activity, ease of labeling, ease of endpoint determination, associated hazards, and possibilities for convenient assay formulation or operation.

Label	Substance	Detection Methods
Radioisotopes	^{125}I ^{3}H	Scintillation counting
Enzymes	Horseradish peroxidase Alkaline phosphatase ß-D-galactosidase Malate dehydrogenase Glucose-6-phosphate dehydrogenase	Colorimetry, fluorimetry, luminometry
Fluorescence	Fluorescein Rhodamine Coumarin derivative Phycoerythrin Europium (Eu^{3+}) Samarium (Sm^{3+}) Terbium (Tb^{3+})	Fluorimetry Time resolved fluorimetry
Chemiluminescent compounds	Acridinium ester Isoluminol derivative	Luminometry
Particles	Colloidal gold Latex particles etc.	Visual assessment nephelometry, particle counting, turbidimetry
Ligands	Biotin/Avidin	Indirect labeling with radioisotopes, enzymes, fluorophores, or luminescent compounds

Table 1.2: Some common labeling substances and measurement methods

1.1.4.2.1 Radioisotopes Labels

The most common radioisotopes used in immunoassays is ^{125}I. It has many useful attributes as general radioisotopic labels. For example, ^{125}I is chemically very reactive and can be effectively incorporated into many types of molecules using straightforward methods[17] (iodide oxidation or conjugation with the Bolton-Hunter reagent). ^{125}I is inexpensive, and commercially available with virtually 100% radioisotopic purity for labeling. Radioisotopic decay yields low-energy gamma radiation which is easily and efficiently detected with a scintillation counter. Another advantage of radioisotope labeling to measurements in complex biological material is negligible background. Unlike many other labels, the background measurement for radioisotopes like ^{125}I in almost all biological samples is virtually zero. Also, radioactive disintegration is unaffected by changes in physico-chemical parameters such as pH, concentration, temperature, etc. This means that the full specificity of radioisotopic detection can be realized which may partly account for the widespread opinion that RIA and IRMA methods are inherently stable, with low between-assay variability.

A problem when using radioisotopes is the potential health hazard. Care must be used to protect anyone handling isotopes. The most useful radioisotopes have a short half-life, which makes practical shelf life of labeled reagents limited to a few weeks, or in a few instances to a few months. No matter how stable the radiolabeled material can be made, a fresh preparation will be required when the radioactive disintegration rate falls to such a level that the count rate is too low for practical counting time. The use of ^{125}I with a 60-day half-life is a convenient compromise between effective shelf life and waste disposal.

1.1.4.2.2 Enzyme Labels

Antibodies and many antigens can be linked to functional enzymes.[17] These labeled reagents can then be detected by the addition of appropriate substrate for the enzyme. This is commonly achieved by using chromogenic substrates (Figure 1.3).

The ideal enzyme for immunoassays needs to be inexpensive, very stable, small, and easily conjugated. It should have a high catalytic activity and a range of substrates. High catalytic activity gives a high turnover rate of substrate to product, thus maximizing the amplification of the final signal. The enzyme activity should also be minimally susceptible to interference from factors likely to be present in the sample. These factors include pH, presence of common preservatives (some of which may

inhibit the enzyme), enzyme cofactors, enzyme substrates or inhibitors and other enzymes which may compete for the substrate.

A large number of different enzymes have been used to label antibodies.[17, 18] Commonly used enzymes in immunoassays are listed in Table 1.2. The enzymes malate dehydrogenate and glucose-6-phosphate dehydrogenase have been used in homogeneous enzyme immunoassays[20] exemplified by the Syva EMIT (Enzyme Multiplied Immunoassay Technique) system. Both enzymes are monitored by the conversion of the cofactor NAD to $NADH_2$. The enzymes most favoured in the ELISA method are horseradish peroxidase, alkaline phosphatase, and β-galactosidase. The popularity of horseradish peroxidase is at least partly due to its high turnover number, the variety of sensitive assays systems available, its suitability for diverse conjugation procedure (because it is a glycoprotein, the "periodate method" may be used), and its small molecular size (40 000 Da. vs. 100 000 and 500 000 Da. for alkaline phosphatase and β-galactosidase, respectively).

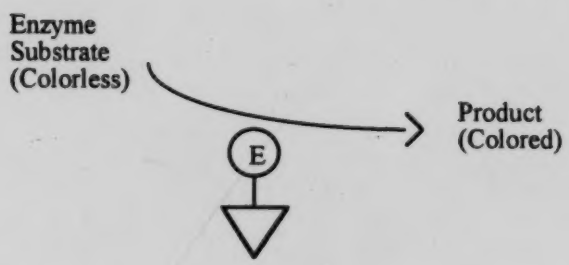

Figure 1.3: The use of an enzyme to label immunological reagents. The conversion of substrate to product is determined by monitoring color development visually or in a spectrophotometer. The amount of product (or colour) is proportional to the concentration of enzyme, which in turn is proportional to the concentration of either antigen or antibody, depending on which is labeled.

The most attractive feature of using an enzyme for labeling is the intrinsic amplification of the signal by the enzyme action. The amplification provides assays with extremely sensitive detection. A single enzyme molecule can turn over thousand of substrates molecules to products. Even the relatively poor conjugates available can prove exceptionally sensitive and detection levels in the picomolar range are commonly reported. Enzyme labels also offer the advantage of an instant visual result, but are more difficult to use in quantitative assays than other types of labels. This is because of the need to measure the rate of the enzyme reaction to get a true measure of the amount of bound reagent, and because antigen-antibody reaction may results in change in enzyme activity (see homogeneous assays section below).

1.1.4.2.3 Fluorescent Labels

The high sensitivity and selectivity achieved with fluorescing compounds make fluorescent detection procedures ideal for many immunological and biological techniques such as immunohistochemistry, flow cytometry, fluorescence-activated cell sorter analysis and molecular structure and function studies. Fluorescent detection is among the most sensitive, and eliminates many of the problems associated with radiochemical labeling methods.

A few common fluorescent compounds used as labels in immunoassays are also listed in Table 1.2. Each fluorophore has distinct and characteristic excitation and emission spectra. Both fluorescein and rhodamine show good chemical stability. They are very satisfactory fluorophores in many respects and have been very extensively used. They are readily available in activated forms (isothiocyanate) for direct coupling to antibody or other proteins and the coupling process is very readily and simply achieved.[17] They also have very high quantum yield. However, both have relatively small Stokes shift (the difference between the peak wavelengths of excitation and emission) and fluorescence is susceptible to change in pH and different levels of impurities in sample. These factors limit the methodology in some respects. However, similar to enzyme labels, the fluorescence properties of fluorophores is susceptible to changes in molecular environment and are useful for development of homogeneous assay where a separation step is not needed.

Interference from background fluorescence is a drawback of using fluorescent labels. However, background present in most biological material has a relatively short lifetime of a few nanoseconds. This is in contrast with the lifetime of the lanthanide

chelates, which is on the order of 100 microseconds. This long lifetime aspect has led to a particular method of detection: time-resolved fluorimetry[20, 21] in which it is possible to measure fluorescence at a time when virtually all the background fluorescence has disappeared.

1.1.4.2.4 Chemiluminescent Labels

Chemiluminescence is a very similar phenomenon to fluorescence.[20] Whereas the exciting energy in fluorescence is in the form of light, in luminescence it is provided by a chemical reaction. Depending on the rate of the luminescent reaction, the light emitted can be measured as a single pulse or as a continuous signal.

Similar to fluorophores, chemiluminescent compounds can also be used as labels in immunoassays.[20] A number of chemiluminescent substrates are available, but most use has been made of the isoluminol derivatives and the acridinium esters. Isoluminol derivatives can be coupled to immunological reagents through a reactive amino group ($-NH_2$) using a simple coupling reagent, e.g. carbodiimide. The main problem with the use of isoluminol is its low solubility. This generally leads to inferior performance when it is used to label reagents. Acridinium esters are more luminescent than luminol and can be used as chemiluminescent labels to give assays with enhanced sensitivity.

Although luminescence has the potential to compete with other labels for maximum sensitivity, the detection system is prone to interference. Variation in both pH and temperature can have critical effects on luminescence. Not only can a change in pH reduce quantum yield, but it can shift the light emission spectrum leading to a change in maximum wavelength.

1.1.4.2.5 Particle Labels

Antibody or antigen (or hapten) may be labeled by coupling to small particles[20] [e.g., latex particles, inorganic colloidal particles, or erythrocytes to give agglutination or particle-counting immunoassays. Agglutination tests can be observed visually (latex agglutination test can be carried out on a simple slide without the aid of any instrumentation) or with nephelometers or turbidimeters. This indirect detection method has similar draw backs as mentioned for the immunoprecipitation method.

1.1.4.2.6 Ligand Labels

A recurring approach to signal amplification for sensitive immunoassays can achieved by coupling small molecules such as biotin as the primary label to specific reagents. Then biotin specific proteins such as avidin or streptavidin, attached with multiple copies of detectable labels (secondary labels), is used to detect the biotin-labeled reagent or complex.

Labeling antibodies or proteins with biotin is simple when using biotin derivatives such as succinimide ester.[17] Biotinylation normally does not have any adverse effect on the antibody, and the coupling conditions are mild. Biotinylated antibodies can be detected using labeled streptavidin or avidin. Both are available commercially, labeled with enzymes, fluorescent dyes, or iodine. Biotin-avidin system (or Streptavidin) are typically chosen because of their high affinity of their binding reaction ($K_a = 10^{14}$ L mol^{-1}) and the quadravalency of avidin or streptavidin to increase the size of the detection complex and thus the strength of the signal.

1.1.5 Quantitation

1.1.5.1 Separation-Free Assays

Homogeneous immunoassays[22] arise because the binding reaction interferes in some ways with the detection of the label. This feature results in modulation (inhibition, enhancement, quenching or polarization) of signal from the label (enzyme activity, fluorescence, luminescence). Note that signal modulation is not always a feature of all antibodies and is also not applicable to the measurement of large molecule-like proteins.

The modulation of the signal from the label allows the binding reaction to be monitored in the complete reaction mixture, without the necessity for a separation step. Consequently they are referred to as separation-free or homogeneous immunoassays. Most homogeneous assays are of the competitive type, i.e. limited reagent. With proportionately increasing concentration of antigen, there will be less binding of the labeled-antigen conjugate, with the corresponding change either decrease or increase in the signal from the label. An ideal homogenous assay requires 100% modulation of signal from the label by the binding reaction. In practice this is very difficult to achieve, so that separation-free assays are often much less sensitive than immunoassays with separation steps. They are characterized by simplicity and speed and are widely

employed in monitoring blood and urine levels of therapeutic drugs and of drugs of abuse when low detection limits ($<10^{-6}$ mol/L) are not required.

1.1.5.2 Assays with Separations

Classically, determination of bound and free fractions of analytes or reagent in immunoassays was achieved by precipitation of the antibody/antigen complex first, then the actual separation was achieved by centrifugation. Though such procedures are still in common use, solid-phase antibodies or antigen/haptens predominate in new assays because of their convenience and efficiency. A wide range of solid phases are commonly used (microtiter plates, membranes, tubes, magnetic beads) and reagents can be covalently coupled to, or strongly adsorbed onto to different types of solid surface to bind analyte. Separation is then achieved by simply removing the reaction mixture solution containing the free fraction from the solid surface. When the sample is a complex biological fluid such as serum, a solid phase method also conveniently allows washings, which is often very useful in removing factors that would otherwise interfere with in the label activity. The separation and washing processes involve more steps and make heterogeneous assays slower, but generally more sensitive than homogeneous assays.

1.2 Automated Analyzers

1.2.1 Total Analysis Systems

A typical chemical analysis method includes the following procedures: sampling, sample transport or delivery to the laboratory, sample preparation; separation; detection; and finally data interpretation and reporting of results. Since these laboratory procedures are labor intensive, integration of these steps into a single analyzer with high level of automation will reduce cost by reducing the dependency on the labor requirement, both the number and the skill level of the technologists. Beside enhanced reproducibility and accuracy due to less human involvement, automation also improves efficiency by reducing the analysis time and increasing speed of reporting results.

The extensive automation and integration of analysis procedures result in the concept of the "Total Analysis System" (TAS)[23, 24]. This combination of automation and integration of analysis procedures makes TAS an ideal approach for continuous monitoring of chemical concentrations in industrial chemical and biochemical process. As such, the TAS concept has many potential applications in biotechnology, process

control, and the environmental and medical sciences, fields in which continuous monitoring has become increasingly important. Examples of TAS[25] include many commercially available analyzers using flow injection analysis (FIA), and those more sophisticated systems that incorporate FIA with either a chromatograph or a selective enzyme reactor.

1.2.2 Immunoassay Systems

Over the last few years, there has been a drive in immunoassay toward total automation for clinical testing[26] (i.e., from test request to result reporting), in order to reduce cost and improve the service aspect of the laboratory, by reducing the turnaround time for analysis. The automated laboratory process starts with the ordering of tests by computer order entry. A complete test menu is provide with instructions for a particular sample container with a bar code label for positive identification. The sample (taken from a patient elsewhere and delivered to the lab) is transferred onto the analyzer. Robotics are often used for sample handling and preparation. The actual analysis procedure may include a step to separate the bound from the unbound antigen if it is a heterogeneous immunoassay. The detection system could be multiapproach, e.g., spectrophotometry and fluorimetry. Finally, electronic data processing and quality control facilitate result verification and reporting. Discrete and random access automated analyzers provided a wide spectrum of tests around the clock to meet the demands of rapid testing. By combining computer technology for order entry and result reporting, an automated analyzer includes all but the sampling and sample transport steps of TAS.

Immunoassay systems with varying degree of automation are now well established in central clinical laboratories. However, these units are normally large, expensive and dedicated to routine analysis at fixed locations in a large institution. In contrast, micro-immunoassay devices such as those presented in this thesis can contribute toward development of smaller, less-expensive, and removable automated systems so that testing can be performed "near patient," i.e., point-of-care testing (POCT). POCT can be performed at various locations, both within and outside the traditional hospital environment. POCT can be performed routinely at nursing units, physician office or urgently at intensive care unit, surgery or emergency room to provide almost immediate test results so that appropriate treatment can be quickly applied. A POCT unit could also be relocated to areas where the desired patient population is residing. Testing at the

patient's home may become the most convenient. In some cases, this may be necessary due to the patient's medical condition.

1.3 Miniaturized Systems

Miniaturization of chemical measurement instruments using microfabrication technology was first demonstrated by Terry et al in 1975[27], when an integrated gas chromatograph was fabricated on a 5 cm diameter silicon wafer. The significance of this initial work was not well recognized until the late 1980s, when Manz et al.[28, 29] argued that miniaturized instruments are potentially more useful for liquid than gas analysis. Since then, integration of several laboratory steps on a single device (chip) for analysis of fluid samples has been proposed and demonstrated.[30-41]

The proposed concept is to include all the steps in TAS, in miniature form, to give a micro-total-analysis-system (μ-TAS) and provide the equivalent of a laboratory on a microdevice (chip). Such devices have all the potentials benefits of TAS and the added advantages of being small. μ-TAS provides automation of chemical procedures at a volumetric scale (nL to pL) several orders of magnitude below conventional system. These features will allow sophisticated procedure to be carried out under computer control while greatly reducing reagent consumption and waste generation. Added economic benefits over large automated analyzers include reduction of cost by reducing consumption of expensive reagents (antibodies, enzymes) and generating less waste for disposal (toxic or biologically contagious samples). Production costs can also be prominently low when mass production of devices is applicable. Miniaturization can also offer improved performance such as higher efficiency, faster analysis time and allows massive design and fabrication of parallel structures.

1.3.1 Miniaturization techniques

Miniaturization here refers to the fabrication of 3-dimensional microstructures in small devices in silicon or other materials using microelectronics fabrication technology. Microfabrication involves the processes of film deposition, photolithography, etching, and bonding, all of which have been using in integrated circuit manufacture. Using microfabrication technology, many micromechanical structures have been fabricated and reported in the literature.[42] For example, microfabricated pumps and valves have been designed, and even integrated into chemical sensors to handle liquid or gas flows. Other examples include micromachined motors, rotators, mass flow meters, neural

probes, atomic force probes. Many of the applications are not related to chemistry. However, for chemical analysis, microfabrication allows the formation of complex systems of branched channels of almost any shape in a planar substrate. Such a network is capable of sample preparation, processing, injection, separation and detection. The strength of this technology lies in the ability to make miniaturized structures integrated together and to produce them in large batch processes. Mass production can result in excellent reproducibility, and potentially inexpensive devices.

1.3.2 Pumping and Separation with Capillary Electrophoresis

Capillary electrophoresis, in which the driving force is an electric field, has proven to be a powerful separation method and a convenient means for fluid pumping.[31-41] Its potential for automated, rapid, high-efficiency separations makes it appealing as a replacement for some of the more labor-intensive assays carried out in electrophoretic gels and as a complement to companion techniques such as HPLC. Among the many attractive characteristics of this technology is its versatility for separation of a diverse spectrum of analytes, ranging from small organic ions to macromolecular protein complexes or DNA. Capillary electrophoresis not only gives efficient separation but also generates the electroosmotic flow (EOF) which can be used to pump and mix solution before separation.

With capillary electrophoresis, sample is introduced into a buffer-filled capillary either hydrodynamically (with pressure or suction) or electrokinetically (with voltage). Both ends of the capillary and electrodes are then placed into a buffer solution that also contains the electrodes, and high voltage is applied to the system. The applied voltage causes charged analytes in a sample to migrate (electrophoretic migration) and separate according to their charge and mass while moving through the capillary (Figure 1.4). The electroosmotic flow is the solvent flow induced by the applied voltage and charges (usually negative) on the interior capillary wall. With these two transport phenomena, the solvent and solutes all migrate due to electroosmotic motion of the solvent, while the ions are additionally driven by migration in the electric field. The electroosmotic flow rate is usually larger than that of electrophoretic migration, so that all the sample components move in one direction and past a detector window placed near the outlet of the capillary, where information is collected and stored by appropriate data-acquisition system.

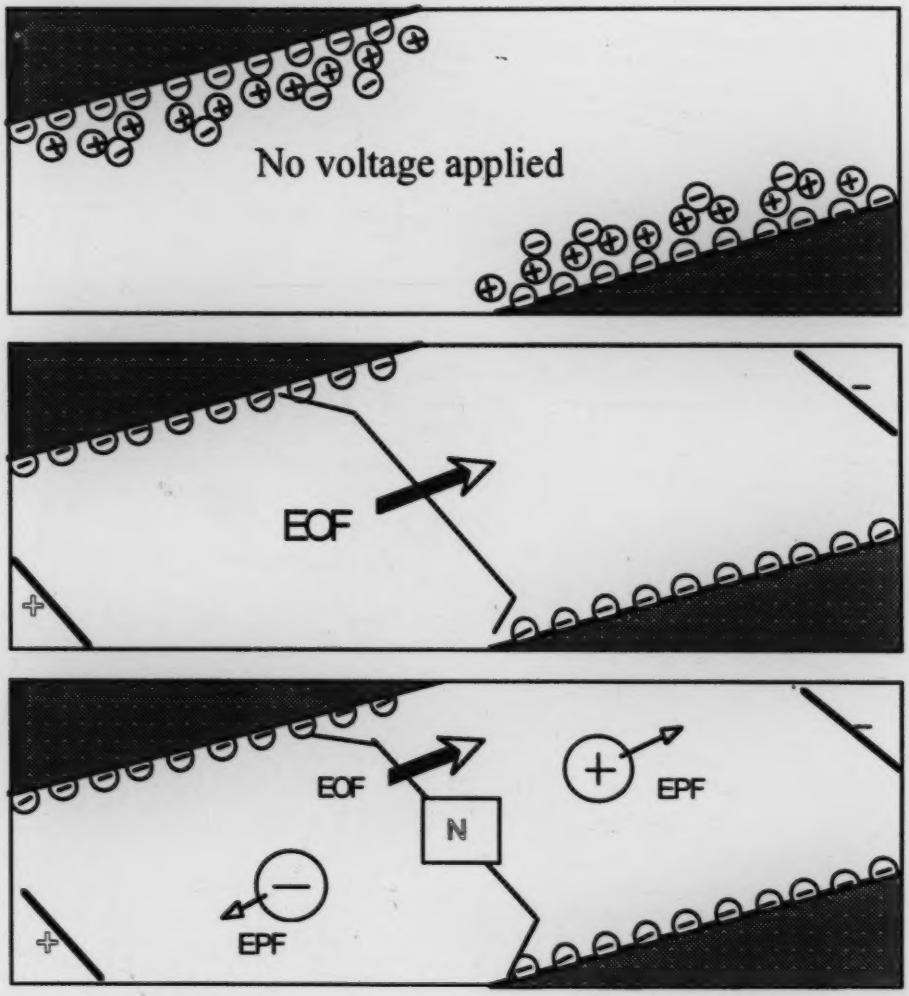

Figure 1.4: Simplistic view of electroosmotic flow (EOF) and electrophoretic flow (EPF). (Top) negatively charged glass or silica surface and hydrated cations accumulating near surface; (middle) solvent flow towards the cathode upon application of electric field; (bottom) differential solute migration superimposed on electroosmotic flow. (Adapted from HP manual "High performance capillary electrophoresis-an introduction").

Because of electroosmotic flow, electric fields may be used to control fluid within a valveless microchannel system. Integration of different functional components such as mixers and injectors are greatly simplified and automated fluid control are readily achieved with external electronic relays. In contrast, microvalves and micropumps are not well developed and are more difficult to incorporate into a microchannel system. Methods utilizing more conventional pumps would develop extremely high back-pressures with small capillary dimensions and are not well suited to delivery of low volumes.

1.3.3 CE-based microfabricated immunoassay systems

Figure 1.5 shows a schematic diagram of a CE-based microfabricated immunoassays systems. A system of microchannels and reservoir (30 - 250 μm) is fabricated on a small planar substrate. Insulating substrate, e.g., glass, and fused silica are used rather than semiconducting substrates, to allow high voltages to be applied to the chips to transport samples and reagents through the channel manifolds. A computer program is used to control the power supplies, electronic relays, data collection and processing. Using electrokinetic effects with appropriate application of voltage, sample and reagents (antibody, secondary reagents, tracer ...) are delivered to the reaction chamber, allowed to mix and react. After a period of incubation, a portion of the reacted mixture is delivered to the injector, an intersection (slightly offset) between the sample and separation channels. By switching the voltage to separation buffer and waste, a small volume of the mixture is injected into the separation channel and the components are separated in solution by capillary electrophoresis. For simplicity and sensitivity, laser-induced-fluorescence is used. Depending on the assay format, fluorescent-labeled tracer, fluorescent-labeled primary or secondary reagents can used for quantitation.

Potential advantages of such flow-based immunoassays include simplicity of design for system automation and integration, rapid analysis, minute consumption of reagents, little generation of waste and use as portable monitors for environmental or industrial testing or quantitative point-of-care clinical diagnosis.

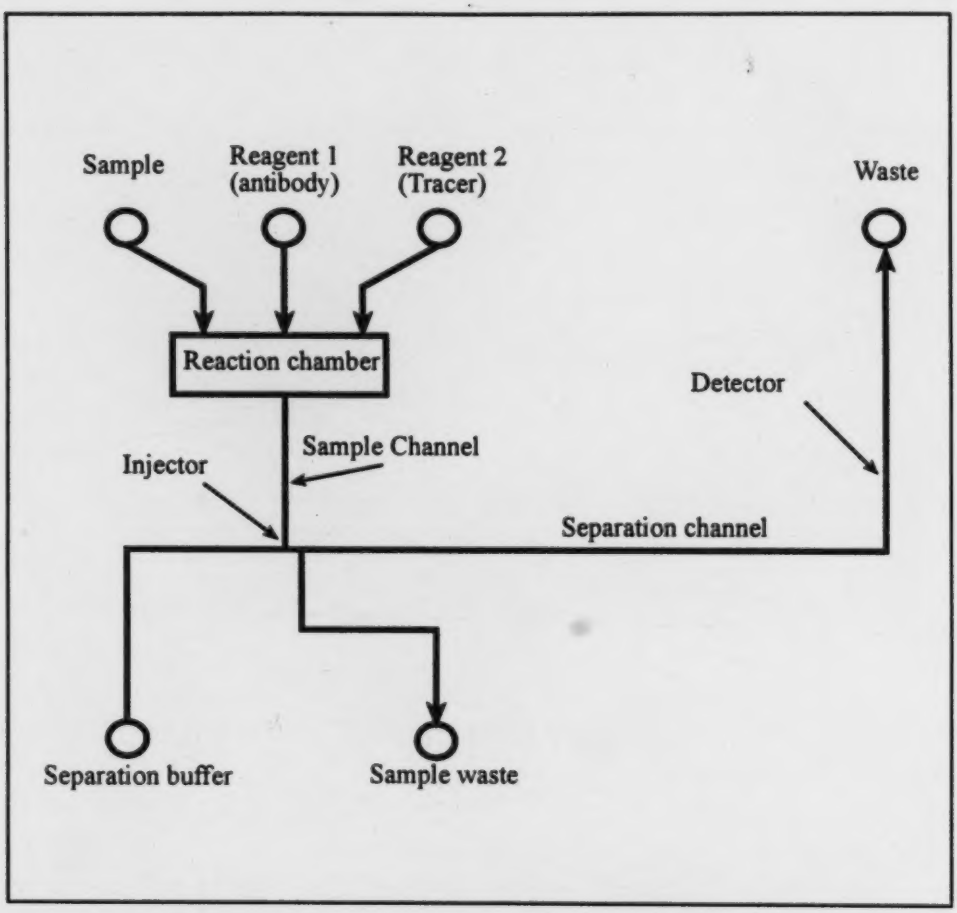

Figure 1.5: Schematic diagram of a microdevice for immunoassays. Circles are solution reservoirs for buffer, sample, reagents and wastes. Lines represent microchannels (30-250 μm) fabricated on planar substrates. Injector is formed at the intersection (slightly offset intersection to prolong length) of sample and separation channels. Arrows on channels indicate the direction of the fluid flow. Detection can be located at any point on the separation channel between the injector and the separation waste.

1.4 Scope of Present Work

The development of miniaturized, microfabricated devices for useful and relevant applications such as clinical diagnostics or environmental monitoring is currently under rapid growth. Potential benefits of using microdevices for these applications include improvement in analysis time, increased cost effectiveness, better performance and portability. To this end, one of the objectives of this work is to demonstrate the feasibility of developing microfabricated devices for immunoassay. The focus of the present work is on the design and evaluation of microfabricated glass devices for small automated immunoassay systems using CE and laser induced fluorescence as the separation and detection techniques, respectively. A key element in utilizing electrokinetically driven microfluidic devices for immunoassays is the demonstration that separation of immunological reaction products can be performed on-chip. This element is emphasized throughout the remaining chapters.

Chapter 2 gives the experimental details of chip fabrication, instrumentation, and a simple chip layout with only two crossing channels for sample injection and separation. This layout was used to optimize separation and detection on-chip. Optimization of separation efficiency for simple molecules (such as amino acids) and large complex proteins such as antibodies is discussed along with the theory of electroosmotic pumping and electrophoretic separation. The need for, and the results of, optimization to reduce antibody adsorption on glass chips are discussed. The optimization of detection using laser induced fluorescence is also covered in this chapter.

In chapter 3, optimization of separation is evaluated for glass devices bonded at room temperature. This contrasts to the devices fabricated by permanent bonding of two glass plates at high temperature, which were used in chapter 2 and in the later chapters. Some of the advantages of using room-temperature-bonded devices are also discussed.

Chapter 4 reports on the use of microchip-based capillary electrophoresis for studying antigen/antibody interactions. Antibody binding affinity is a measure of this interaction and is a determining factor in immunoassay sensitivity. Fluorescein-labeled BSA was used to determine the affinity of monoclonal anti-BSA in the complex ascites fluid matrix. The antibody affinity constant for the BSA/anti-BSA was compared with published results. Antibody/antigen complex speciation is also reported in this chapter.

In chapter 5, separation, detection and quantitation of reagents and products in immunofluorometric and fluoroimmunoassay formats are reported. The simple chip design was used to separate the immunological products within about 40 s. The determination of monoclonal mouse IgG in mouse ascites fluid and drug theophylline in serum samples were demonstrated in this chapter.

Chapter 6 describes a more complex layout of channels for integration of sample processing with separation and detection. This layout was used for competitive immunoassays in which on-chip mixing of serum samples with a labeled tracer and the specific antibody is followed by separation and detection of the components. Diffusional dispersion was a convenient and effective mechanism for mixing fluids in microchannels. Issues affecting layout design such as dilution accuracy, diffusion and reaction time are discussed for rapid immunoassay systems using electrokinetic pumping and diffusional mixing.

Finally, Chapter 7 provides a brief summary of each of the preceding chapters, with some discussion of future work.

1.5 References

1. Yalow, R.; Berson, S. *Nature* **1959**, *184*, 1648-1649.
2. Anderson, D. J.; Kricka, L. J.; Skogerboe, K. J.; et al. *Anal. Chem.* **1997**, *69*, 165R-229R.
3. Price, C. P.; Newman, D. J.; Eds. *Principles and Practice of Immunoassay*; Stockton Press: London, 1991; pp 643.
4. Diamandis, E. P.; Christopoulos, T. K. Eds. *Immunoassay*; Academic: San Diego, CA, 1996.
5. Wild, D. G., Davies, C. J. In *The Immunoassay Handbook*; Wild, D. G., Ed. Stockton Press: New york, 1994; pp 49-82.
6. Gosling, J. P. In *Immunoassay: Laboratory Analysis and Clinical Application;* Gosling, J. P.; Basso, L. V., Eds. Butterworth-Heinemann: Newton, MA, 1994; pp 1-30.
7. Glynn, L. E.; Steward, M. W., Eds. *Structure and Function of Antibodies;* John Wiley and Sons: New York, 1981; pp 1-52.
8. Harlow, E.; Lane, D. Eds. *Antibodies: A Laboratory Manual;* Cold Spring Harbor Laboratory: New York, 1988; Chapters 4-5.
9. Köhler, G.; Milstein, C. *Nature* **1975**, *256*, 495-497.
10. Karawajew, L.; Behrsing, O.; Kaiser, G.; Micheel, B. *J. Immunol. Methods* **1988**, *111*, 95-99.
11. Görög, G.; Gandolfi, A.; Paradisi, G., et al. *J. Immunol. Methods* **1989**, *123, 131-140.*
12. Moore, G. P. *Clin. Chem.* **1989**, *35*, 1849-1853.
13. Whicher, J. T.; Perry, D. E. In *Practical Immunoassay;* Butt, W. R., Ed. Marcel Dekker, Inc: New York, 1984; pp 117-177.
14. Maynard, Y.; Scott, M. G.; Nahm, M. H.; Ladenson, J. H. *Clin. Chem.* **1986**, *32*, 752-757.
15. North, J. *Trends Biotechnol.* **1985**, *3*, 180-186.
16. Schlatter, D.; Barnes, R.; Fattinger, C.; et al. *Biosens. Bioelectron.* **1993**, *8*, 109-116.
17. Harlow, E.; Lane, D. Eds. *Antibodies: A Laboratory Manual;* Cold Spring Harbor Laboratory: New York, 1988; Chapter 9.

18. Gosling, J. P. In *Immunoassay;* Diamandis, E. P.; Christopoulos, T. K., Eds.; Academic: San Diego, CA, 1996, pp 287-308.
19. Jaklitsch, A. In *Enzyme-mediated Immunoassay;* Ngo, T. T.; Lenhoff, H. M., Eds.; Plenum Press: New York, 1985; pp 33-35.
20. Collins, W. P., Ed. *Complementary Immunoassays;* John Wiley & Sons: New York, 1988; Chapters 11, 13, 14, 16.
21. Sabbatini, N.; Guardigli, M.; Manet, I.; Ziessel, R.; Lehn, J. M. *Med. Biol. Environ.* **1995**, *23*, 101-107
22. Chan, D. W., Ed. *Immunoassay A Practical Guide;* Academic Press, Inc: Orlando, Fl, 1987; Chapter 1.
23. Graber, N.; Lüdi, H.; Widmer, H. M. *Sensors and Actuators* **1990**, *B1*, 239-243.
24. Manz, A.; Harrison, D. J.; Verpoorte, E.; Widmer, H. M. In *Advances in Chromatography*, Brown, P. R.; Grushka, E., Eds.; Marcel Dekker: New York, 1993; pp 1-65.
25. Widmer, H. M. In *Proceedings 2nd International Symposium on μTAS (Basel. Nov. 19-22);* Widmer, H. M.; Verporte, E.; Barnard, S., Eds, 1996; pp 3-8.
26. Anderson, D. J.; Kricka, L. J.; Skogerboe, K. J.; et al. *Anal. Chem.* **1997**, *69*, 203R-208R.
27. Terry, S. C. A gas chromatography system fabricated on a silicon wafer using integrated circuit technology. Ph.D. Dissertation, Stanford, University, 1975.
28. Manz, A.; Graber, N.; Widmer, H. M. *Sens. Actuators* **1990**, *B1*, 244.
29. Manz, A.; Fettinger, J.C.; Verpoorte, E.; Lüdi, H.; Widmer, H.M.; Harrison, D.J. *Trends Anal. Chem.* **1991**, 10, 144-149.
30. Harrison, D.J.; Fluri, K.; Seiler, K.; Fan, Z.; Effenhauser, C.S.; Manz, A. *Science* **1993**, 261, 895-897.
31. Chiem, N.; Harrison, D.J. *Anal. Chem.* **1997**, 69, 373-378.
32. Cheng, J.; Fortina, P.; Surrey, S., Kricka, L.J., Wilding, P. *Mol. Diagn.* **1996**, 1, 183-200.
32. Harrison, D.J.; Manz, A.; Fan, Z.; Lüdi, H.; Widmer, H.M. *Anal. Chem.* **1992**, 64, 1926-1932.
33. Manz, A; Harrison, D.J.; Verpoorte, E.; Widmer, H.M. . In *Advances in chromatography* ; Brown, P.R.; Grushka, E. eds.; Marcel Dekker: New York, **1993**, pp 1-66.

34. Koutny, L.B.; Schmalzing, D.; Taylor, T.A.; Fuchs, M. *Anal. Chem.* **1996**, 68, 18-22.
35. Jacobson, S.C.; Hergenröder, R.; Moore, A.W.; Ramsey, J.M. *Anal. Chem.* **1994**, 66, 4127-4132.
36. Fluri, K.; Fitzpatrick, G.; Chiem, N.; Harrison, D.J. *Anal. Chem.* **1996**, 68, 4285-4290.
37. Jacobson, S.C.; Ramsey, J.M. *Anal. Chem.* **1996**, 68, 720-723.
38. Woolley, A.T.; Hadley, D.; Landre, P.; deMello, A.J.; Mathies, R.A.; Northrup, M.A. *Anal. Chem.* **1996**, 68, 4081-4086.
39. Seiler, K.; Fan, Z.H.; Fluri, K.; Harrison, D.J. *Anal. Chem.* **1994**, 66, 3485-3491.
40. Effenhauser, C.S.; Manz, A.; Widmer, H.M. *Anal. Chem.* **1993**, 65, 2637-2642.
41. Branebjerg, J.; Fabius, B.; Gravesen, P. In *Micro total analysis systems*; van den Berg, A.; Bergveld, P. eds. Kluwer Academic Publishers: Netherlands; 1995, pp 141-151.
42. Technical Digest, Transducers 97, 9th International Conference on Solid-State Sensors and Actuators, Chicago, June 16-19, 1997.

Chapter 2

Optimization of Separation and Detection

2.1 Introduction

Immunoassays permit a highly selective and sensitive detection of macromolecules (e.g. proteins and polysaccharides) and of smaller molecules (e.g. peptides, hormones, and drugs) in complex biological matrices.[1] Their selectivity is based on the high specificity of recognition of the antibody to the antigen, whereas the sensitivity results from the use of labeling techniques such as radioactivity, fluorescence, chemiluminescence, or enzyme amplification. Many immunoassay formats rely on separation of bound and free forms of antibody and antigen using a solid polymer as a supporting medium for an immobilized antibody or antigen. The procedure is often relatively slow and tedious when performed manually, as it requires many steps. Capillary electrophoresis (CE) has proven to be a powerful tool to separate species in solution and chip-based CE has been used successfully to manipulate minute quantities of solution and provides very rapid separation. Therefore, chip-based CE is being examined as an automated and rapid method for performing immunoassays. A number of aspects of experimentation needed to be developed and refined before on-chip immunoassays could be performed. These are presented in this chapter. Section 2.2 covers the theory of electroosmotic pumping and CE separation. Section 2.3 gives the experimental details of chip fabrication, instrumentation, chip layout and procedures to optimize separation and detection on-chip. Section 2.4.1 discusses the need for, and the results of, optimization to reduce IgG adsorption on-chip. Section 2.4.2 shows the evaluation of chip design, and optimization of separation efficiency, while Section 2.4.3 shows the optimization of detection with laser induced fluorescence.

2.2 Theory

2.2.1 Electroosmosis and Electrophoresis

A capillary electrophoresis (CE) system consists of a glass capillary channel filled with a buffering medium across which a voltage is applied. Charged species introduced at the inlet of the channel migrate under the influence of the electric field to the outlet. If

a suitable detector is placed near the outlet, the passage of each zone of the species may be recorded, yielding an electropherogram.[2]

The migration velocity of a particular species is given by

$$v = \mu E \quad [1]$$

with

$$E = V/L \quad [2]$$

where v is the velocity, μ is the electrokinetic mobility of the species, E is the electric field gradient, V is the total applied voltage, and L is the length of the channel. In equation 2 it is assumed the channel geometry is constant throughout the entire device. Adjustment can be made to obtain E in each region if this is not the case. The time, t_m, required for a zone to migrate a distance, d, from the injection to the detection location is

$$t_m = d/v = d/(\mu E) \quad [3]$$

Most capillaries used for CE contain silanol groups which become negatively ionized in the presence of a buffer (pH buffer > pK_a of silanols). The negative charge on the surface of a capillary wall is balanced by a positively charged layer of hydrated cations in the solution at the wall-solution interface. Upon application of the electric field, this layer begins to move toward the cathode and, owing to viscous drag, transports the bulk liquid inside the capillary. This transport process is known as electroosmotic flow. With this flow, μ in equation 1 can be divided into two components

$$\mu = \mu_{ep} + \mu_{eo} \quad [4]$$

where μ_{ep}, is the electrophoretic mobility and μ_{eo} is electroosmotic mobility. The electrophoretic mobility is a characteristic property of a given ion in a given medium at a given temperature

$$\mu_{ep} = q/(6\pi\eta a) \quad [5]$$

where q is the charge of the ion, η the solution viscosity, and a the radius of the molecule assuming it has a spherical shape. The viscous drag of the solvent, the charge and size of the molecule thus determine the electrophic mobility and ultimately the

separation of the charged species in an applied electric field. The electroosmotic mobility, μ_{eo}, is given by

$$\mu_{eo} = \varepsilon\zeta/(4\pi\eta) \qquad [6]$$

where ε is the dielectric constant of the solvent, and ζ the zeta potential of the capillary wall. It is important to note that under electrophoretic conditions where electroosmosis is suppressed, anions and cations would move in opposite directions. However, in capillaries such as those etched in glass, the electroosmotic flow is usually strong and its corresponding electroosmotic mobility is larger than the electrophoretic counter part for each individual ion in the sample. Consequently, the net total mobility, μ, in equation 4 is positive and both cations and anions migrate in the same direction toward the cathode.

2.2.2 Diffusion Effects on Separation Efficiencies.

As in chromatography, we are interested in the resolution of two or more components and the speed with which separation can occur. The irreducible minimum peak broadening in CE is due to longitudinal diffusion. The corresponding spatial variance, σ_L^2, is given by

$$\sigma_L^2 = 2Dt_m \qquad [7]$$

where D is the molecular diffusion coefficient of the solute in the zone. Substituting the expression for time from equation 3 into equation 7 yields

$$\sigma_L^2 = 2Dd/(\mu E) \qquad [8]$$

The rate of generation of variance per unit length or height equivalent to a theoretical plate, H_L, due to longitudinal diffusion alone is given by

$$H_L = \sigma_L^2/d \qquad [9]$$

substituting equation 8 into equation 9 yields

$$H_L = 2D/(\mu E) \qquad [10]$$

and the corresponding number of theoretical plates, N_L, is given by

$$N_L = d/H_L \qquad [11]$$

Substituting H from equation 10 into equation 11 gives

$$N_L = \mu dE/2D = \mu V_{id}/(2D) \qquad [12]$$

where V_{id} is the potential difference between the injection and the detection points.

2.2.3 Off-Column Effects Contribution to Separation Efficiencies.

In practice, injected and detected volumes as well as detector response time also contribute to the variance. Equation 7 can be modified to

$$\sigma_{tot}^2 = \sigma_L^2 + \sigma_{inj}^2 + \sigma_{det}^2 + \sigma_o^2 \qquad [13]$$

where σ_{tot}^2 is the total spatial variance, σ_{inj}^2 is the variance due to injection, σ_{det}^2 is the variance due to detection. The extra term, σ_o^2, is the variance due to other non-ideal factors including sample overloading, Joule heating in the capillary, sample adsorption to the capillary wall, and solute microheterogeneity. Sample overloading only occurs at high concentration of analytes. For microchip-based CE with fluorescent detection, analyte concentration is typically low and the variance due to sample overloading is minimal. The contribution of the adsorption effect to the total variance is minimal for small solutes but becomes important for complex molecules such as proteins which tend to adsorb to the wall of an uncoated channel. The contribution of solute microheterogeneity (either natural or by non-uniform labeling with multiple dye molecules) to the total variance becomes important if the analyte's mass or charge becomes distributed over a broad range.

The variances due to injection and detection are the results of finite volumes of the injector and detector, as well as the response time of the detection electronics. There is an additional contribution due to dispersion of the sample during the injection period, and the variance contributed due to this term can be approximated as $2Dt_{inj}$ where t_{inj} is the injection time.[3] Assuming that both the injection and detection volumes have a rectangular-shaped profile along the capillary axis, the variances σ_{inj}^2 and σ_{det}^2 can be approximated by

$$\sigma_{Inj}^2 = l_{inj}^2/12 + 2Dt_{inj} \qquad [14]$$

$$\sigma_{det}^2 = l_{det}^2/12 + (\mu E\tau)^2 \qquad [15]$$

where l_{inj} and l_{det} are the lengths of the injector and detector and τ is the time constant for the detection system. τ can be estimated by $1/(2\pi f)$ where f is the cut-off frequency of the low-pass filter. By substituting equations 7, 14 and 15 into equation 13, the total variance can be rewritten in detail as

$$\sigma_{tot}^2 = 2Dt_m + 2Dt_{inj} + l_{inj}^2/12 + l_{det}^2/12 + (\mu E\tau)^2 + \sigma_o^2 \qquad [16]$$

and similar to equation 9, the total plate height can be written as

$$H_{tot} = 2Dt_m/d + 2Dt_{inj}/d + l_{inj}^2/(12d) + l_{det}^2/(12d) + (\mu E\tau)^2/d + \sigma_o^2/d \qquad [17]$$

The sum of the second and third terms of the right hand side of equation 17 is an estimate of the injection plate height and the sum of the fourth and fifth terms is an estimate of the detection plate height.

2.2.4 Separation Resolution

According to Giddings,[4] with later modification by Jorgenson,[5] the resolution of two solutes in CE is

$$R = \frac{1}{4}\left[\frac{\mu_{ep,1} - \mu_{ep,2}}{\bar{\mu} + \mu_{eo}}\right] N^{\frac{1}{2}} \qquad [18]$$

where $\mu_{ep,1}$ and $\mu_{ep,2}$ are the electrophoretic mobilities for the two solutes and $\bar{\mu}$ is the average electrophoretic mobility. Substituting N with the expression in equation 12, equation 18 becomes

$$R = \frac{1}{4}\left[\mu_{ep,1} - \mu_{ep,2}\right]\left[\frac{dE}{2D(\bar{\mu} + \mu_{eo})}\right]^{\frac{1}{2}} \qquad [19]$$

According to equation 19, all four variables, the difference in μ_{ep} of the two solutes, the electroosmotic flow, the separation distance and the electric field affect separation resolution in CE. Variation of these values may allow one to meet the separation requirements. While changes of separation distance and electric field are

trivial, modification of electroosmotic flow or electrophoretic mobility is more complicated.

2.3 Experimental

2.3.1 Materials and Reagents

Borosilicate glass (Pyrex, Borofloat) was from Paragon Optical (Reading, PA). Photomask glass was from Agfa-Gevaert (Belgium) and cover-slip (0211) glass was from Corning Glass (Parkridge, IL). Microscope slides and Sparkleen detergent were from Fisher Scientific (Edmonton, Canada). The hollow diamond drill bit was purchased from Lunzer (Saddle Brook, NJ). Crystal bond came from Aremco (Ossining, NY). Glass vials (one-dram), microtiter plates, chloroform were from Fisher Scientific (Edmonton, Canada). Dimethylsulfoxide (DMSO), HCl, NaH_2PO4, Na_2HPO4, NaOH, HNO_3, NaCl, and sodium bicarbonate were from BDH while boric acid was from J.T.Baker (all via Fisher Scientific). Tween 20, polyvinyl alcohol (PVA), Nafion solution (5% w/v in aliphatic alcohol & H_2O) and polydimethylsiloxanes (PDMS) were from Aldrich (Milwaukee, WI). H_2O_2 was from Caledon (George Town, Canada). All chemicals were reagent grade. Fluorescein, fluorescein isothiocyanate isomer I (FITC), amino acids, tris(hydroxymethyl)-aminomethane (tris), tricine, and fluorescein-labeled bovine serum albumin (BSA*), human immunoglobulin G (H-IgG) and fluorescein-labeled goat anti-human IgG $F(ab')_2$ fragment (anti H-IgG* $F(ab')_2$) came from Sigma (St. Louis, M0). Fluorescein-labeled theophylline and antitheophylline were part of the Abbott TDx reagent set (from Sigma). Fluorescein-labeled goat anti-human IgG (anti H-IgG*) was purchased from Molecular Probes (Eugene, OR). The fluorescein to protein (F/P) ratio was 11.2 for BSA* and 7.6 for anti H-IgG*, according to the suppliers. 0.45 μm and 0.22 μm pores sizes syringe filters were from Millipore (Bedford, MA). Unless otherwise indicated, all solutions were prepared with doubly distilled water and were filtered with 0.22 μm pore filters (Millipore) before use. Detergent solution was prepared by dissolving one teaspoon of detergent per liter of water.

The "tris" buffer (pH 9) contained 100 mM, tris and 20 mM boric acid. The "10 mM tricine", low ionic strength buffer contained 10 mM tricine adjusted with sodium hydroxide to pH 8.0 and 0.01% w/v Tween 20. The "50 mM tricine" high ionic strength buffer contained 50 mM tricine adjusted with sodium hydroxide to pH 8.0, 0.01% w/v Tween 20, and 26 mM NaCl.

2.3.2 Procedures

2.3.2.1 Amino Acid Labeling

Amino acids were labeled using the method recommended for protein labeling.[6] Stock solutions of amino acid (3 mM) were prepared in 0.1 M sodium bicarbonate (pH 9.0). A 10 mM fluorescein isothiocyanate (FITC) solution in DMSO was diluted with water to 1 mM. While stirring, 100 μL of 1 mM FITC solution was added in 20 μL aliquots over 2 minutes to 900 μL of each of the seven 3.3 mM amino acid solutions. The mixtures were left in the dark at 4° C overnight before use. Prior to analysis, reacted solutions were mixed and serially diluted with separation buffer.

2.3.2.2 Labeling of H-IgG

H-IgG was labeled as described for labeling of amino acids. Purified H-IgG (3.4 mg) was dissolved in 1 mL of 0.1 M sodium bicarbonate (pH 9.0). While stirring, 50 μL of 1 mg/mL of FITC in DMSO was slowly added in 5 μL aliquots. The mixture was left in the dark at 4° C overnight, then 150 μL of freshly prepared 1 M hydroxylamine (pH 8.0) was added and incubated for 30 min. to stop the reaction. The 1.2 mL solution was concentrated and dialyzed down to 150 μL by spinning a 10,000 MWCO Filtron Macrosep concentrator with a centrifugal force of 7000 g at 4° C. Then 1 mL of water was added to the mixture and the dialysis process was repeated twice more. The final concentrated sample was reconstituted to 1 mL with antibody dilution buffer (25 mM Tris-boric acid, 10 mM NaCl (pH 9), 0.0025 % Tween 20 (w/v), 0.0025% sodium azide (w/v)) and stored at 4° C in the dark.

2.3.2.3 Mass Spectrometry of Bovine Serum Albumin

Mass spectra of BSA and fluorescein-labeled BSA were obtained from matrix assisted laser desorption ionization (Kratos Kompact MALDI) using a sinapinic acid sample matrix and 20 kV acceleration. This work was performed by R. Whittal at the University of Alberta.

2.3.3 Device Fabrication

Devices were fabricated at the Alberta Microelectronic Centre (AMC) using microlithographic patterning and an HF/HNO_3 etchant.[7] Devices consisted of two glass plates bonded together, one with etched channels and the other with holes drilled in it.

2.3.3.1 Microlithography and Etching

The photomask layout of the channel patterns was designed with PC based L-Edit software (Tanner Research Inc., Pasadena, CA), and the master chrome mask (5x5 inch square) was manufactured by Precision Photomask (Montreal, Canada). The glass to be etched was first prepared by cleaning in H_2SO_4/H_2O_2 (3:1) for 30 minutes. Care should be taken when using this concentrated acid mixture. Then a Cr/Au/Cr coating (25/100/25 nm thickness) was sputtered onto the glass substrates before spin coating with 1.5 μm of photoresist (Waycoat HPR 504, Olin Hunt) and soft-baking at 110 °C for 30 minutes (Figure 2.1a). A contact mask aligner (Karl Suss MA4) was used to align the mask with the glass substrate. The photoresist was then exposed to UV light (365-405 nm) for about 3 s (Figure 2.1b), developed with Microdeposit developer (Shipley, Newton, MA) to remove the exposed resist and baked at 120 °C for 0.5 hour (Figure 2.1c). The chrome and gold layers were etched with a commercial Cr etch (KTI Chemicals, Sunnyside, CA) and Aqua Regia ($HCl:HNO_3$ 3:1 volume ratio), respectively (Figure 2.1d). The exposed glass was etched using a freshly prepared mixture of concentrated $HF:HNO_3:H_2O$ (20:14:66) (Figure 2.1e). The channel depth during etching was monitored with an alpha-step profilometer (Tencor Ind., Mountain View, CA). Typical etched depth was 13 to 15 μm. The remaining photoresist and metal coatings were then stripped with acetone and the etches described above (Figure 2.1f).

Cover plates with drilled access holes were prepared as follows: Microscope slides were glued with Crystal Bond to both sides of a glass plate, for protection against chipping or scratching during drilling of 2 mm diameter holes with a diamond bit. The protecting glass slides were then removed with the aid of acetone.

2.3.3.2 Bonding

2.3.3.2.1 Room Temperature Bonding

Before bonding, the top plates were rinsed three times with acetone to remove excess Crystal Bond, then cleaned in hot (100 °C) piranha acid solution (H_2SO_4 : H_2O_2 3:1 V/V) for 15 min. Both plates were then cleaned in a class 100 clean hood with a high-pressure cleaning station (MicroAutomation). The plates were spun under a high pressure (3000 psi) jet of water for about 50 s, to remove most of the particles on the surface of the glass. A clean sponge and detergent solution were then used to rigorously scrub the surface of the substrates for about two minutes to remove strongly

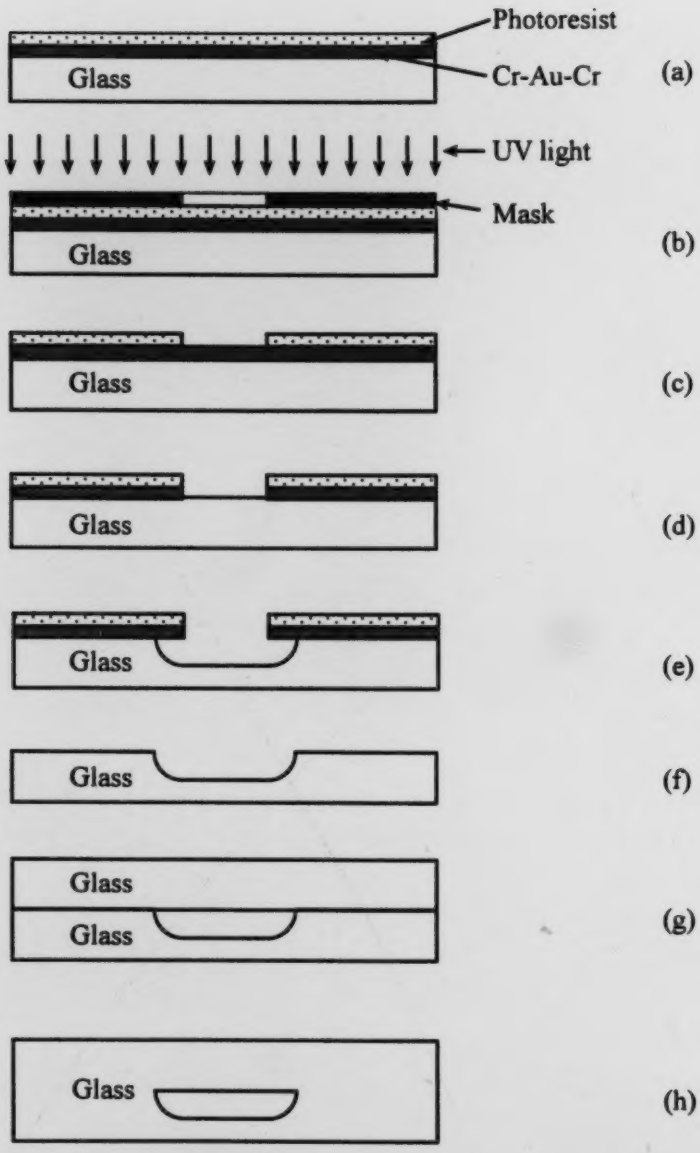

Figure 2.1: The sequence of device fabrication: Glass plate is coated with metal and photoresist (a); Photoresist is exposed to UV light through contact mask (b); Photoresist is developed (c); Exposed metal is etched (d); Exposed glass is etched (e); Resist and metal are stripped (f); Cover plate is aligned and room-temperature bonded to etched plate (g); Thermal bonding at high temperature (h).

adsorbed particles. The substrates were then spun again under the water jet for 1.5 minutes, and finally dried under the IR lamp for about one min. The top plate was aligned with the etched plate immediately after cleaning (Figure 2.1g). Air trapped between the plates was squeezed out by manually applying pressure until the Newton's ring disappeared. The plates were separated and recleaned if any particulate prevented complete contact. When separating, care was taken to prevent damage to the glass surfaces. Shear forces caused by sliding the plates over each other must be avoided; instead, a modest force should be applied to bend the glass, causing the edges of the plates to lift apart and this separation can then be induced to propagate inwards.

2.3.3.2.2 High Temperature Bonding

Room-temperature bonded devices were thermally bonded (Figure 2.1h) in a Model 6-525 programmable furnace (J. M. Ney Co., Yucaipa, CA) at 590 °C for Photomask and 0211 glass and 650 °C for Pyrex glass. The temperature program for Pyrex glass was: (1) 40 °C/min up to 550 °C, then held at this temperature for 30 min, (2) 20 °C/min up to 610 °C and held for 30 min, (3) 10 °C/min up to 650 °C and held for 6 h, and (4) natural cooling of the furnace to room temperature. For Photomask and 0211 glass, the heating rates and temperatures in step 1 to 4 were changed to (1) 40 °C/min, 440 °C; (2) 2 °C/min, 473 °C; and (3) 2 °C, 590 °C respectively then (4) cooling at 4.0 °C/min to 473 °C before natural cooling to room temperature.

2.3.4 Chip Layout

The chip layout is shown in Figure 2.2a. The thick lines represent channels about 250 μm wide at the mouth, and the thin lines depict regions about 52 μm wide at the top and about 25 μm wide at the bottom. A double-T injector design was used,[8, 9] with an approximate length of 150 μm between the two arms of the T, and a volume of ~100 pL. The distance from the injector region to the separation channel waste reservoir (#4) was 7.5 cm. The typical injector to detector distance was 5 cm. A 250 μm wide line forms a rectangle around the whole device, but does not contact any of the fluid channels. This rectangle was used in the leak tests discussed in Chapter 3 "Evaluation of Room Temperature Bonded Glass Devices".

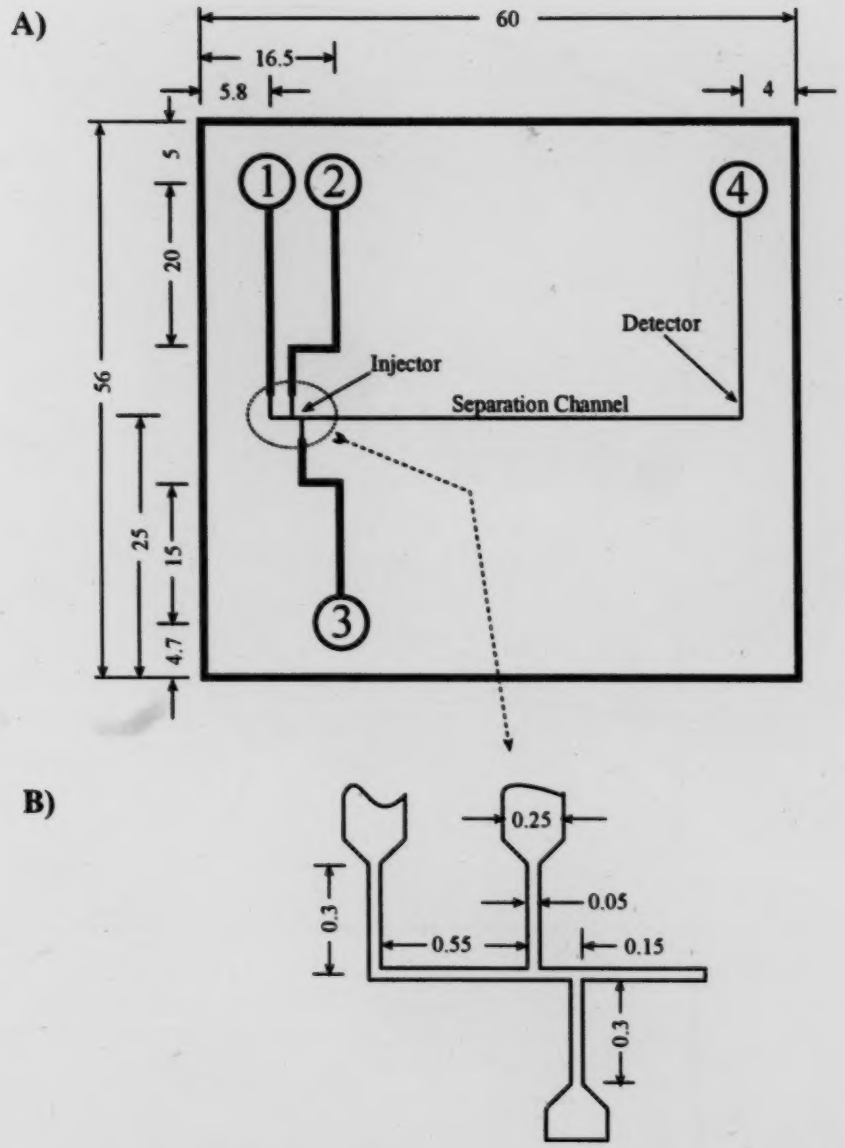

Figure 2.2: A simple chip-layout showing channels with dimensions. Solution reservoirs are numbered for reference in the text. Glass devices are typically 76 X 76 mm. Channel dimensions are in mm.

2.3.5 Instrumentation

Figure 2.3 shows a block diagram of the instrumental setup. The computer controlled the power supplies and switching of high voltage applied to the chip reservoirs through a system of relays, as described previously.[10, 11] Laser induced fluorescence (LIF) and collection optics were used to detect fluorescent species directly on-chip. A photomultiplier tube (PMT) (Hamamatsu) was used to transduce fluorescent signals to electrical signals, which were then filtered, digitized and stored on the computer. Figure 2.4 shows a schematic diagram of the optical setup. The optics were arranged on an optical breadboard (3 ft x 3 ft, Melles Griot) as shown in Figure 2.4a. A microchip device was secured at a fixed location on a chip holder, which was mounted on an x-y translation stage. A 488-nm air-cooled Ar ion laser (Cyonics/ Uniphase, Model 2011-20SL, Newport Research) operated at 4.6 mW served as the fluorescence excitation source. The beam from the laser was split into two with a beam splitter (BS) (Optikon, Ontario, Canada). Mirrors M1, M2, M3, M4 were used for beam deflection in the directions as indicated by arrow heads. The 90-degree-deflected low-intensity beam (30% of the laser output) was focused with a 15 cm focal-length lens at the double-T injector for visual observation. The undeviated beam (70% of the laser output or 3.2 mW) was focused with a 15 cm focal-length lens (lens 1) at the detection point on the separation channel, at an incident angle of 56°, measured from the plane of the chip (Figure 2.4b). Emission was collected with a 25x Leitz Fluotar (0.35 NA) objective, then directed onto the PMT after passing through an 800 μm pinhole (located at the image plane) and an optical bandpass filter (508-533 nm). The detector observes an 11 pL volume as defined by the field limited pinhole. The PMT was operated at 1.1 kV for all studies. PMT signal was filtered through a six-pole Butterworth filter (Krohn-Hite model 3342) with 15-50 Hz low-pass cut off frequency. The filtered signal was recorded simultaneously on a strip chart recorder and a computer. The A/D board sampling rate was 20 Hz, except in the case of rapid separation of amino acids where 100 Hz was used. Optimized signal detection was achieved by first moving the detection microscope to a selected detection location on the separation channel, focusing the laser beam to about a 50 μm spot (slightly smaller than the channel width observed visually) at this location, visually aligning the pinhole with the laser spot and fine tuning PMT positions in the vertical position for maximum signal from a flow of 0.5 nM fluorescein solution through the channel.

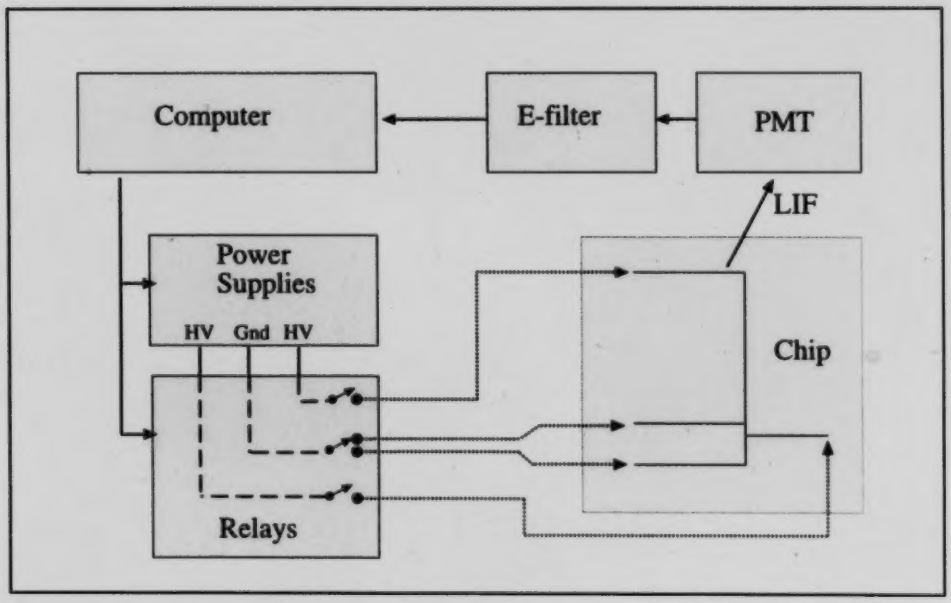

Figure 2.3: Schematic layout of the instrumental setup. The computer controlled the high voltage (HV) power supplies and HV relays which are activated with a 24 V power supply via a digital relay controller (not shown). Laser induced fluorescence (LIF) and microscope collection optics (see Figure 2.4) were used to detect fluorescent species directly on-chip.

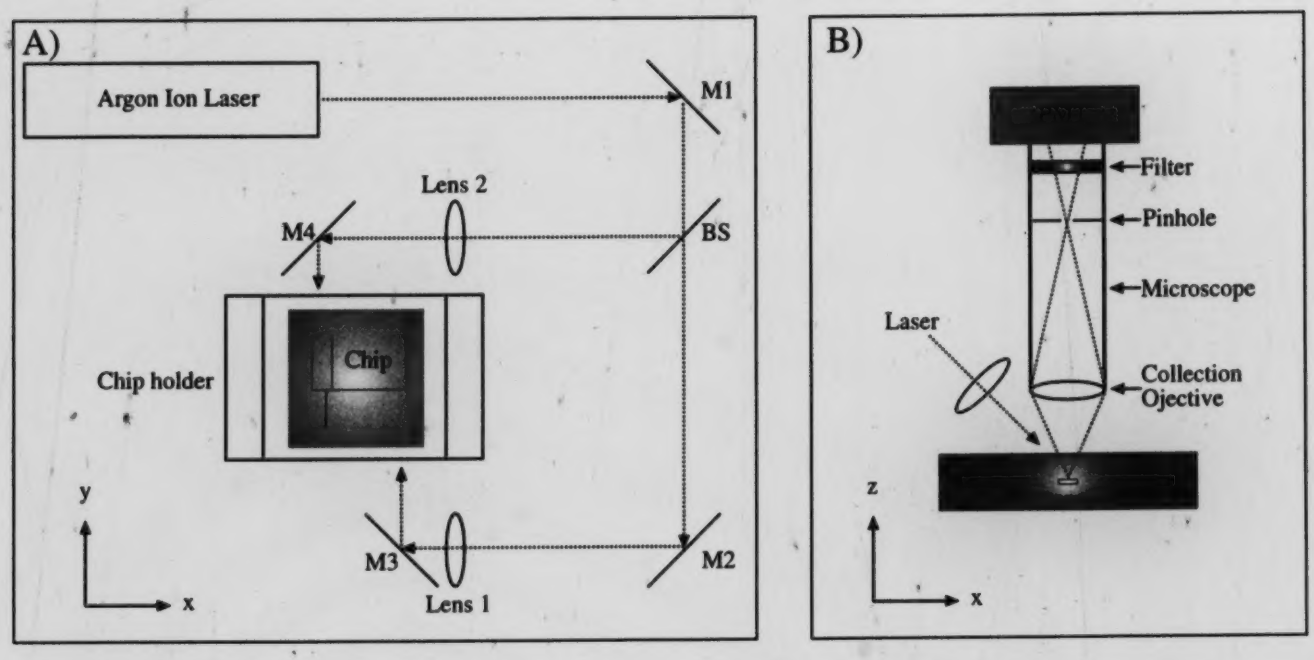

Figure 2.4: Schematic diagram of the laser excitation (A) and fluorescence detection (B) setup on an optical bread board (3 ft x 3 ft). Laser beam was splitted with a beam splitter (BS). Undeviated beam (70% of output intensity) was focused with lens 1 at the detector point on the separation channel. Deflected beam was focused with lens 2 at the injector for visual observation. Mirrors M1-M4 were used for beam deflection in directions indicated by arrows. Chip holder was mounted on an x-y translation stage. Microscope body was mounted on an x-z translation stage.

2.3.6 Chip Operation

2.3.6.1 Electrokinetic Injection

Plastic pipette tips were cut so that they fit into the holes of the top plate to form larger reservoirs for the solutions. Approximately 10 μL of sample was added to the sample reservoir (#2), with 10 μL of buffer in the other reservoirs. Fine Pt wires were insulated using Teflon sleeves and were inserted into the reservoirs on the device. Sample was injected using the double-T injector by applying -1 kV at the injection waste reservoir (#3) and ground at the sample reservoir (#2), as shown in Figure 2.5b. Separation was effected by switching to -6 kV applied at the waste reservoir (#4) and ground at the buffer reservoir (#1) Figure 2.5c.

2.3.6.2 Vacuum Injection

Fluorescein samples of 0.1, 0.5, 1.0, 10 nM were prepared by serial dilution with the 50 mM tricine buffer (pH 8) described above. Electrokinetic injection of fluorescein samples was described above. Pump driven injections were used to create sample plugs large enough that dispersion would not reduce the concentration for the majority of the plug length. A vacuum was applied to reservoir 3 to pull a 2 cm long plug of dye introduced via reservoir 4 towards the detector. Suction was then stopped while dye in reservoir 4 was removed and replaced with buffer, then the vacuum was turned on again to pull the plug of dye past the detector. Width at half maximum of the 2 cm long vacuum injected plugs were about 5.6 s and the vacuum-flow velocity is estimated to be about 0.36 cm/s. The software Igor (Wavemetrics, Lake Oswego, OR) was used for data smoothing (9 point box) and statistical analysis. Average and SD (noise) of base line signals were taken over 100 points of data. Peak values were 100 point averages when the peaks were broad enough. Analyte signal was obtained by subtracting baseline from peak average.

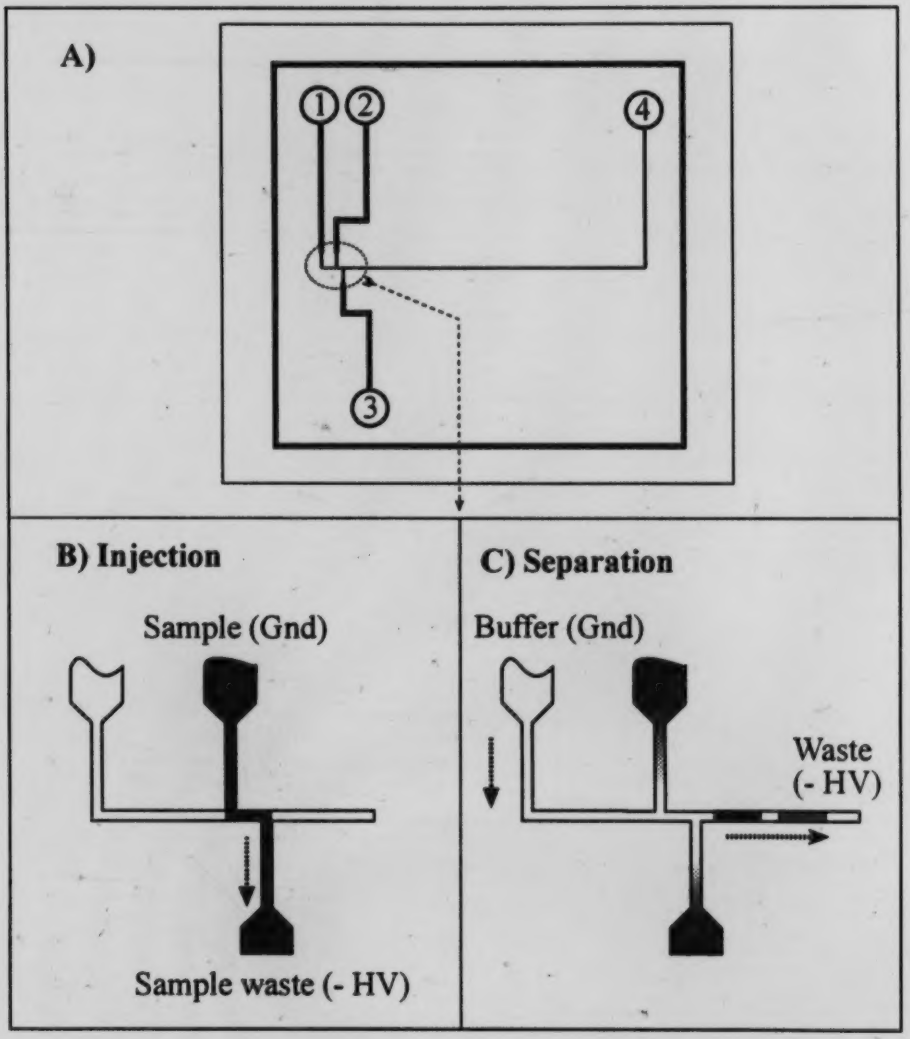

Figure 2.5: Schematic diagram of electrokinetic sample loading, injection and separation steps.

2.3.7 Coatings

25 % and 1% (v/v) of polydimethylsiloxane (PDMS) solutions were prepared by dilution with chloroform then filtered through a 0.45 μm pore PFTE-membrane syringe-filter. Chloroform is a good solvent for many polymers so polypropylene pipette tips, glass vials and glass syringes were used to handle chloroform solutions.

Before coating, glass vials were rinsed 3 times with doubly distilled water and dried in an oven at 110 °C overnight. To each vial, 200 μL of PDMS solution was added, covered, swirled and allowed to sit at room temperature for about 5 minutes then removed from the vial. A thin layer of PDMS solution remaining on the inner surface of the vials was air-dried in a fume hood. The vials were then placed in the programmable Ney oven and heated at 10 °C per minute up to 200 to 500 °C, held at this temperature for 0.5 hour, then the oven was turned off to allow natural cooling to room temperature.

Other coatings were also tested. A 200 μL solution of 5% w/v of Nafion in alcohol solution was added to the vials to be coated. The solution was allow to sit in the vial overnight at 4 °C then poured out. The film of Nafion remaining on the vial wall was allowed to dry in air, then baked in an oven at 130 °C under N_2 atmosphere for 1 hour. PVA solution was prepared by dissolving in hot water (~ 90 °C) to make 10% w/v. Other concentrations were prepared by dilution of the 10% solution with hot water. For vial coating, PVA solution was added, allowed to sit for 1 hr at room temperature before withdraw from the vial. The vial was put in an oven (model 5831, Nation Appliance Co., Portland, Or) at 140 °C under N_2 atmosphere for 1 hour. Coatings with protein were prepared by adding 200 μL of protein solution (protein concentration is given in Table 2.2) to the vials, allowing them to sit at room temperature for 3 hours, then rinsing.

To coat a glass chip, PDMS solution was added to one of the holes giving access to a large channel. Capillary forces caused the solution to flow into the channels without the need for an external pressure. After waiting a few minutes to allow the solution to fill all the channels, the remaining solution in the reservoir was removed with a syringe. The chip was put into a vacuum oven and the oven pressure was lowered to less than 80 kPa to allow chloroform in the channels to evaporate at room temperature (~ 21°C). The chip was then transferred to the programmable oven and heated to 400 °C as described above.

2.3.8 Vial IgG Adsorption Test

Prior to the adsorption test, 50 mM phosphate buffer (pH 7.5) was prepared by mixing 75 mL of 50 mM NaH_2PO_4 with 250 mL of 50 mM Na_2HPO_4 solutions. This phosphate buffer was used to prepare solutions of human IgG (H-IgG) (200 μg/mL), BSA (10 mg/mL), and fluorescein-labeled anti-human IgG $F(ab')_2$ fragment (20 μg/mL), and to rinse the vials in the procedure described below. Microtiter wells were also used instead of the glass vial. The adsorption test procedure was divided into four steps. First, to each vial or well 100 μL of the H-IgG solution was added, incubated for 1 to 3 hours at room temperature, discarded, and the vial was rinsed twice with buffer. Second, 200 μL of the BSA solution was added to block any remaining protein-binding sites on the glass surface, incubated for 1-3 hours, discarded and then rinsed twice. Third, 100 μL of the anti H-IgG* $F(ab')_2$ solution was added, incubated 1-3 hours, discarded then rinsed twice and finally, 200 μL of buffer was added. A 488 nm argon ion laser beam was used to illuminate the bottom of the vials and fluorescence was observed by eye through a 515 nm long-pass filter (OG515).

2.4 Results and Discussions

2.4.1 Conditions to Reduce Antibody Adsorption On-Chip

Antibodies such as immunoglobulin G (IgG) are required for immunoassays. These proteins tend to adsorb to silanol bearing surfaces such as those of fused-silica capillaries or glass channels through ionic, hydrophobic, and hydrogen-bonding interactions.[12, 13] Protein adsorption leads to complex flow profiles within the capillary,[14] significant zone broadening, non-reproducible migration times, low detection sensitivity and error in quantitation. Many strategies are used to reduce protein adsorption in conventional CE. These include the use of high and low pH buffers,[15] high salt concentration,[16, 17] zwitterions and other additives in the samples and running buffers,[18] as well as capillary coatings.[12, 17, 19-24] However, most of these strategies are mainly designed to optimize separation and are not necessarily useful for immunochemical reactions. Extreme pH can decrease protein adsorption but also reduces antibody/antigen binding. Buffer additives can denature proteins and also reduce antibody/antigen interaction. High salt concentration creates extra band broadening and decreases resolution if Joule heat is not sufficiently dissipated. Polymer coatings suffer from the fact that no synthetic polymer has been found to prevent all

proteins from adsorbing.[25] For example, polyacrylamide is an excellent coating to reduce adsorption of many proteins and gives excellent separation efficiency[26] but cannot prevent IgG from adsorbing.[27] Several authors have resolved this problem by cleaving the F_c fragment (the bottom portion of the Y shape IgG molecule) which seems to be responsible for most protein/wall interactions. However, fragmentation requires modification of the antibody molecules and is limited to assays where it is the antigen which is determined.

Immunoassay with glass microchip CE not only requires good separation, but should preferably be simple, reproducible and as low a cost as existing immunoassays methods. Efficient capillary coatings such of those of Schmalzing,[26] Town,[14] or Cobb[23] require derivatization of the fused silica surface and immobilization of a sufficiently thick layer of polymer (e.g. polyacrylamides, epoxydiol) to cover the surface silanol groups. Typically, an individual capillary is coated then evaluated by CE separation of proteins. This serial method of coating and testing is sophisticated but very time consuming, labour intensive and expensive when a coating procedure is not well established. Exploratory work with capillary coating following the published literature showed that the existing procedures are complex and time consuming, and not always successful with IgG. When applied to chips, coating is further complicated by the presence of a large number of intersecting channels.

This section discusses the efforts to find a method to reduce IgG adsorption. The objective was to find a simple, cost effective, reproducible and immunoreaction-compatible method suitable for on-chip immunoassays. A variety of coatings were tested. The large combination of coating and buffer conditions required a simple, rapid and inexpensive method of evaluation. Therefore the procedure to find a method suitable for on-chip immunoassays was divided into 2 stages. First inexpensive glass vials were used for coating and evaluation of IgG adsorption; then materials offering the least IgG adsorption were further optimized and evaluated on-chip. Surface modified by adsorption of polymers such as polydimethylsiloxane, PVA, Nafion, or with basic proteins, Tween 20 and other buffer additives were tested for IgG adsorption. Polydimethylsiloxane was tested since it was used for coating ampoules to store blood[28a] and the coating procedure was simple. Basic proteins adsorb to glass surfaces via electrostatic interactions with deprotonated surface silanols, and could potentially be used to prevent IgG adsorption. Tween 20 has been used for blocking of non-specific adsorption in immunoassays. Dynamics coatings with surfactant and tricine zwitterions were also tested. The results showed that PDMS coated surfaces heated to 400 °C,

used in combination with NaCl and Tween 20 added to the running buffer was effective. Alternately, uncoated chips used with tricine buffer containing NaCl and Tween 20 had reduced IgG adsorption, and gave relatively good separation efficiency.

2.4.1.1 IgG Adsorption Test on Glass Vials

Based on immunosorbent techniques, glass vials were used as a solid support to test for adsorption of IgG, which is then recognized by a fluorescein-labeled antibody. Visual observation of fluorescence provided a rapid means to screen for good coatings or methods which prevent IgG and protein adsorption. A lack of fluorescence from the vial surface indicates a potentially good coating, provided that the antigen-antibody binding is not degraded by the conditions used (denaturing conditions which degrade antibody/antigen binding also give negative fluorescence test results). To check for the latter case, uncoated vials and microtiter wells were also used for the test. The strong fluorescence observation from both uncoated glass and microtiter wells validates that IgG adsorption on glass vials is detectable by eye. The non-denaturing 50 mM phosphate pH 7.5 buffer did not interfere with antibody/antigen interaction, as expected.

Table 2.1 shows the results obtained from PDMS coated vials. The level of adsorption of IgG was qualitatively judged by comparing fluorescence from each vial with that from uncoated vials. Polymer chain length (indicated by the viscosity), curing temperature and the presence of surfactants affected the level of protein adsorption. All PDMS coated vials baked at 400 °C showed less IgG adsorption. PDMS with 100 cts viscosity gave better coating than other viscosities, for unknown reasons. The decrease in IgG adsorption with PDMS polymer films cured at high temperature (400 -500 °C) can be explained by a better film coverage of the glass surface.[28b] The adhesion of PDMS films is increased and the coated surface is more hydrophobic with high temperature treatment, with maximum hydrophobicity at about 400 °C. Noll[28c] suggests that better adhesion of the film is due to occasional cleavage of the Si-CH_3 bonds of PDMS followed by covalent bond formation through condensation with Si-OH group. He also suggests that a rise in temperature forces the polydimethylsiloxane chains preferentially into an orientation such that the interface of PDMS with air is covered by methyl groups in close packing, which gives a higher density of methyl groups and better coverage of the surface.

Low adsorption of IgG is indicated by weak fluorescence. It may result from hydrophobic interaction of IgG with the PDMS film, or with residual silanol groups on

PDMS viscosity (cts)	PDMS concentration (W/V)	Heated Temperature (°C)	Additive in IgG solution	Additive concentration (mg/mL)	Fluo-rescent results
0.65	100%	400	none	-	medium
1.0	100%	400	none	-	medium
5	100%	400	none	-	medium
10	100%	400	none	-	medium
20	100%	400	none	-	medium
50	100%	400	none	-	medium
100	100%	400	none	-	weak
1000	100%	400	none	-	medium
1000	25%	400	none	-	medium
100	25%	400	none	-	weak
100	1%	400	none	-	weak
100	1%	21	none	-	strong
100	1%	200	none	-	strong
100	1%	500	none	-	weak
100	1%	400	Tween 20	2.5 mg/mL	no
100	1%	400	Brij 35	2.5 mg/mL	no

Table 2.1 PDMS coating conditions and fluorescence results from vial adsorption tests (see text in section 2.3.8 "Vial IgG adsorption Test" for testing procedure). Chloroform was used to dilute some PDMS where applicable. Laser (488 nm) beam was used as excitation source and fluorescence was visually observed through a 515 nm long-pass filter. In the results, "Strong" indicates that the level of fluorescence was high and about equal to that of uncoated vials, while "no" indicates that fluorescence was not observable by eye. "Weak" and "medium" are relative levels in between none and strong fluorescence.

the surface not completely shielded by the film. Addition of a neutral surfactant such as Tween 20 or Brij 35 further reduced protein adsorption, to a level not observable by eye. These results show that a 100 cts PDMS coating cured at 400 °C, combined with using a buffer containing a neutral surfactant (Brij 35 or Tween 20) can significantly reduce adsorption of IgG.

Tables 2.2 shows the results from other types of tested coatings. PVA was cured at 140 °C according to Schromburg.[29] The results show that this coating reduces adsorption of IgG, and the level of adsorption varied with the coating thickness. Vials coated with 10% solution did not show any observable adsorption. However, PVA solution at this concentration was very viscous, so was difficult to introduce into small channel of the glass devices (high pressure fittings coupled to the chip reservoir were not available at that time). PVA coating was also reported to suppress electroosmotic flow and work best at low pH (pH 3); therefore, it was not selected for further investigation.

Nafion coating cured at 130 °C was not effective to prevent IgG adsorption as shown by the strong fluorescence result in Table 2.2. The Nafion film did not adhere and was removed from the glass surface when the IgG solution was added to the vial.

Basic proteins such as cytochrome c and lysozyme (pI = 10.2 and 11.0, respectively) have net positive charge in pH 7.5 buffer. These proteins were previously shown to adsorb to an uncoated glass surface.[19] They were selected as reagents to block binding sites on the glass surface. The medium fluorescence results shown in Table 2.2 indicate the blocking method was not efficient at reducing IgG adsorption. These results suggest the proteins were probably not irreversibly adsorbed to glass surfaces and exchanged with IgG during the IgG incubation step in the test procedure. BSA and Tween 20 have been used as reagents to block non-specific binding sites in conventional immunoassays with microtiter wells. These were also used for the adsorption test and the results were similar to those of the basic proteins.

The adsorption test procedure was also used for uncoated vials with a 100 mM tricine, 5 mg/mL Tween 20 buffer. Tricine buffer was selected from Good's listing[30] of biological buffers, as it has a pK_a around 8, which is close to that used in the Abbott TDx theophylline kit discussed in later chapters. The neutral surfactant, Tween 20, was selected to reduce protein adsorption, since it is commonly present in immunological reagent preparations and does not negatively affect the reagents or the immunoreaction.[31] This buffer was also found to be effective in reducing IgG adsorption to glass vials to an undetectable level.

Coating	Coating solution concentration	Heated Temperature (°C)	Additive in IgG solution	Additive concentra-tion (mg/mL)	Fluo-rescent results
PVA	5 mg/mL in water	140 in N_2 for 1 hour	none	-	medium
	10				medium
	25				weak
	50				weak
	100				no
Nafion	5% weight in alcohols incubation overnight	130 under N_2 1 hr	none		strong
Cyto-chrome c	1 mg/mL in buffer	21	Cyto-chrome c	0.1 mg/mL	medium
Lysozyme	2 mg/mL in buffer	21	Lyso-zyme	0.1 mg/mL	medium
BSA	12 mg/mL in buffer	21	BSA	1.2 mg/mL	medium
Tween 20	50 mg/mL in buffer	21	Tween 20	5 mg/mL	medium
Uncoated	-	21	a) tricine b)Tween 20	a) 100 mM b) 0.5% w/v	no

Table 2.2 Other coating conditions and fluorescence results from vial adsorption tests (see text in section 2.3.8 "Vial IgG adsorption Test" for testing procedure). With proteins and Tween 20 coatings, the BSA blocking step in the Adsorption Test was omitted. The explanation for fluorescence results was given in Table 2.1.

2.4.1.2 Adsorption Testing On-Chip

Adsorption of proteins leads to poor separations in capillary electrophoresis. The best PDMS coating conditions and the tricine buffer were further optimized for protein separation efficiencies on-chip. Figure 2.6 shows the results obtained from 70 μg/mL of fluorescein-labeled anti-human IgG (whole molecule, not the $F(ab')_2$ fragment) with a PDMS-coated glass chip. A Tris, boric acid buffer at pH 9 was used for separation of amino acids and gave excellent separation efficiency (described in Section 2.4.2.2 "Separation Efficiency" below). Towns and Regnier[19] reported the use of nonionic surfactants (0.001% to 0.1% of Tween 20 or Brij 35) with hydrophobic coatings (octadecylsilane) improves separation efficiency of proteins. Consequently, we added these surfactants to the above buffer to improve the performance. Using this buffer in PDMS coated chips gave good IgG separation efficiency, with 15,300 theoretical plate (N) for the antibody in Figure 2.6.

The use of tricine buffers with salt and Tween 20 also reduced IgG adsorption in uncoated chips. The ionic strength was adjusted with NaCl, since the presence of 40-100 mM salt has been reported to accelerate complex formation.[32] A value of 26 mM NaCl was chosen in order to minimize Joule heating effects. Figure 2.7 illustrates the separation of fluorescently labeled, polyclonal, human IgG and BSA. The IgG peak gave a clean, symmetrical peak with 750-1000 theoretical plates with 6 kV applied (750 V/cm), indicating the buffer/surfactant system selected is reasonably effective in uncoated chips. The BSA peak is well separated from IgG. The large breadth of the BSA main peak and the presence of several other nearby peaks is due to the very heterogeneous character of the commercially labeled BSA (MALDI mass spectrometry showed the fluorescein-labeled BSA had a full width at half maximum of 6,000 Daltons, compared to the 1,000 Daltons width of native BSA from the same commercial source).

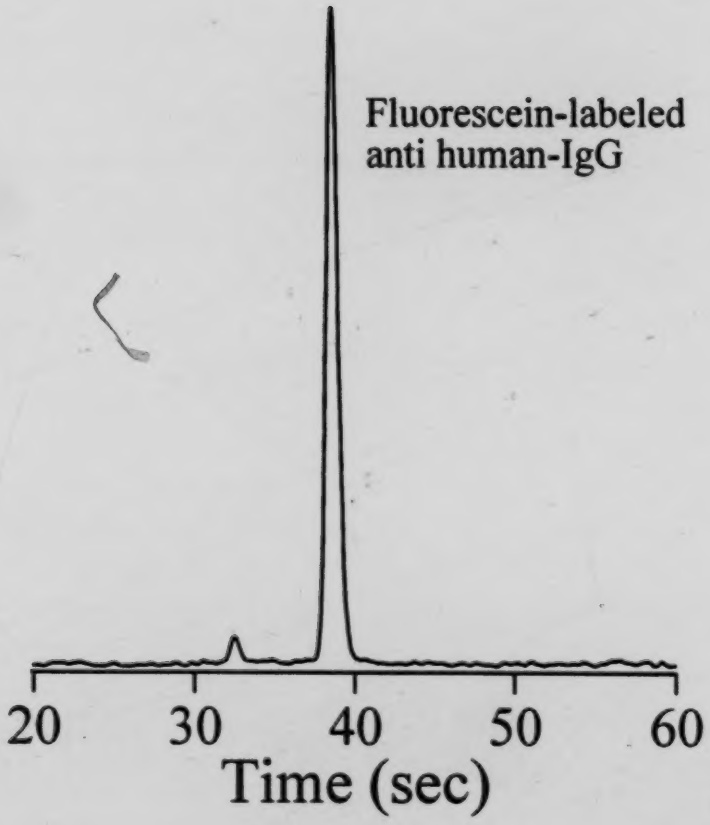

Figure 2.6: Electropherogram of fluorescein-labeled anti human-IgG (70 μg/mL) obtained with a PDMS coated chip. Separation buffer was 100 mM tris, 20 mM boric acid, pH 9, with 20 mM NaCl and 0.01% Tween 20. Separation distance was 4.9 cm. Injection voltage was -1 kV applied at the sample waste. Separation was -6 kV applied at buffer waste. Laser excitation was at 488 nm and fluorescent detection was between 508-533 nm.

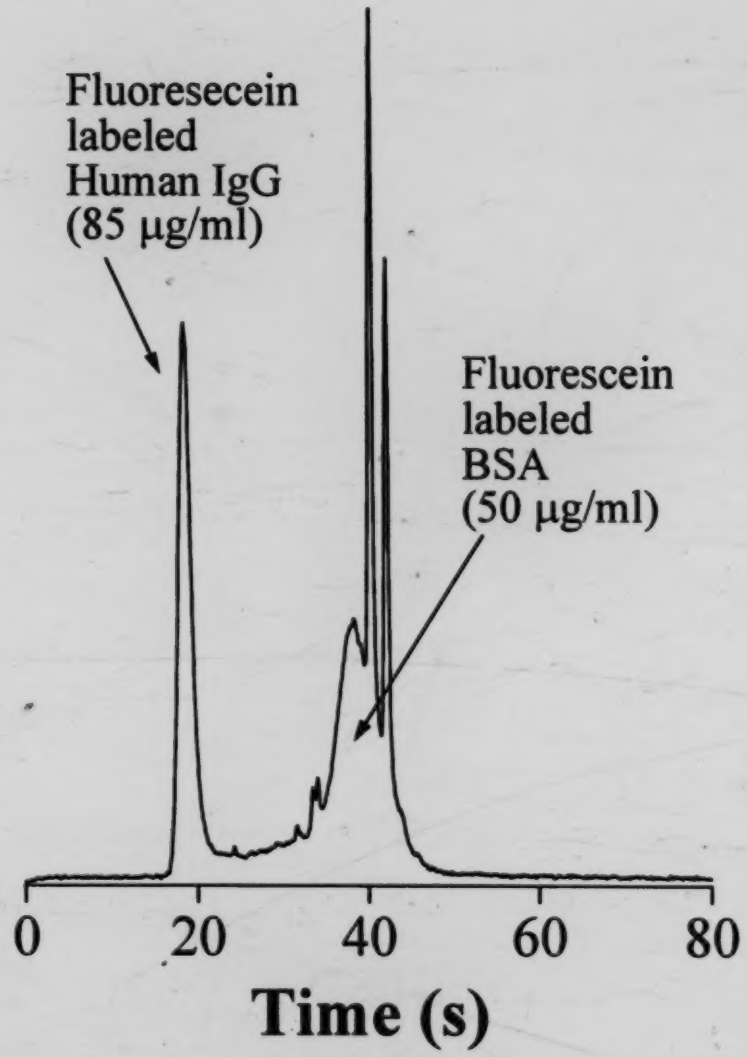

Figure 2.7: Electropherogram of fluorescein-labeled human-IgG and fluorescein-labeled BSA obtained with an uncoated chip. The separation buffer was 50 mM, pH 8, tricine buffer with 26 mM NaCl and 0.01% Tween 20. Separation distance was 6.39 cm. Injection voltage, separation voltages, excitation and detection wavelengths were same as in Figure 2.6.

2.4.2 Evaluation of Chip Design and Optimization of Separation Efficiency

Controlling electroosmotic flow is of interest in chip-based CE, since electroosmotic flow provides a useful mechanism for sample pumping used in preparation and delivery. Electroosmotic flow has proven to be quite convenient in many forms of CE for 3 reasons. First, without this flow, cations and anions would move in opposite directions, so that both species could not be analyzed in a single run with a single detector. Second, without electroosmotic flow, control of sample pumping in a desired fashion from different channels would be more difficult, since advanced knowledge of the charge of the species of interest are required to determine their flow direction. Third, without the flow, very large and/or weakly charged ions may require great lengths of time to travel the length of the separation channel. Conversely with electroosmotic flow, ions of a variety of size and charge may be analyzed in a shorter period.

Rapid separation is one of the major benefits of using chip-based CE . The chip uses a glass surface, non-cylindrical channels, and usually much shorter separation lengths than in conventional CE. However, shorter channel distance generally means lower applied voltages as arcing becomes more problematic. The short separation lengths also mean the volume contribution of injection and detection can become more significant. It is useful to explore the effects of d, μ and E on on-chip separation efficiency, since the situation is slightly different than in conventional CE. Several researchers[33, 34] have conducted detailed studies of these effects in conventional CE, thereby providing a basis for comparison. Effenhauser has also examined the role of separation length on on-chip resolution and separation speed,[8] providing further comparisons.

In this section, the effects of E and ionic strength on mobility, separation efficiency, speed and resolution for chip-based CE will be presented.

2.4.2.1 Flow Evaluation

In order to evaluate the chip design and separation conditions, electrokinetic and separation parameters such as velocity, mobility, plate number and plate height were determined from a series of injections with different separation voltages. The

fluorescent species used was fluorescein-labeled phenylalanine. The electric field was varied from 625 to 1,375 V/cm (5 to 11 kV applied voltage) and the distance between the points of injection and detection, d, was 4.9 cm. Figure 2.8 shows a plot of v vs. E for fluorescein-labeled phenylalanine. The plot is linear with a zero intercept ($r^2 = 1.000$ and intercept = - 0.002 ± 0.002 cm/s) as predicted by equation 1. The electrokinetic mobility, μ, obtained from the slope of the linear regression line is 3.52 ± 0.01 x 10^{-4} cm^2/Vs. The small standard deviation in μ indicates a stable electrokinetic mobility and shows that velocity is linearly proportional to electric field up to at least 1,375 V/cm. The linear relationship of v vs. E confirms that Joule heat in the separation channel is sufficiently dissipated in this device. This is consistent with a previously reported result that the Joule heating effect only becomes apparent within glass chips at an electric field of 2,500 V/cm or higher.[11]

2.4.2.2 Separation Efficiency

To evaluate separation efficiency, the number of theoretical plates, N, was determined from peak profiles by using the formula[35]

$$N = 5.54 (t_m/w_{1/2})^2$$

where t_m is the migration time and $w_{1/2}$ is the full peak width at half-maximum expressed in terms of time. Figure 2.9 shows a plot of N vs. the electric field E. The plot is linear (slope = 65.6 ± 2.6 cm/V, intercept = 4.9 ± 0.3 x 10^4 and $r^2 = 0.991$). At a V_{td} of 6,738 V (E = 1,375 V/cm) N is 138,500, which indicates relatively high efficiencies can be achieved within this small device. This is in agreement with results previously demonstrated by Effenhauser et al, who used a very similar device layout.[8] The non-zero intercept indicates that there are other factors (as described in Section 2.2.3) contributing to the zone broadening besides longitudinal diffusion alone, following Equation 17.

In Figure 2.10, a plot of H vs. migration time is shown for fluorescein-labeled phenylalanine. The plate height increases linearly with migration time ($r^2 = 0.991$ and slope = 1.62 ± 0.06 x 10^{-2} μm/s). The diffusion coefficient of fluorescein-labeled phenylalanine determined from the slope according to equation 17 was 3.9 ± 0.2 x 10^{-6} cm^2/s which is comparable to 3.4 ± 0.3 x 10^{-6} cm^2/s previously reported by Effenhauser. The intercept, 0.19 ± 0.01 μm, represents an invariant plate height which is a significant contribution to the total plate height.

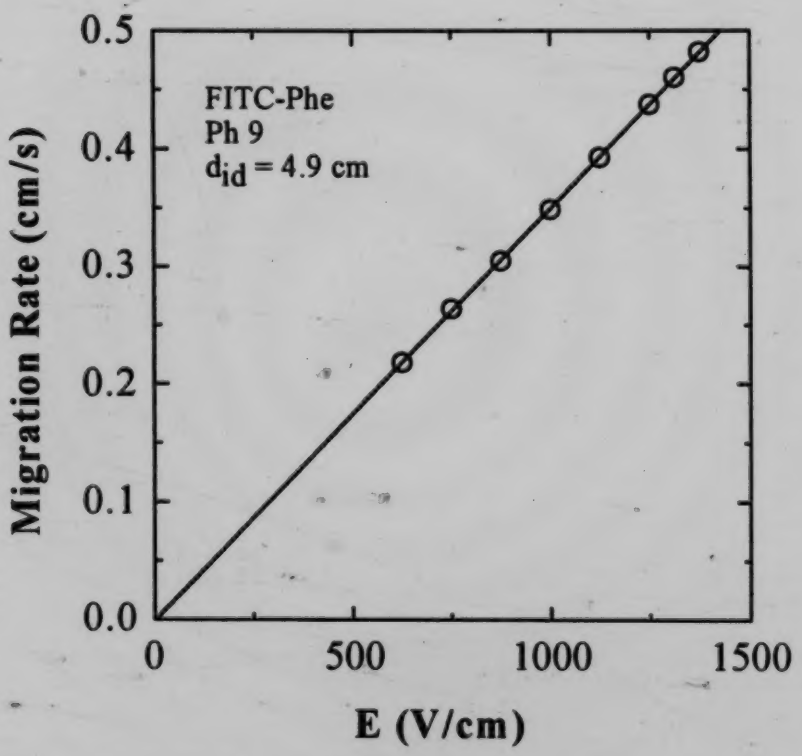

Figure 2.8: Plot of migration rate versus electric field for 10 μM fluorescein-labeled phenylalanine in 100 mM, pH 9, Tris buffer. Injection-separation distance, d_{id}, was 4.9 cm.

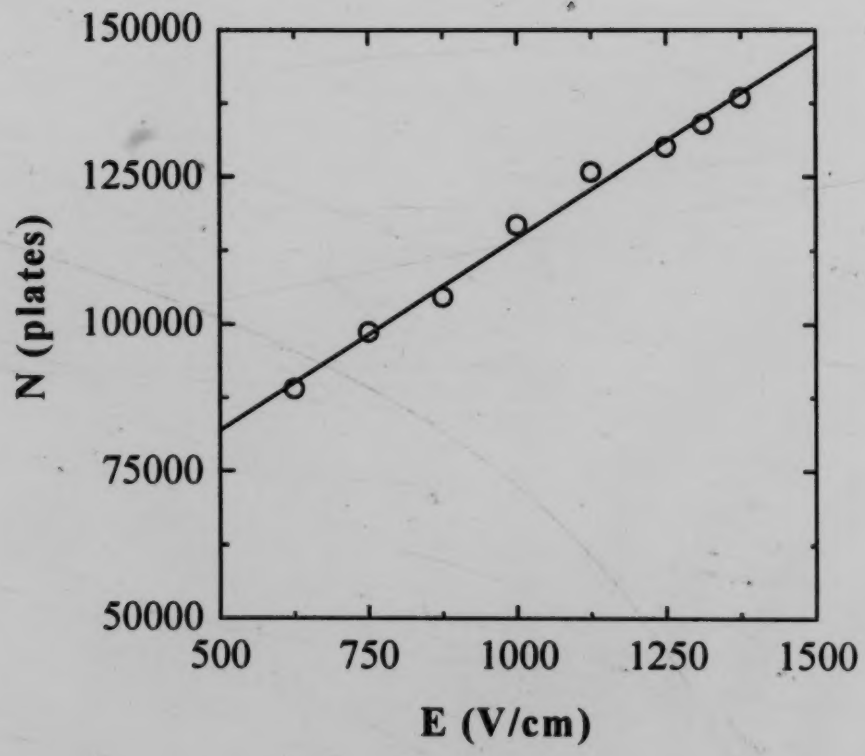

Figure 2.9: Plot of theoretical plate number versus electric field for 10 μM fluorescein-labeled phenylalanine in 100 mM, pH 9, Tris buffer. Injection-separation distance, d_{id}, was 4.9 cm.

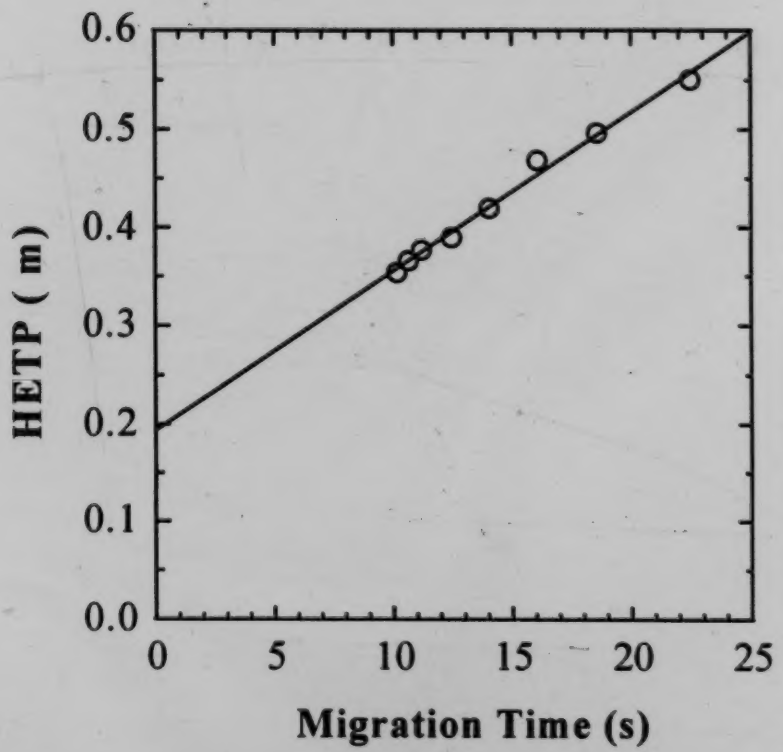

Figure 2.10: Plot of height equivalent to theoretical plate (HETP) versus migration time for 10 μM fluorescein-labeled phenylalanine in 100 mM, pH 9, Tris buffer. The injection separation distance, d_{id}, was 4.9 cm and the electric field ranged from 625 to 1375 V/cm.

The intercept in Figure 2.10 is the sum of all the migration time-independent terms which can be estimated from the appropriate terms in equation 17. The injection contribution to the time-independent plate height is due to the injection time and volume. An injection time, t_{inj}, of 1.4 s corresponds to 0.023 μm plate height or 12.1% of the total time-independent plate height. The length of the injector region used in this study was 152 μm. However, diffusion and the field lines at the corners distort the injection plug, which adds approximately 65 μm of extra length (sample was visually observed to expand at both ends of the injector), giving a total injection plug length of approximately 217 μm. This value gives 0.080 μm plate height and together with the injection time plate height, gives an injection contribution of 0.103 μm or 54 % of the total time-independent plate height.

The detection contribution to the time independent plate height is due to detection volume and detection electronics. The detection volume (l_{det} = 100 μm) corresponds to 0.017 μm plate height. The detection electronics contribution can be estimated by $(\mu E\tau)^2/d$ where E is 1,375 V/cm, d is 4.9 cm and μ for the fastest migrating component is 3.52 x 10^{-4} cm^2/Vs. With the low-pass filter set at f = 50 Hz, the time constant of the detector can be determined to be $\tau = 1/2\pi f$ = 3.2 ms. This corresponds to an electronic contribution of 0.0048 μm plate height. The net detection contribution is then 0.022 μm or 11.5 % of the time-independent plate height.

In total, the sum of the injector and detector contributions to the total time-independent plate height is only 0.125 μm or 66.5% of time independent plate height. The remaining contributions could, in part, be due to underestimating the 100 μm detection window (the detection set-up for these analyses was not optimized and the field limited pinhole might not be exactly at the focal plane of the collection objective). Distortions in the shape or size of the injection plug could also be a factor. Other possible contributions are represented by the term σ_o^2/d in equation 17, as discussed in the theory section.

While the time-independent contributions to plate height are significant for small molecules, it is useful to know how relevant they are to the separation of proteins, where adsorption, multiple labeling and protein heterogeneity can play a major role. The proteins anti H-IgG and BSA are large molecules with an average molecular weight before labeling of 155,000 and 66,500 Daltons, respectively. These molecules were multiply-labeled with fluorescein. The average number of fluorescein molecules per protein was 7.6 and 11.2 (provided by suppliers) for anti H-IgG* and BSA*,

respectively, and the distribution of products can be quite large. MALDI mass spectrometry showed fluorescein-labeled BSA had a full width at half-maximum of 6,000 Daltons, compared to the 1,000-Daltons width of native BSA from the same commercial source.

Figure 2.11 shows an electropherogram obtained from the separation of these two labeled proteins in the 50 mM tricine separation buffer. The separation distance and the electric field were 6.39 cm and 678 V/cm, respectively. The plate heights for the anti H-IgG* and BSA* were 188 and 128 μm, respectively. The calculated contribution to zone broadening from diffusion ($D = 4.0 \times 10^{-7}$ cm^2/s for IgG), injection and detection only accounts for about 0.13 μm or less than 0.1 % of these values. Therefore, in protein separation the major factors affecting separation efficiency in glass chips are sample microheterogeneity and adsorption to the capillary walls, as is found in conventional CE.

2.4.2.3 Resolution of Amino Acids

Equation 19 shows that resolution will be proportional to the square root of dE/μ. The effect of E was described above, here we discuss the effect of varying ionic strength on mobility and on and resolution in chip based CE.

fluorescein-labeled arginine (Arg), histidine (His), tryptophan (Trp), phenylalanine (Phe), glycine (Gly), glutamic acid (Glu), and aspartic acid (Asp) were used for this study. The results of the separation of a mixture of the seven amino acids (AA) using the injection scheme outlined in the Experimental Section are shown in Figures 2.12 and 2.13. Both electropherograms were recorded at an electric field strength of 678 V/cm and an injector-detector distance of 6.39 cm. The assignment of the various peaks was based on single runs of each of the amino acids. The fluorescein-labeled AA had a net negative charge[5,8] but migrated toward the cathode due to high electroosmotic flows in the separation channel.

Data in Figure 2.12 were obtained using the 10 mM tricine, low ionic strength separation buffer with an observed current of 1.6 μA. The concentration of each labeled AA was 2 nM assuming 100% conversion of FITC to labeled acids. Elution of all labeled AA was achieved within 26 s. However, tryptophan and phenylalanine were

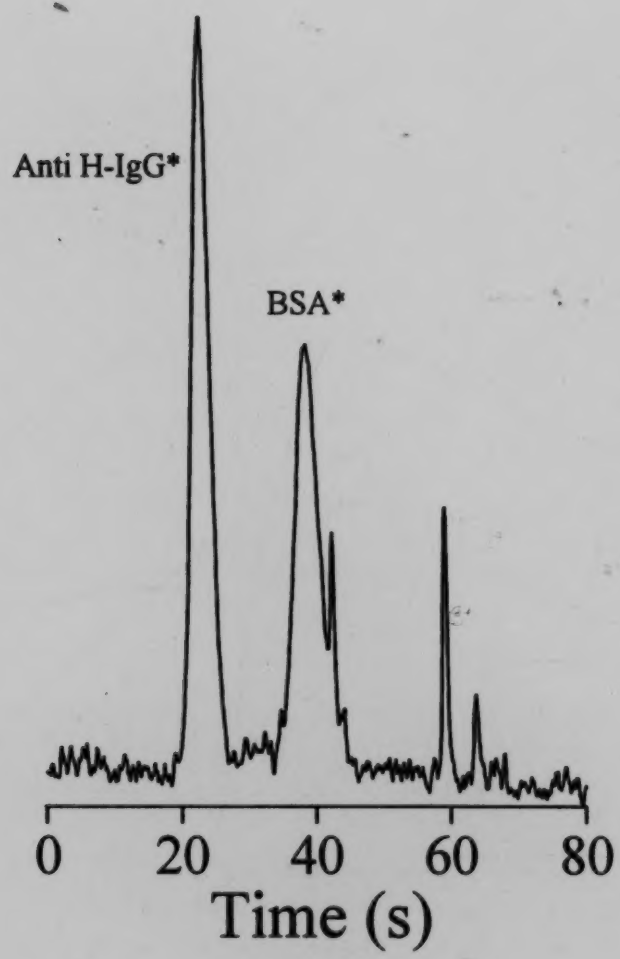

Figure 2.11: Electropherogram of a mixture of 3.2 nM fluorescein-labeled goat anti H-IgG and 15 nM fluorescein-labeled BSA obtained with an uncoated, Borosilicate glass device. Separation buffer was 50 mM pH 8 tricine buffer. Injection separation distance was 6.39 cm and electric field was 678 V/cm. Optical detection parameters are as listed in Figure 2.15.

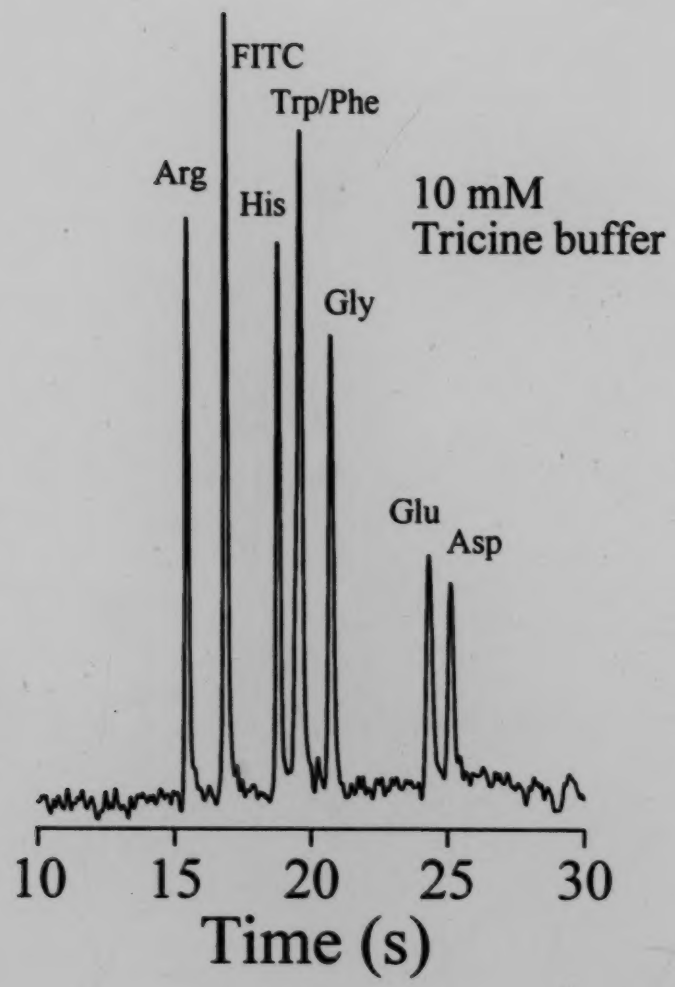

Figure 2.12: Electropherogram of a mixture of seven fluorescein-labeled amino acids with 10 mM, pH 8, low ionic strength tricine buffer. Concentration of each labeled amino acid was approximately 2 nM. Injection-separation distance, d_{id}, was 6.39 cm and electric field was 678 V/cm.

not resolved. The observed electrokinetic mobilities listed in Table 2.3 vary from 3.70 x 10^{-4} to 6.02 x 10^{-4} cm^2/Vs for FITC-Asp to FITC-Arg, respectively.

Figure 2.13 was obtained from the 50 mM tricine, high ionic strength separation buffer, with an observed current of 22 μA. The concentration of each labeled AA was 5 nM. The higher ionic strength reduces the size of the charged double-layer at the channel wall, decreased the zeta potential, ζ and so, according to equation 6, decreases the electroosmotic flow. Consequently, migration of all components required about 120 s. However, the resolution is much better, giving near baseline resolution of trytophan and phenylalanine. The migration rate and the electrokinetic mobilities also decreased, and are included in Table 2.3.

The ionic strength also affects the plate numbers. A high electroosmotic flow obtained from a low ionic strength buffer will reduce the time for longitudinal broadening. Figure 2.14 shows a plot of N versus μ for the species analyzed in both 10 and 50 mM tricine buffers. The theoretical plate number varies from 77,800 to 129,500 for 10 mM Tricine buffer and from 27,000 to 76,200 for 50 mM tricine buffer. Despite the scatter, the data from both buffers lies on the same linear regression line (r^2 = 0.938) indicating that the differences in N for the labeled AA are mainly due to longitudinal diffusion effects. Any extra Joule heat created from the higher current in the 50 mM tricine buffer must be effectively dissipated, as it did not seem to degrade separation efficiency.

μ (x 10^{-4} cm^2/Vs)	Arg	His	Trp	Phe	Gly	Glu	Asp
in 10 mM tricine	6.02	4.94	4.77	4.77	4.48	3.82	3.70
in 50 mM tricine	2.62	1.67	1.58	1.53	1.30	8.72	7.99

Table 2.3 Comparison of electrokinetic mobilities of seven fluorescein-labeled amino acids in the 10 mM tricine low ionic strength and the 50 mM high ionic strength buffer. The separation distance was 6.39 cm and field was 678 V/cm.

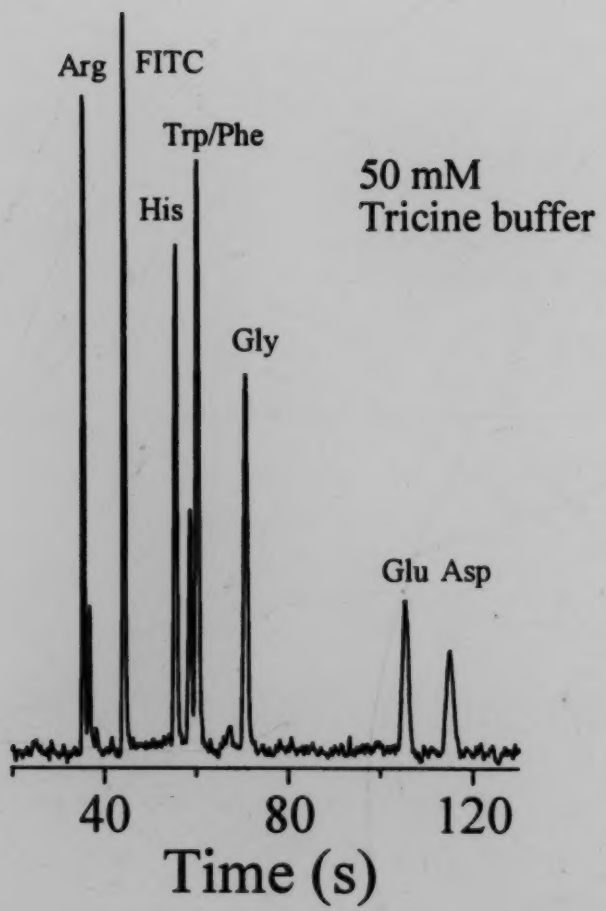

Figure 2.13: Electropherogram of a mixture of seven fluorescein-labeled amino acids with 50 mM, pH 8, high ionic strength tricine buffer. Concentration of each labeled amino acid was approximately 5 nM. Separation distance and electric field were the same as in Figure 2.12.

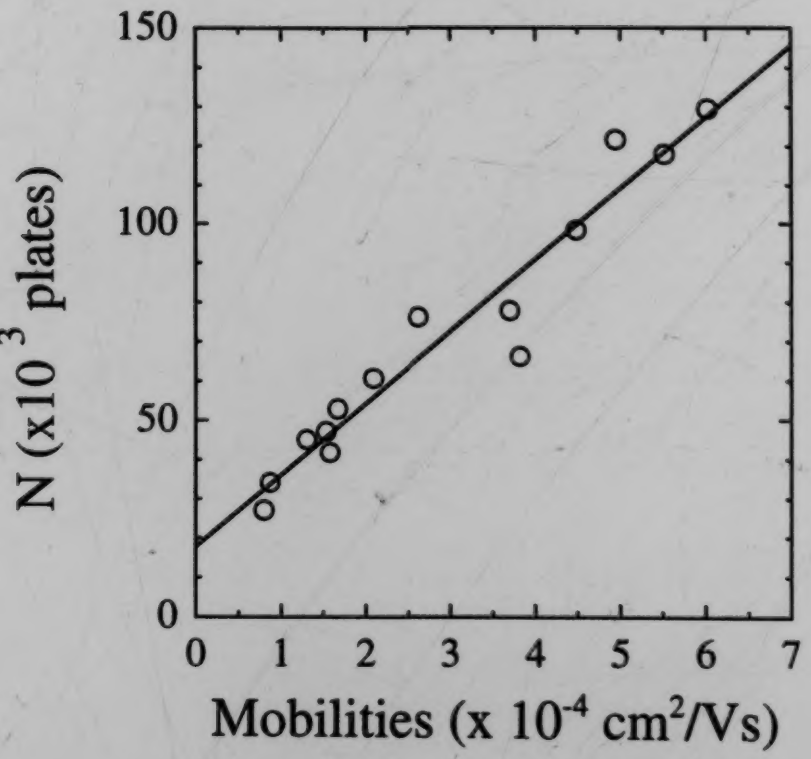

Figure 2.14: Plot of theoretical plate number versus electrokinetic mobilities for fluorescein-Labeled amino acids in 10 and 50 mM, pH 8 tricine buffers. The injection-separation distance was 6.39 cm and the electric field was 678 V/cm.

2.4.3 Optimization of Detection Limit

Fluorescence detection provides a high degree of sensitivity, which is useful in chip-based CE where the sample volume is usually very small. Good detection limits (DL) in the range of high nanomolar (200 nM)[8] to low nanomolar (3 nM)[36] were demonstrated for labeled amino acids and fluorescein. Nevertheless, in order to perform immunoassays on-chip where concentration of reagents and products may be in the picomolar range, it was necessary to substantially improve upon detection limits cited in these earlier reports.

The detection limit is defined as the smallest concentration that can be reported as being present in a sample with a specified level of confidence. It is often operationally defined as the analyte concentration yielding an analytical signal equal to some confidence factor k times the standard deviation of the blank measurement (s_{blk}).[37] This can be directly calculated from

$$DL = 3\, s_{blk} / m$$

where 3 was taken for k (99.9% level of confidence), s_{blk} is the standard deviation or noise of the blank and m is the calibration sensitivity (slope of an analyte signal versus concentration plot). According to this expression, low DL is achieved by minimizing the noise from the blank and maximizing the detection sensitivity.

2.4.3.1 Sensitivity Optimization

Sensitivity is a parameter which needed to be optimized in order to achieve the lowest detection limit. For the detection system used, careful alignment of the field limiting pinhole with the focus laser spot on the separation channel was critical for good detection sensitivity. The procedure described in the experimental section was used to get optimum detection. Significant change of detection signal was observed with a detector displacement (either in the vertical or in the horizontal direction) of about 15 μm (estimated by a micrometer mounted with the translation stages supporting the microscope tube or the chip holder) from the optimum condition.

Peak signals were measured across a range of 10 to 1000 pM fluorescein concentrations. Fluorescein sample plugs were large enough that longitudinal diffusion did not decrease the concentration at the center of the plug over the time taken to reach the detector. Figure 2.15 shows the results obtained from the fluorescein samples with

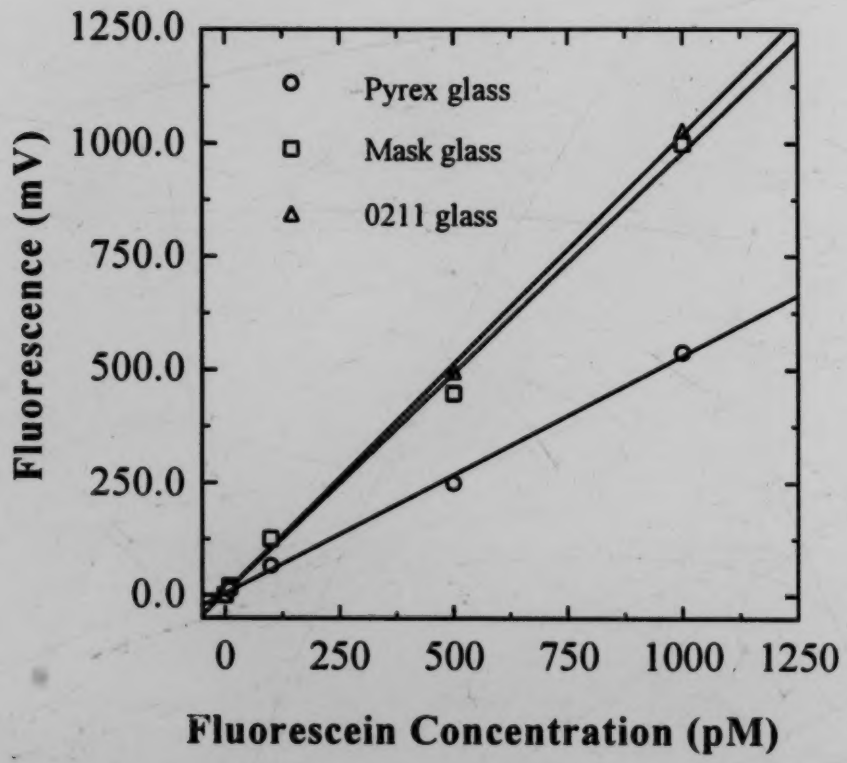

Figure 2.15: Fluorescein signal versus concentration detected from 2 cm plug sample in devices made from three different types of glass. The 50 mM pH 8 tricine buffer was used for sample dilution. Excitation with 488 nm laser operated at 3.2 mW. Fluorescent signal collected by a 25x (0.35 NA), filtered through a 508-533 nm interference filter and detected with PMT operated at 1.1 kV.

large injection plugs in three different glass devices. The PMT was operated at 1.1 kV for all devices. The peak signals were plotted versus the concentration of fluorescein. The plots are linear and the calibration sensitivity obtained from the slope of each plot for 0211, mask and Pyrex devices are 1.01 ± 0.02; 0.97 ± 0.04, 0.53 ± 0.01 mV/pM, respectively. For 0211 and photomask devices, the detection was set at optimum and good sensitivities were achieved whereas for the Pyrex device, a poorer sensitivity was observed due to a slight misalignment of the pinhole and the laser spot. The misalignment was noticed after the measurements by removing the PMT from the microscope and by observing the laser spot through the pinhole.

2.4.3.2 Limiting Noise and its Origin

Noise is a parameter which needed to be reduced in order to achieve the lowest detection limit. The glass wafer bonding process was optimized to reduce formation of light scattering centers on the surface of the glass devices. Careful alignment of the laser beam, to eliminate scattering from the curved walls of the channels was also beneficial. Optimal alignment involved directing the beam along the axis of the channel instead of across it, with adjustment of the angle of the incident beam to minimize background.

Background signals were determined by taking the difference of the signal levels with PMT settings at 0 and 1.1 kV while the laser was on and the channel was filled with buffer (blank). This signal includes background from fluorescence and scattering of glass, buffer scattering, detection electronics and stray light. However, all experiments were performed in a dark room and when the laser beam was blocked, the background signal was decreased to 5%, which indicates that electronic and stray light backgrounds were minor. Replacing buffer with water did not change the background significantly, indicating a glass matrix or solvent origin for background fluorescence. The fluorescence and Raman scattering from glass were high enough to be observed by eye through a 515 nm long pass filter when the laser was focused at a location in the glass.

The background noise is the sum of background fluorescent noise and detector noise. Fluorescent noise originating from glass is an irreducible parameter; therefore, background signal and noise from several different types of glass typically used for fabrication of planar CE devices were investigated. Figures 2.16 and 2.17 show the background fluorescent signal and background noise determined from blanks in

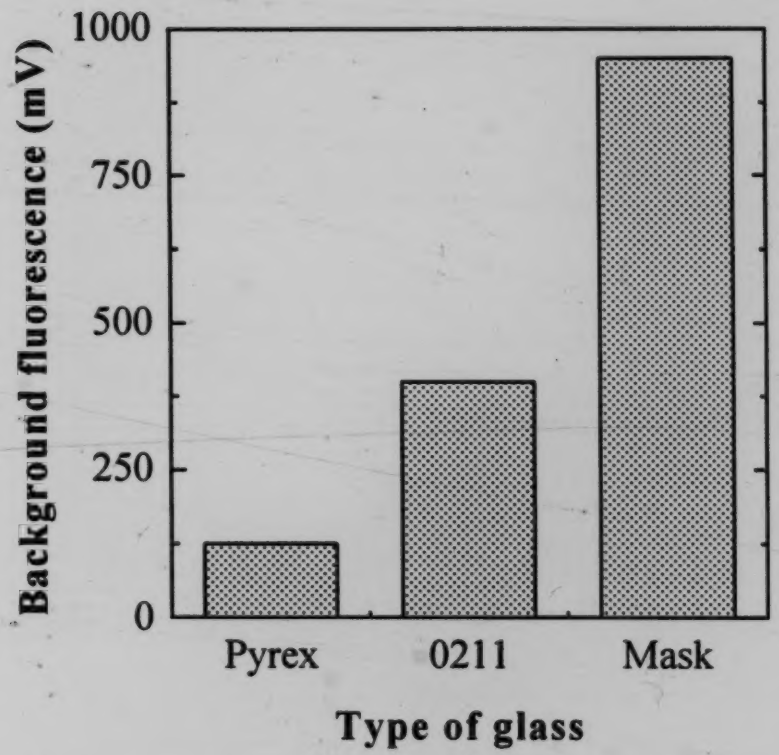

Figure 2.16: Background fluorescence of devices made from three different types of glass: Borosilicate (Pyrex), zinc titania (0211) and soda lime (photomask). Optical detection parameters are as described in Figure 2.15.

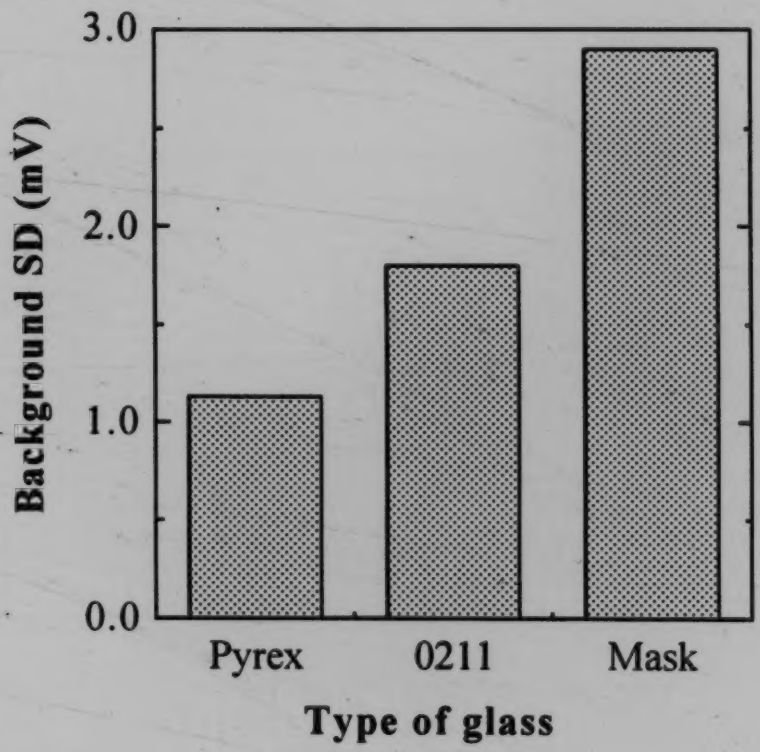

Figure 2.17: Background noise from Pyrex, 0211 and photomask glass devices described in Figure 2.16. Optical detection parameters are as listed in Figure 2.15.

Borosilicate Pyrex, Zinc Titania 0211 and Soda Lime Photomask glass devices. The devices' channel depths were similar (13, 13 and 14 μm for the three types of glass, respectively). The background signals were 9-point smoothed and the SD of the smooth signals was taken as the background noise. The background fluorescence and noise increase in the order: Pyrex, 0211, and photomask glass. In Figure 2.18, the background noise of the three glass types was plotted versus the square root of the background signals. The linear plot (slope 0.091 ± 0.007 $mV^{1/2}$ and intercept = 0.0 ± 0.2 mV) indicates shot noise, which is due to the random fluctuation in the background fluorescent signal. A zero intercept of the plot indicates that the detector noise was relatively small compared to the background noise. Fourier transform of signals (1024 points) obtained from 10 pM solution gave a frequency spectrum approximately flat and random above 2 Hz. This result indicates that flicker noise (1/f noise) is insignificant and shot noise is the limiting noise type as discussed above.

Overall, the main factor contributing SD of the blank is the noise from the glass fluorescence background. Therefore, according to the DL expression for a given sensitivity, Borosilicate Pyrex glass would give the lowest DL of the 3 glass types.

2.4.3.3 Detection Limit

2.4.3.3.1 Detection limit of Fluorescein

DLs of 6.30 ± 0.06; 5.35 ± 0.09; and 9.20 ± 0.15 pM for fluorescein were obtained from Pyrex, 0211, and photomask, respectively. Ideally for a given sensitivity, the Pyrex device with a lower background noise should give the lowest detection limit, but a less than optimized detection set up made its DL higher than that of the 0211 device. These results show the importance of optics alignment in chip-based CE for detection of low concentration. Note for this study, sample plugs were large enough that longitudinal diffusion did not decrease the concentration at the center of the plug over the time taken to reach the detector and the effect of diffusion on peak signal was minimal. However, for a typical electrokinetic injection with a plug length of about 217 μm (as discussed in section "Separation Efficiency"), the diffusional broadening reduced the peak signal by approximately a factor 3. The corresponding DL for fluorescein samples was about 19, 16 and 28 pM, respectively. These correspond to 1500, 1260 and 2200 injected molecules, respectively (injection volume =130 pL).

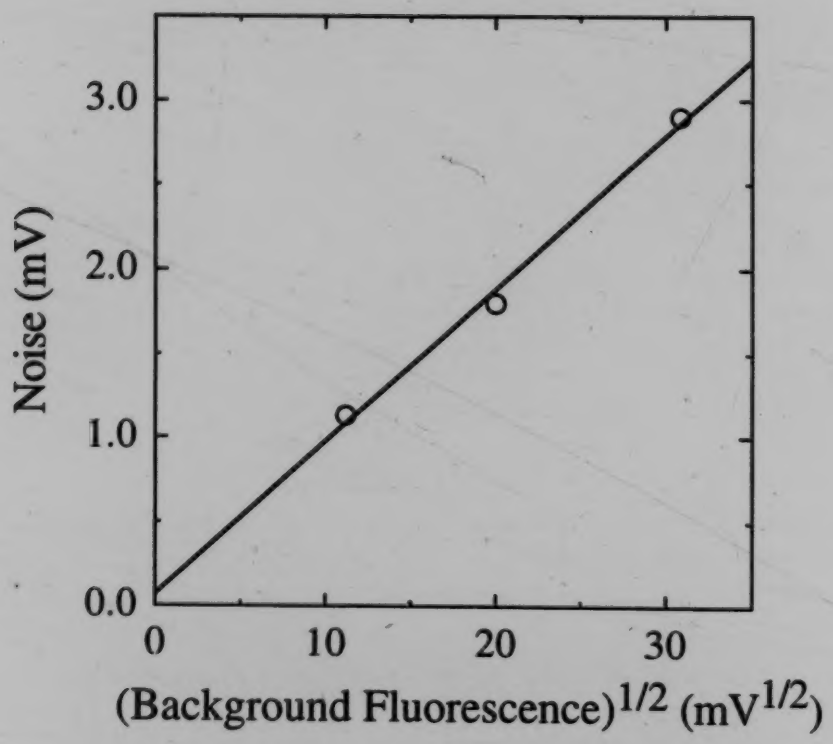

Figure 2.18: Noise vs square root of background fluorescence of glass devices described in Figure 2.16. Optical detection parameters are as listed in Figure 2.15.

2.4.3.3.2 Detection limit of Amino Acids and Proteins

As shown above, optimization of the detection set-up was used to determine the sensitivity and DL of fluorescein at 488 nm excitation. However, most analytes such as amino acids and proteins do not fluoresce at this excitation wavelength and need to be labeled with a dye. The effect of labeling on the detection limit of simple molecules such as amino acids and of more complex proteins such as anti human immunoglobulin G (anti H-IgG) and bovine serum albumin (BSA) are discussed below.

Figure 2.19 shows separation of 7 fluorescein-labeled amino acids in a Borosilicate glass device. If 100 % conversion of FITC to labeled amino acids is assumed, then the concentration for each labeled amino acid would be 500 pM in the sample. For labeled arginine in Figure 2.19, the signal to noise is 15.4. Assuming a linear calibration sensitivity, the DL was estimated at 97 pM for the labeled arginine. However, the separation shows that some FITC still remained after 2 days of incubation at 4 °C, indicating that conversion to the labeled product was less than 100% and the 97 pM reported above is a conservative estimate of DL for labeled arginine.

DLs were also obtained for more complex analytes such as fluorescein-labeled anti-human immunoglobulin G (anti H-IgG*) and fluorescein-labeled bovine serum albumin (BSA*). Figure 2.11 shows an electropherogram obtained from a mixture of 3.2 nM of anti H-IgG* and 15 nM of BSA* in Borosilicate glass. The multiple labels per protein molecule (7.6 for H-IgG and 11.2 for BSA given by supplier), effectively increase the fluorescence yield per unit of protein. Therefore, we should expect a higher calibration sensitivity and a lower detection limit for the proteins. However, the signal to noise ratios for anti H-IgG* and BSA* in Figure 2.11 were 126 and 72 and the corresponding calculated detection limits were 80 pM and 667 pM, respectively. The protein peaks were broad and significantly lower than those observed for equivalent concentrations of fluorescein. Sample microheterogeneity gives a broad spread of protein mass to charge ratio, leading to broadened peaks. Also, sample adsorption to capillary walls was a likely cause of the broadened peaks.

These results together with those for fluorescein and amino acids show that DLs varied for different analytes. However, the combined results shows DLs in the low to mid picomolar range are achievable in chip-based CE devices for fluorescein-labeled analytes, including proteins such as H-IgG and BSA

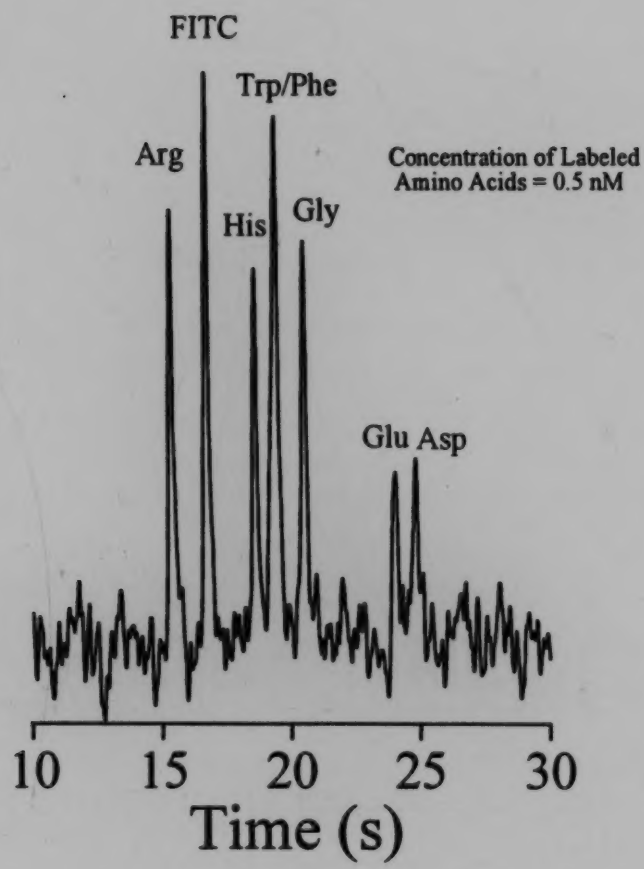

Figure 2.19: Electropherogram of 0.5 nM fluorescein-labeled amino acids obtained with a Borosilicate glass device. Separation buffer was 50 mM, PH 8, tricine buffer. Injection separation distance was 6.39 cm and electric field was 678 V/cm. Optical detection parameters are as listed in Figure 2.15.

2.5 Conclusion

In summary, a simple and inexpensive, vial-based, IgG adsorption test was developed to screen and evaluate coatings and buffer conditions for immunoassay on-chip. A PDMS coating combined with neutral surfactant significantly reduced IgG adsorption and gave good separation efficiency. The use of the zwitterionic tricine buffer in combination with a neutral surfactant and salt was also effective in reducing IgG adsorption, and gave sufficiently good separation of proteins in uncoated chips. Although inferior in separation efficiency, the use of the tricine buffer with uncoated chip is simpler (no coating was needed) and more reproducible from chip to chip while separation resolution is sufficient for many assays, as will be shown in the following chapters.

Separation performance of a microchip-based CE design was evaluated by comparing flow profiles and separation efficiency with current theories. The data shows that performance close to the theoretical limit can be achieved for this design. Complete analysis with high separation efficiency can be obtained on a time scale of seconds. Theoretical plate numbers of 139,000 and associated plate height of 0.35 μm were obtained. Band broadening due to diffusion, injector and detector are the main factors affecting the separation efficiency for small molecules whereas for proteins, other factors such as adsorption to the capillary walls and microheterogeneity are most likely the main limiting factors. While rapid separation is a desired characteristic, short separation time limits the resolution of the analytes. Ionic strength can be used as an effective means to control electroosmotic flow and separation time, to allow a desired separation speed and resolution. These studies also show the dependency of separation efficiency on separation distance, electric field, electroosmotic flow and the type of analyte(s) used. These results are consistent with those obtained from fused silica capillary in conventional CE. Therefore, these factors should be considered when separation performance of different devices are compared.

The detection system set up was optimized for planar chip-based CE devices. Better limits were obtained by optimizing the glass wafer bonding process to reduce formation of light scattering centers on the surface of the glass devices. Careful alignment of the laser beam, to eliminate scatter from the curved walls of the channels was also beneficial. Optimal alignment involved directing the beam along the axis of the channel instead of across it, with adjustment of the angle of beam incidence to minimize

background. Background fluorescence of glass varied with different types of glass (Soda lime > Zinc Titania > Pyrex) and was the limiting factor for very low concentration detection. Under optimized detection conditions, the observed detection limits were in the range of low picomolar for fluorescein and labeled amino acid samples, to high picomolar for protein such as BSA. These results are a substantial improvement over the 2 nM limit we obtained previously[36] and are adequate for many immunoassay targets.

2.6 References

1. Masseyeff, R. F. In *Methods of Immunological Analysis*; Masseyef, R. F., Albert, W. H., Staines, N. A., Eds.; VCH: New York, 1993; Vol.1, pp 115-130.
2. Li, S. F. Y. *Capillary Electrophoresis: Principles, Practice and Application*; Elsevier: Amsterdam, 1992; Chapter 1.
3. Seiler, K.; Harrison, D. J.; Manz, A. *Anal. Chem.* **1993**, *65*, 1481-1488.
4. Giddings, *J. C. Sep. Sci.* **1969**, *4*, 181-189.
5. Jorgenson, J. W.; Lukacs, K. D. *Anal. Chem.* **1981**, *53*, 1298-1302.
6. Harlow, E.; Lane, D. Eds. *Antibodies: A Laboratory Manual; Cold Spring Harbor Laboratory*: Cold Spring Harbor, N.Y. 1988; pp 174-243 and 354-355.
7. Fan, Z. H. *PH.D Thesis, University of Alberta, Chemistry Dept.* 1994, Chapter 3.
8. Effenhauser, C. S.; Manz, A.; Widmer, H.M. *Anal. Chem.* **1993**, *65*, 2637-2642.
9. Harrison, D. J.; Fluri, K.; Seiler, K.; Fan, Z.; Effenhauser, C. S.; Manz, A. *Science* **1993**, *261*, 895-897.
10. Seiler, K.; Harrison, D. J.; Manz, A. *Anal. Chem.* **1993**, *65*, 1481-1488.
11. Fan, Z.; Harrison, D. J. *Anal. Chem.* **1994**, *66*, 177-184.
12. McCormick, R.M. *Anal. Chem.* **1988**, *60*, 2322-2328.
13. Monnig, C. A., Kennedy, R. T. *Anal. Chem.* **1994**, *66*, 280R-314R.
14. Town, J. K.; Regnier, F. E. *Anal. Chem.* **1992**, *64*, 2473-2478.
15. Lauer, H. H., McManigill, D. *Anal. Chem.* **1986**, *58*, 166-170.
16. Green, J. S.; Jorgenson, J. W. *J. Chromatogr.* **1989**, *478*, 63-70.
17. Swedberg, S. A. *Anal. Biochem.* **1990**, *185*, 51-56.

18. Bushey, M. M.; Jorgenson, J. W. *J. Chromatogr.* **1989**, *480*, 301-310.
19. Town, J. K.; Regnier, F. E. *Anal. chem.* **1991**, *63*, 1126-1132.
20. Town, J. K.; Regnier, F. E. *J. Chromatogr.* **1990**, *516*, 69-78.
21. Bruin, G. J. M.; Chang, J. P.; Kuhlman, R. H.; Zegers, K.; Kraak, J. C.; Pope, H. *J. Chromatogr.* **1989**, *480*, 339-345.
22. Hjerten, S. *J. Chromatogr.* **1985**, *347*, 191-198.
23. Cobb, K. A.; Dolnik, V. Novotny, M. *Anal. Chem.* **1990**, *62*, 2478-2483.
24. Mosely, M. A.; Deterding, L. J.; Tumer, K. B.; Jorgenson, J. W. *Anal. chem.* **1991**, *63*, 109-114.
25. Garbassi, F.; Morra, M.; Occhiello, E., Eds. *Polymer Surfaces: From Physics to Technology*, John Wiley & Sons: NewYork, 1994, pp 395-430.
26. Schmalzing, D.; Piggee, C. A.; Foret, F.; Carrilho, E.; Karger, B. L. *J. Chromatography A* **1993** , *652*, 149-159.
27. Schmalzing, D.; Nashabeh, W.; Yao, X.-W.; Mhatre, R.; Regnier, F. E.; Afeyan, N. B.; Fuchs M. *Anal. Chem.* **1995**, *67*, 606-612.
28. Noll, W. *Chemistry and Technology of Silicones*, Academic Pres, New York, 1968. a) p 581; b) pp 447-453; c) p 445.
29. Gilges, M.; Kleemiss, M. H.; Schomburg, G. *Anal. Chem.* **1994**, *66*, 2038-2046.
30. Good, N. E.; Winget, G. D.; Winter, W.; Connolly T. N.; Izawa, S.; *Singh*, R. M. M. *Biochem.*, **1966**, *5*, 467-477.
31. Engval, E.; Perlmann, P. *J. Immunology* **1972**, *109*, 129-135.
32. Reif, O.-W.; Lausch, R.; Scheper, T.; Freitag, R. *Anal. Chem.* **1994**, *66*, 4027-4033.
33. Hayes, M. A.; Kheterpal I.; Ewing, A. G. *Anal. Chem.* **1993**, *65*, 2010-2016.
34. Wu, C. T.; Huang, T. L.; Lee, C. S.; Miller, C. J. *Anal. Chem.* **1993**, *63*, 2010-2013.
35. Karger, B. L.; Snyder, L. R.; Horvath, C. *An Introduction to Separation Science*, John Wiley & Sons: New York, 1973; pp 136-137.
36. Liang, Z. L.; Chiem, N.; Ocvirk, G.; Tang, T.; Fluri, K.; Harrison, D. J. *Anal. Chem.* **1996**, *68*, 1040-1046.
37. Ingle, J. D.; Crouch, S. R. *Spectrochemical Analysis* Prentice Hall: New Jersey, 1988; Chapters 5-6.

Chapter 3

Evaluation of Room Temperature Bonded Glass Devices

3.1 Introduction

Microfluidic devices etched in glass substrates provide an on-chip fluidic network in which chemical reactions, sample injection and separation of reaction products can be driven using electrokinetic phenomena.[1-11] Devices fabricated in glass use a cover plate to close the channels in the etched plate, which is bonded at high temperatures to allow softening and flow of the glass plates.[1-11] It would be convenient to lower the temperature required for bonding, or even to make the bonding step reversible in order to reduce fabrication time and cost, and increase the flexibility of device fabrication.

Oxidized silicon wafer bonding has been extensively studied.[12, 13] Wafer bonding is thought to arise from bonds formed between hydroxyl groups on opposing silicon dioxide surfaces during the initial cold contact stage. This is referred to as cold or contact bonding, or cold welding. Frequently, the cold welded bond formed during the initial contact between wafers is strong enough to allow further handling of the bonded structure without additional treatment. Glass bonding should be similar to oxidized semiconductor wafer bonding, since glass is mainly silicon dioxide and its surface bears hydroxyl groups. We have examined the question of whether a cold weld between two glass surfaces can be reliably used for the fabrication of microchip devices used for separations.

It was not clear whether the glass substrates we used in fabrication were smooth enough to provide the good contact required for cold welding. Silicon wafers tend to be acceptable for bonding if their microscale roughness is less than 5 Å.[13] However, the surface roughness of glass was determined to be 50 -70 Å for fired or mechanically polished glass.[14a] Consequently, it was not immediately obvious that we could obtain the intimate contact needed for formation of a strong cold contact bond of glass plates without extensive polishing. However, we recently reported that temperatures could be lowered to 440 °C with extensive cleaning,[15] while Ramsey and co-workers have reported a chemical treatment used in silicon bonding which can lower the bonding temperature of glass to about 90 °C.[16]

In this chapter, a simple method based on rigorous cleaning[11, 15, 17] to bond glass at room temperature for microfluidics applications is reported. This method was successfully used to bond a wide range of the same or different types of commercially available glass without the need for thermal treatment. Microchip-based CE devices bonded through this method did not leak under normal operating conditions and showed good separation and performance.

3.2 Experimental Section

Materials, reagents, and chip fabrication were previously described in Chapter 2. The chip layout was described in Figure 2.2 and also shown in Figure 3.1. The thick lines represent channels about 250 μm wide at the mouth, and the thin lines depict regions about 52 μm wide at the top and about 25 μm wide at the bottom. A double-T injector design was used with an approximate length of 150 μm between the two arms of the T, and a volume of ~100 pL. The distance from the injector region to the separation channel waste reservoir (#4) was 7.5 cm. The typical injector to detector distance was 5 cm. A 250 μm wide line forms a rectangle around the whole device, but does not contact any of the fluid channels. This rectangle was used in the leak tests discussed below.

3.2.1 Chip Characterization

Cut polypropylene pipette tips (Fisher Scientific) were inserted and glued into each access hole with five-minute epoxy, to serve as solution reservoirs. Channels were pressure tested with buffer or 20 μM FITC dye loaded into the reservoirs. Nitrogen gas was then coupled to the reservoirs via Nalgene tubing and 10-30 psi was applied to the reservoirs for 10-30 min. Leaking of solution to the border channel, which is not in contact with the channels containing fluid (Figure 3.1a), was checked visually by eye and with a 200x microscope. If FITC dye was used then the channel and its proximity were also scanned with a focused, Ar-ion laser beam (488 nm, 3.2 mW output). Fluorescence was visually check through a 250x microscope and a 515 nm long-pass filter (OG515, Omega Optical, Brattleboro, VT).

Current-voltage curves were measured using increasing voltage steps applied to channels filled with tricine buffer.

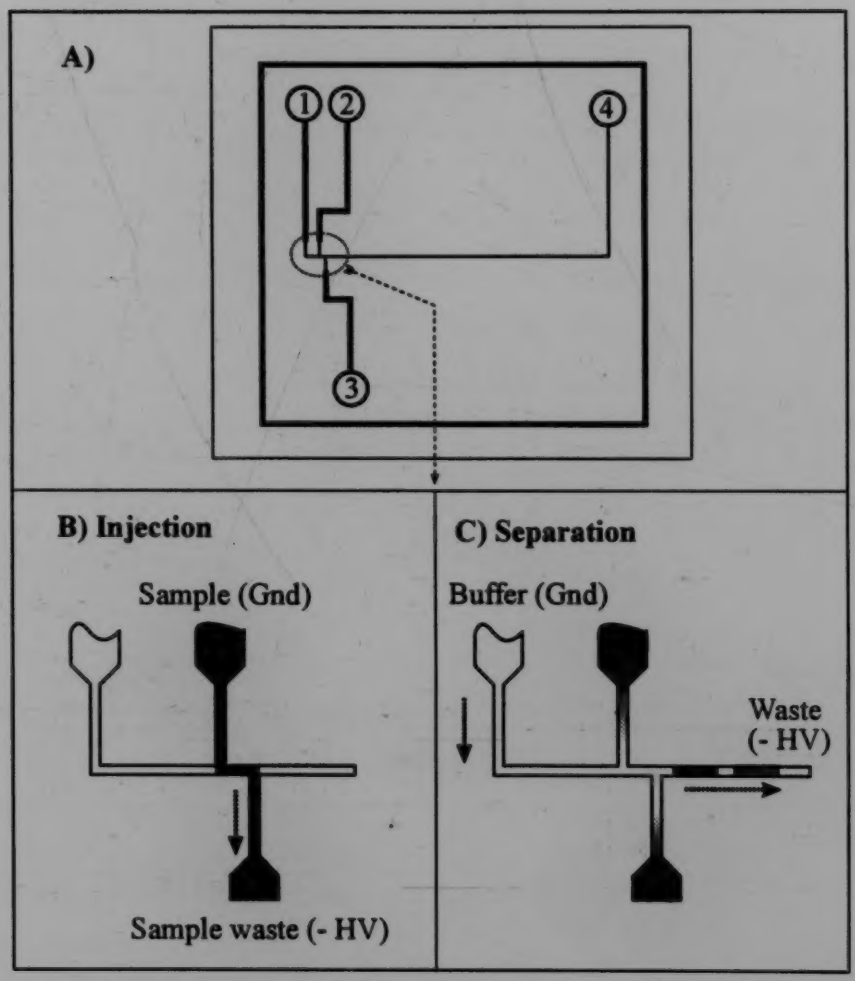

Figure 3.1. Schematic layout of the channels for room temperature bonded glass devices. In the upper diagram, the thick lined rectangle shown is 6.0 by 5.6 cm. Channel reservoirs are marked for reference in the text. Thick lines are 250 μm wide, thin lines are 55 μm wide at the top of the channel. The two lower figures show the sample loading and injection steps.

3.2.2 Instrumentation and Chip Operation

The computer controlled power supply and relay arrangement has been described previously in Chapter 2, as has the 488-nm argon ion laser induced fluorescence detector.

Approximately 10 μl of sample was added to the sample reservoir (#2), with 10 μl of buffer in the other reservoirs. Sample was injected using the double-T injector by applying -1 kV at the injection waste (#3) and ground at the sample (#2), as show in Figure 3.1b. Separation was effected by switching to -6 kV applied at the waste (#4) and ground at the buffer (#1) reservoirs, Figure 3.1c. Separation performance was determined from elution time and the peak width at half height in the conventional fashion.[2]

3.3 Results And Discussion

3.3.1 Conditions for Absence of Interference Fringes

The glass types tested for room temperature bonding (RT) are listed in Table 3.1. The first criterion of importance is the glass smoothness and its preparation during manufacture of the plates. The Pyrex used was ground and polished, while Borofloat, microscope slide and cover slip glass (Corning 0211) were manufactured by a float process. The photomask glass preparation procedure was not available, but it was either rolled or else ground and polished.

All of the glass types tested were flat enough to give RT bonding, as indicated in Table 3.1. However, polished glass was easier to bond than non-polished glass, requiring that substantially less pressure be applied to the plates for good results. Particular care was required during handling, cleaning and hole drilling of the glass as this occasionally introduced surface roughness[14b] that prevented bonding. Extrusion of glass around the rim of the drill holes can prevent good contact of the glass surfaces near the holes. Any method used to prevent these extrusions would be effective. Here, we protected the glass plate during drilling by sandwiching it between two other pieces of glass of the same softness.

Table 3.1 Combinations of glass type tested with room temperature bonding. X marks indicate the combinations. All types of glass were not polished except Pyrex which was mechanically polished. All glass except microscope slide (M. slide) were etched.

Glass Type	Mask	Pyrex	Borofloat	0211	M. Slide
Mask	X				
Pyrex	X	X			
Borofloat	X		X		
0211	X	X	X	X	
M. Slide		X	X		X

A clean surface is probably the most important requirement for RT glass bonding. Organic residue and particles prevent close contact of the glass, resulting in air gaps which are indicated by interference fringes. Observation at the location of an interference pattern on a poorly bonded plate with 500X magnification almost invariably showed at least a particle. Thorough cleaning and particle removal required considerable care, as described in the Experimental Section. Clean glass plates needed to be aligned and bonded together as soon as possible after removal from the rinser-spinner station. Working in a Class 100 clean hood with good flow reduced the likelihood of redeposition of particles, but if interference fringes could not be removed, separation of the glass plates and re-cleaning was required.

We also examined bonding different types of glass together using the RT method. Successful bonding of several combinations of glass is indicated in Table 3.1. These glasses all have significantly different coefficients of thermal expansion. Bonding such glass combinations at temperatures above 440° C gave cracked or shattered devices upon cooling, as was expected due the stress induced by the differences in thermal expansion. The RT bonding method clearly obviates such problems.

The RT bonded devices were found to be quite reliably bonded if all air gaps, indicated by interference fringes, were eliminated. Initial cold welding of the plates upon contact was strong and typically a substantial effort was required to separate them again if necessary. Deliberate separation of the plates was readily achieved within the first few days of contact, but when left in contact for longer periods of time, this proved much more difficult.

Elimination of the air gaps proved to be the best indicator of good bonding, and no such device ever came apart unintentionally. The RT bonded structures which showed no air gaps withstood all normal physical handling they received during mounting in stages, insertion of pipette tips in the fluid reservoirs, or flushing and transfer of solvents. The 30 psi pressure test described below never caused separation of the plates or induced leaking. Even leaving 0.1 M NaOH in the channels for several hours did not degrade the bond or the device performance, indicating good chemical resistance of the bond around the channels. Devices could be used for months of separation studies, and one device remained functional and well bonded after two years of use.

3.3.2 Leakage Testing

Devices used for on-chip capillary electrophoresis and chemical reactions should leak neither fluids nor electrical currents between channels. Leakage of solution was evaluated using pressure testing to 30 psi. Devices that showed no interference fringes after bonding did not leak solution to the surrounding rectangular channel, or to the space between channels. Devices which exhibited some fringes sometimes leaked solution into isolated channels, and showed fluorescence in the regions between channels.

Electrical leakage between channels was tested by comparing the resistances of different channels to their corresponding lengths, as was done previously.[3, 8] Figure 3.2 shows plots of current versus voltage for several channels of different lengths. For devices with no fringes near any channels, the current was stable over time at a fixed applied voltage. Devices which exhibited some fringes showed increasing current with time. For devices with stable currents, the resistance, determined from Ohm's law, ranged from 0.5 to 3.2 GΩ for the different channels. For these devices the ratio of channel resistances was compared to the ratio of channel lengths in Table 3.2, to determine whether the current flow was through the channels alone.[18] The uncertainty of the resistance was estimated from statistical analysis of the least squares fit of the current-voltage curves. The channel resistance ratio agreed with the length ratios within experimental error, indicating that there was no significant electrical leakage.

Figure 3.3 shows that the current through the separation channel was linear to 10 kV, with a slight upward curvature between 10 and 15 kV, indicative of Joule heating effects. Above this potential, the current increased with time, however, it recovered to its original levels when the voltage was reduced. This behavior was seen previously with devices bonded above 400 °C. It is due to electrical leakage or discharge via the leads, contacts or glass surface, and can be eliminated by better shielding of the leads and reservoir contacts, as we have already shown.[3] Our results indicate that room temperature bonded devices withstand high electric fields without substantive leakage effects becoming apparent.

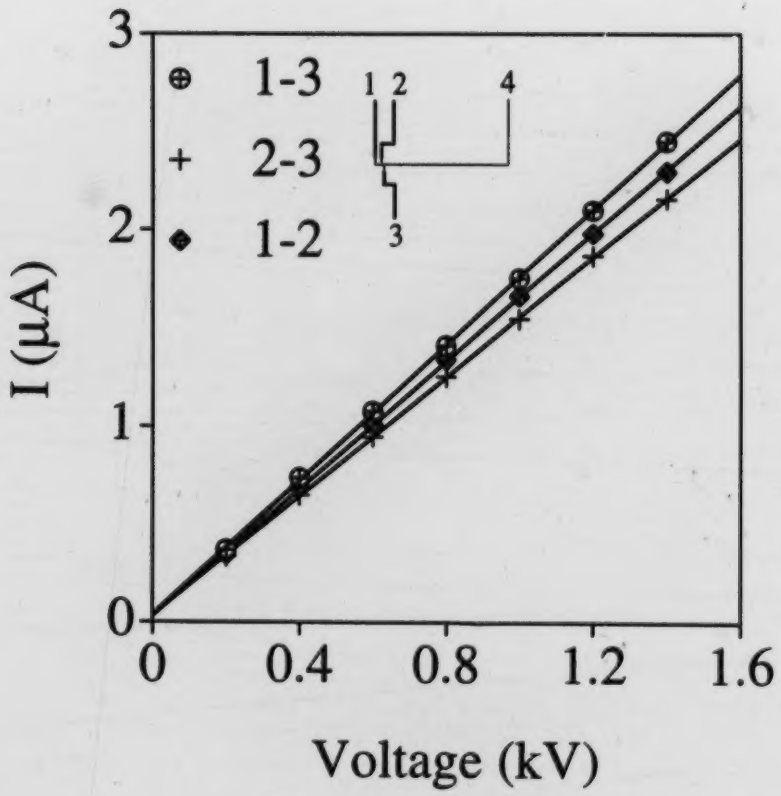

Figure 3.2. Current-voltage curves for potentials applied between the solution reservoirs of a room temperature bonded glass device with the 10 mM, pH 8, low ionic strength tricine buffer.

Table 3.2 Comparison of channel length and channel resistance ratios in room temperature bonded devices.

Channel ratio[a]	Distance ratio[b]	Resistance ratio[c]
(2-3) / (1-3)	1.121 ± 0.005	1.134 ± 0.009
(1-2) / (1-3)	1.076 ± 0.005	1.060 ± 0.009

(a) Numbers refer to channel between the indicated reservoirs, see Fig. 1.

(b) Ratio of equivalent channel lengths, see footnote 19.

(c) Ratio of measured resistances, using pH 8.0 buffer.

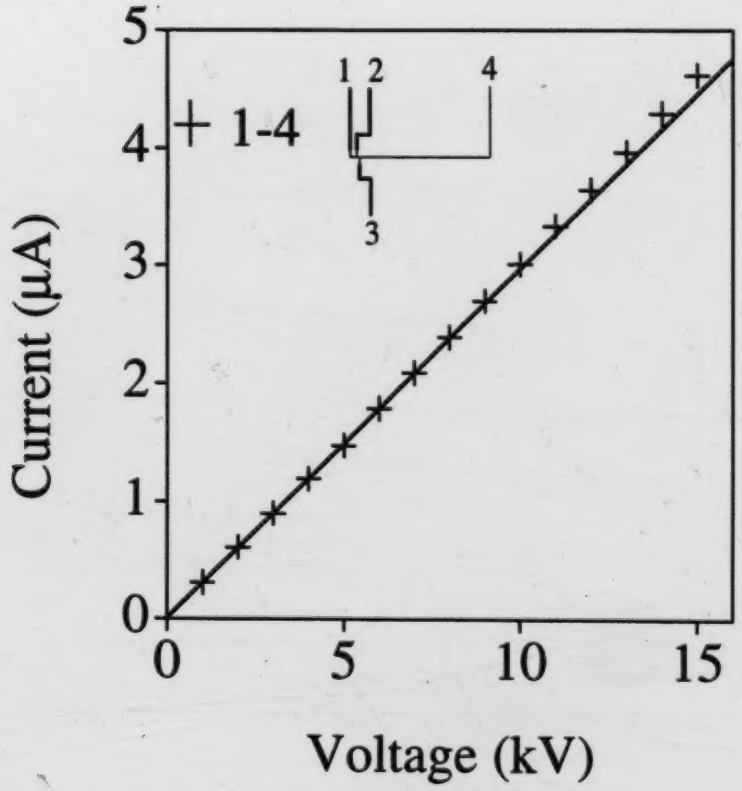

Figure 3.3. Current voltage curve for the highest resistance channel of a room temperature bonded glass device with the 10 mM, pH 8, low ionic strength tricine buffer. The line shows a least squares fit to potentials below 9 kV.

3.3.3 Separation Performance

The most relevant evaluation of the chip is its separation performance, so we have compared devices bonded at 440-650°C with those prepared by RT bonding. Separation of four amino acids in an RT bonded chip is shown in Figure 3.4. Separations were performed at 6 and 8 kV (750 and 1000 V/cm) using mask glass. The peaks are well resolved, except for histidine and phenylalanine. The efficiencies ranged from 17,000 for histidine to 28,000 for glycine with 6 kV applied. Further work with the same device after cleaning the channels with 0.1 M NaOH for about 1 h gave an N of 80,000-90,000 at 6 to 8 kV applied (n = 8) (21-24 plates/volt, 0.63 - 0.56 μm HETP). This compares well with values of 100-120,000 measured in devices bonded at high temperatures. These results shows that rapid separation with high efficiency can be achieved just as readily in room temperature bonded devices as in those bonded at high temperatures.

3.4 Conclusion

The most important factors for successful room temperature bonding were the cleanliness and flatness of the glass surfaces. The performance of these devices, in terms of separations and durability was comparable to that of devices prepared by high temperature bonding. The availability of a low temperature bonding process that does not require additional chemical treatments should prove significant, greatly increasing the flexibility available in fabrication. Greater range in the glass combination with different thermal expansion coefficients may prove useful for optical purposes. The throughput of glass device fabrication is increased by eliminating the time required for thermal bonding. The integration of other components into devices such as waveguides or metal electrodes, which might otherwise be ruined at elevated temperature becomes possible. Similarly, thermally sensitive materials, such as polymer coatings or biochemicals could be introduced before bonding, allowing pre-loading of reagents into open channels before bonding forms the capillaries. Most practically, RT bonding may make devices easily cleaned for reassembly and reuse after they become contaminated by sample solutions.

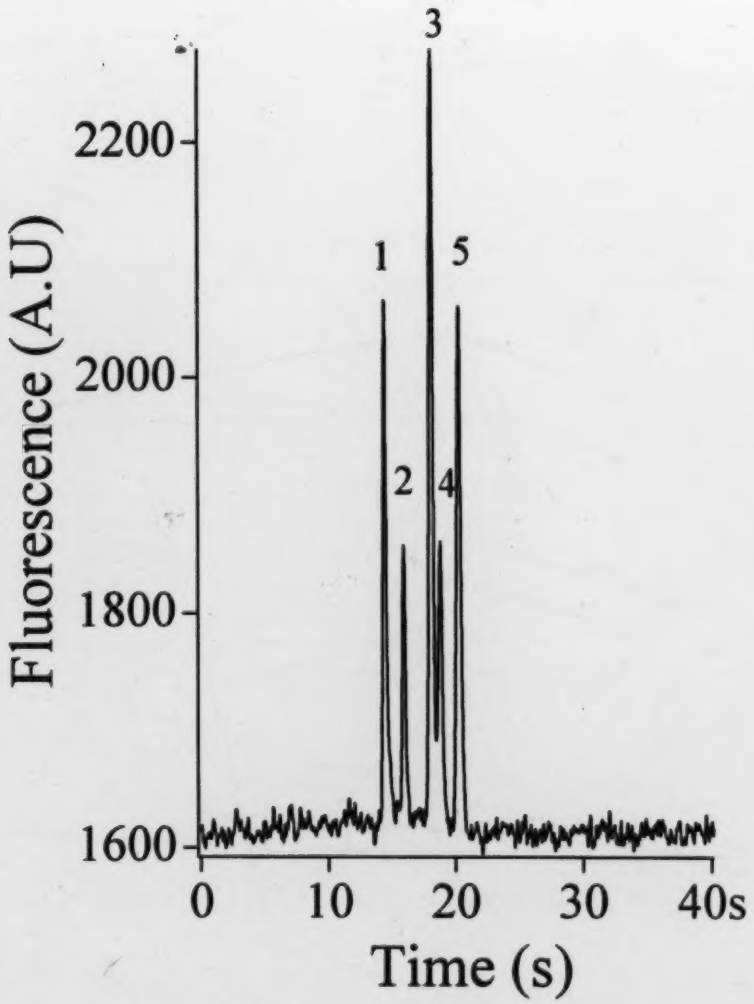

Figure 3.4. Electropherogram of fluorescein-labeled amino acids obtained from a room temperature bonded glass device with pH 8.0, tricine buffer at 6 kV (1) arginine, (2) FITC, (3) histidine, (4) phenylalanine, (5) glycine.

3.5 References

1. Manz, A.; Fettinger, J. C.; Verpoorte, E.; Lüdi, H.; Widmer, H. M.; Harrison, D. J. *Trends Anal. Chem.* **1991**, *10*, 144-149.
2. Harrison, D. J.; Manz, A.; Fan, Z.; Lüdi, H.; Widmer, H. M. *Anal. Chem.* **1992**, *64*, 1926-1932.
3. Seiler, K.; Harrison, D. J.; Manz, A. *Anal. Chem.* **1993**, *65*, 1481-1488.
4. Effenhauser, C. S.; Manz, A.; Widmer, H.M. *Anal. Chem.* **1993**, *65*, 2637-2642.
5. Harrison, D. J.; Fluri, K.; Seiler, K.; Fan, Z.; Effenhauser, C. S.; Manz, A. *Science* **1993**, *261*, 895.
6. Fan, Z.; Harrison, D. J. *Anal. Chem.* **1994**, *66*, 177-184.
7. Jacobson, S. C.; Hergenröder, R.; Koutny, L. B.; Warmack, R. J.; Ramsey, J. M. *Anal. Chem.* **1994**, *66*, 1107-1113.
8. Seiler, K.; Fan, Z. F.; Fluri, K.; Harrison, D.J. *Anal. Chem.* **1994**, *66*, 3485-3491.
9. Harrison, D. J.; Fluri, K.; Chiem, N.; Tang, T.; Fan, Z. *Technical Digest, Transducers 95, 8th Intl. Conf. Solid-State Sensors Actuat.*, Stockholm, June 25-29, 1995, pp 752-755
10. Jacobson, S. C.; Moore, A. W.; Ramsey, J. M. *Anal. Chem.* 1995, *67*, 2059-2063.
11. Fluri, K.; Fitzpatrick, G.; Chiem, N.; Harrison, D.J. *Anal. Chem.* **1996**, *68*, 4285-4290.
12. Bengtsson, S. *J. Electrochem. Soc.* **1992**, *138*, 841-863.
13. Schmidt, M. *Technical Digest, Solid State Sensor Actuator Workshop*, Hilton Head Island, SC, June 13-66, 1994, pp 127-131.
14. Holland, L. *The Properties of Glass Surfaces*; John Wiley & Son, N.Y. 1964; a) pp 119 b) pp 68.
15. Chiem, N. ; Harrison, D. J. *Anal. Chem.* **1997**, 69, 373-378.
16. Wang, H. Y.; Foote, R. S. ; Jacobson, S. C. ; and Ramsey, J. M. *Solid State Sensor and Actuator*. Late-news poster session supplemental digest. June 1996, 17-18, Hilton Head Island, SC.

17. Sobek, D.; Young, A.M.; Gray, M.L., Senturia, S.D. *Proc. IEEE Micro-Electromecahnical Systems Workshop*, Fort Lauderdale, FL, Feb 7-10, 1993; pp 219-224.

18. The channels in the chips tested were not uniform in width, so the equivalent length for an equivalent channel with uniform width was calculated as described earlier [3,8].

$$l_{eq} = l_{true} A_{55} / A_{true}$$

The cross sectional area was calculated based on $[(WxD) + 1/2\pi D^2]$ where W is the channel width on the mask, and D is the etched depth. The area of a 55 μm wide channel was taken as the reference standard.

Chapter 4

Evaluation of Antibody Binding Affinity and Complexes

4.1 Introduction

Antigen/antibody interactions belong to a large group of noncovalent biological binding reactions which depend mainly on structural complementarity between a determinant (or a ligand) and a binding site (receptor) on a macromolecule. These reactions include binding a substrate to its enzyme, binding a hormone to its receptor, and binding of ligands to transporting plasma proteins.[1] The basic theories underlying these binding reactions have much in common; however, antigen/antibody interactions have many unique features originating from their diverse nature. To understand the mechanism and specificity of these interactions, measurements of both binding stoichiometries and their equilibrium constants are important.

Common methods used for assessing antibody/antigen equilibrium constants are based on (1) equilibrium dialysis[2] (2) fluorescence quenching[3] or enhancement[4] (3) equilibrium molecular sieving[5] and (4) ammonium sulfate precipitation.[6] The first two methods are applicable only to systems involving purified or partially-purified antibody. Equilibrium molecular sieving is only suitable for binding systems in which the two components are of very different sizes. The precipitation method uses a high salt concentration which may affect the binding equilibrium. Recently, capillary electrophoresis (CE) has been shown to be a useful and sensitive method for measuring the binding constants of carbohydrates to peptides[7] and ligands to proteins.[8-10] CE allows rapid, efficient separation and detection of different forms of complexes as well as free reactants in a solution mixture of species at equilibrium.

This chapter reports on the use of microchip-based capillary electrophoresis as an alternative CE technique for studying antigen/antibody interactions. The results show that binding constants as well as binding stoichiometries of non-purified antibody preparations, such as ascites fluid, can be rapidly and easily determined. In this study mixing was performed off-chip, but the integration of the reagent mixing, reaction and separation steps on a single chip would also be possible, as demonstrated in Chapter 6. Such integration onto a single chip substrate provides a potentially powerful tool for high throughput screening and evaluation of antibodies currently being developed in medical research and biotechnology.

4.2 Theory

A binding reaction involving antibody and antigen to give a complex can be expressed as

$$Ab + Ag <=> Ab\text{-}Ag \qquad [1]$$

where Ab represents free antibody, Ag free antigen, and Ab-Ag the antibody-antigen complex. The association equilibrium constant K can be defined as

$$K = \frac{[Ab-Ag]}{[Ab][Ag]} \qquad [2]$$

where square brackets denote equilibrium concentration.

The stabilization of the Ab-Ag complexes is achieved by molecular forces commonly involved in stabilizing non-covalent complexes, e.g., hydrogen bonding, London forces, van der Waals forces, hydrophobic and/or coulombic interactions. The higher the affinity of the antibody, the greater the amount of antigen bound to antibody at equilibrium. It is generally not possible to determine experimentally the equilibrium concentration of all three species. Using mass conservation, the equilibrium concentration of antibody can be expressed as

$$[Ab] = [Ab_t] - [Ab\text{-}Ag] \qquad [3]$$

where $[Ab_t]$ is total antibody. Using equations (2) and (3), the following expression may be derived[1]

$$\frac{[Ab-Ag]}{[Ab_t]} = \frac{K[Ag]}{1+K[Ag]} \qquad [4]$$

Equation 4 is a hyperbolic adsorption isotherm. The complex concentration increases as antigen is added to a fixed concentration of antibody, reaching a saturation plateau which is limited by the total antibody concentration.

Equation 4 is derived for antibody with 1 binding site. It can be extended to antibodies with multiple binding sites[11] and rewritten as

$$\frac{[\text{bound Ag}]}{n[Ab_t]} = \frac{K[Ag]}{1+K[Ag]} \qquad [5]$$

where n is the average number of combining sites per antibody molecule used for antigen binding and 'bound Ag' is antigen reacted and bound to the antibody. In

equation 5, it is assumed that (a) K is the same for all the combining sites (i.e. no heterogeneity) and (b) the combination of antibody with one antigen molecule does not appreciably alter its affinity for another molecule. It is important to note that K is the association constant for binding of one molecule to one antibody binding site; and it is generally known as the 'intrinsic association constant'.

Equation 5 is frequently used in the form of a linear transform known as the Scatchard[1, 12] approach

$$\frac{[\text{bound Ag}]}{[\text{Ag}]} = -K[\text{bound Ag}] + n[Ab_t]K \qquad [6]$$

A plot of [bound Ag]/[Ag] versus [bound Ag] allows the determination of the intrinsic equilibrium constant and the average number of binding sites, n.

4.3 Experimental Section

4.3.1 Materials And Reagents:

Fluorescein labeled bovine serum albumin (BSA*) and ascites fluid containing monoclonal anti-BSA antibody were purchased from Sigma (St. Louis, MO). Other reagents were described previously in Chapter 2.

4.3.2 Procedures

Chip layout, injection and separation procedures were described in chapter 2. Briefly, microchip CE devices were fabricated in Borofloat glass and bonded at 650 °C. The simple channel structure design with a double T injector was used, and the depth of the channels was 13 μm. The injection-to-detection distance was 6.4 cm. Injection and separation were performed at -1 kV and -6 kV, respectively.

The 50 mM tricine, high ionic strength, pH 8 buffer used for sample dilution and separation was previously described in Chapter 2. Stock BSA* solution (500 μg/mL or 7.52 μM using 66,500 g/mol for BSA*) was first prepared in the tricine buffer. Then 5, 10, 20, 30, 40, 50 μl aliquots of this stock were added to different microcentrifuge tubes. Tricine buffer was added to each of the tubes to a total volume of 245 μl, and vortexed for about 5 s. Then 5 μl of ascites fluid containing anti-BSA (2.8 mg/mL) was added, vortexed and incubated at room temperature for about 30 minutes before on-chip analysis. The concentration of anti-BSA in each tube was 56 μg/mL or 361 nM

using an average molecular weight (MW) of 155,000 g/mol. For the calibration of peak height to concentration, BSA* stock solution was diluted with tricine buffer to give 250 µl of solution with concentrations between 0 and 30 µg/mL (0 to 451 nM).

The incubation time for equilibration of the binding reaction between BSA* and anti-BSA* was estimated by mixing 750 nM BSA* with 659 nM anti-BSA in a total volume of 500 µl. On-chip analysis was then performed 20, 45, 160, and 850 minutes after mixing. The complex peak height was constant across this entire period. Accordingly, all samples were incubated for about 30 min. before analysis. All incubations took place at room temperature (~21 °C).

4.4 Results and Discussion

The anti-BSA used in this experiment is a mouse monoclonal immunoglobulin G (IgG) which can be taken as being homogeneous in population. The IgG antibody molecule has two identical sites available for antigen binding.[1] Ideally, for antigens with a single antigenic determinant such as haptens, there are two possible forms of complex with the antibody, Ab-Ag and Ab-Ag_2. However, large protein antigens may have two or more antigenic determinants of the same or different types[1] and complexes other than Ab-Ag and Ab-Ag_2 are also possible. Chip-based CE provides separation suitable to studying the speciation of these complexes, without the need for further purification of antibody from antisera such as ascites fluid. It cannot be ruled out completely that the CE separation itself perturbs the equilibria, but past studies have demonstrated that equilibrium constants obtained by CE for peptides binding to Vancomycin are similar to those obtained by other assay methods.[9] Moreover, the separation in chip-based CE is normally rapid (less than 1 minute) which further minimizes any potentially disturbing effects on the equilibrium distribution of the species. Accordingly, the results can be used to determine the association constant of the binding reaction.

4.4.1 Equilibrium Distribution Of The Antigen, Antibody And Complexes

Electropherograms obtained from mixtures of increasing concentrations of BSA* with a fixed concentration of anti-BSA (361 nM) are shown Figure 4.1. For this study we varied the antigen concentration in the sample, to give Ag/Ab ratios in the

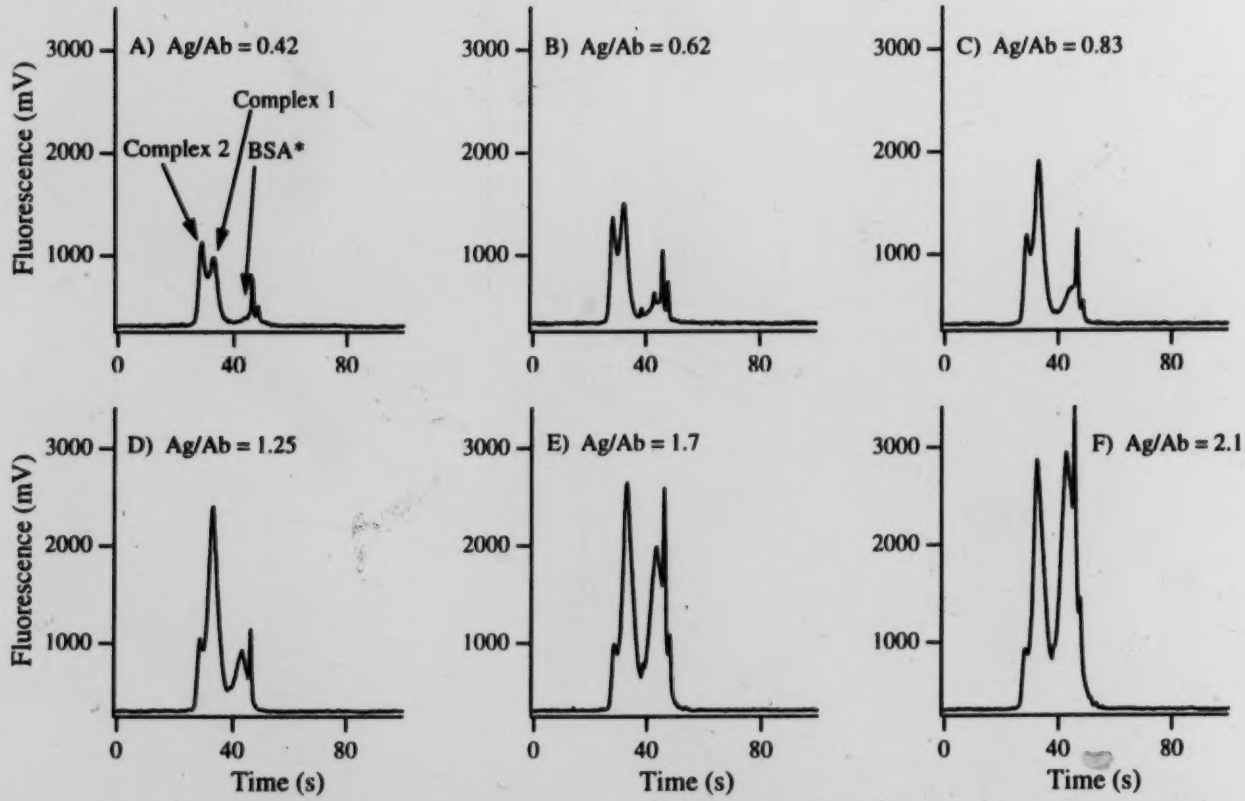

Figure 4.1: Series of electropherograms obtained from mixtures of 361 nM anti-BSA* (Ab) and increasing concentrations of BSA* (Ag). The concentration ratio of BSA* to antibody (Ag/Ab) is given at the top of each electropherogram. Separation was achieved with 50 mM, pH 8 tricine buffer at 678 V/cm with a separation distance of 63.9 cm.

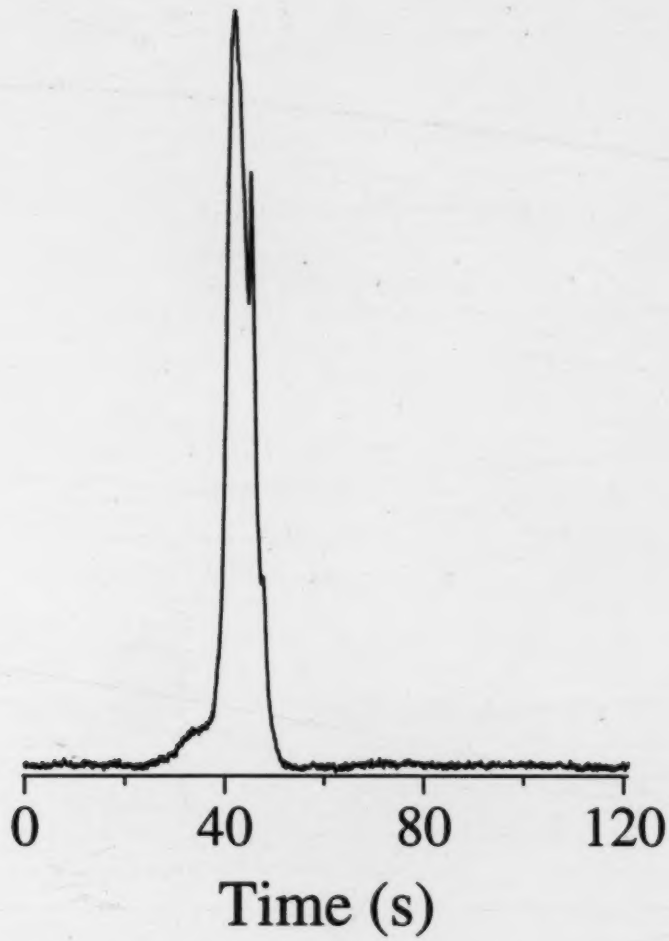

Figure 4.2: Electropherogram of 301 nM fluorescein-labeled BSA. Separation conditions are given in Figure 4.1.

range of 0.42 (antibody excess) to 2.1 (antigen excess). Since laser induced fluorescence was used for detection, only the labeled species (i.e. free BSA*, and antibody-BSA* complexes) could be observed in the electropherograms. The intensity of all peaks increases as the amount of BSA* increases. The distribution of the species at equilibrium is governed by the strength of the antibody affinity. With antibody in excess, most of the BSA* in the solution forms complexes, as indicated by the small BSA* peak observed at about 43 s. The pair of partially overlapped peaks at about 29 and 33 s were assigned to complexes, since they were not present in electropherograms obtained from the BSA* alone, as shown in Figure 4.2. The presence of the two complex peaks indicates at least two different types of complexes were formed. For simplicity, the peak closest to the free BSA* (i.e. at 33 s) is referred to as complex 1, and the other as complex 2. Complex 1 is the dominant species in the concentration range studied.

4.4.2 Binding Constants And Complex Speciations

Using equation 6, the intrinsic association constant can be determined from the equilibrium concentration of free and bound BSA*. To determine concentration of free BSA* in the antibody/antigen mixtures, a calibration curve of BSA* peak height versus BSA* concentration ranging from 0 to 450 nM was first obtained. The calibration plot was linear (slope = 6.3 ± 0.1 mV nM^{-1} and intercept = -8 ± 30 mV) and peak height was then used to evaluate the free BSA* concentration when Ab was present. The bound BSA* concentration were then determined as commonly used in published literature[1,7]

$$[\text{bound BSA*}] = [\text{BSA*}_t] - [\text{BSA*}_{free}] \qquad [7]$$

where "bound BSA*" is complexed BSA*, $BSA*_t$ is the total BSA* and $BSA*_{free}$ is the free BSA*. Note that bound BSA* are complexes which include all stoichiometries (i.e. Ab-$BSA*_2$ etc) and its concentration is equal to the concentration sum of the complexes when the stoichiometry factors are included i.e.

$$[\text{bound BSA*}] = [\text{Ab-BSA*}] + 2[\text{Ab-BSA*}_2] + \ldots \qquad [8]$$

Figure 4.3 shows a plot of bound vs. free BSA* for the BSA* and anti-BSA mixtures. The plot is a saturated binding isotherm with maximum bound BSA* concentration of about 330 nM, close to the total Ab concentration of 361 nM.

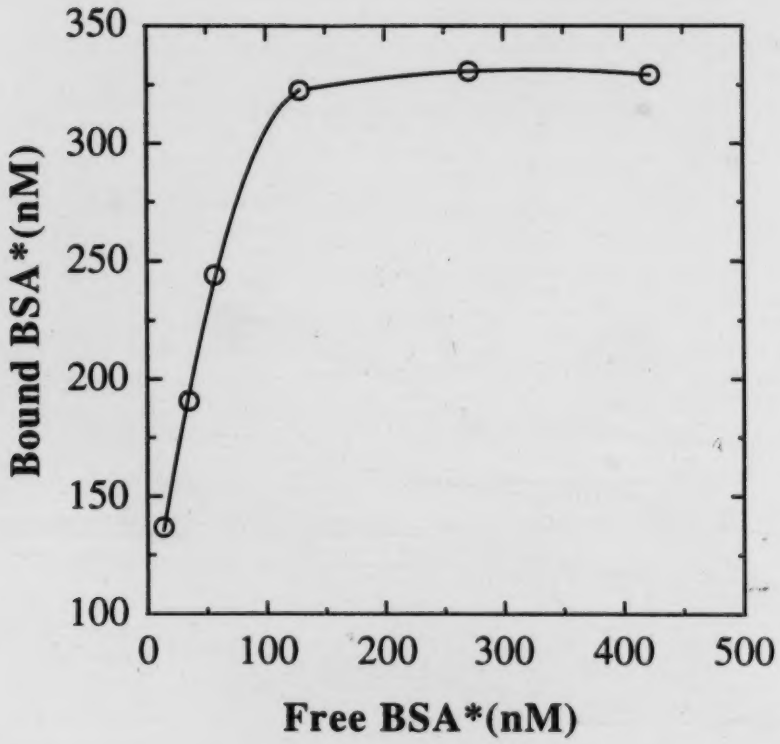

Figure 4.3: Binding isotherm of antibody-bound BSA* versus free BSA for mixtures of increasing BSA* concentration with 361 nM anti-BSA*. Separation conditions are given in Figure 4.1.

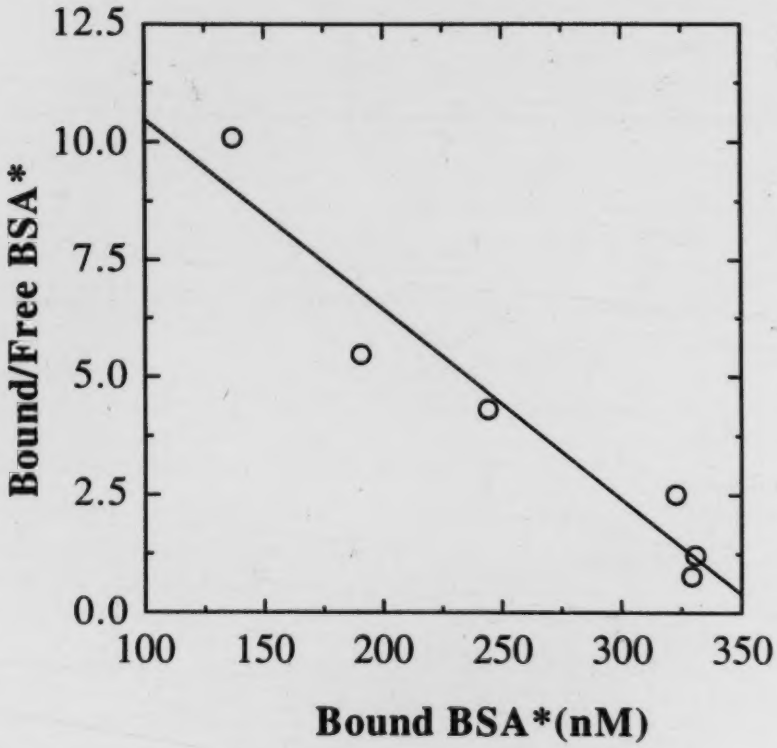

Figure 4.4: Scatchard plot of bound/free versus bound BSA* for the series of electropherograms shown in Figure 4.1.

The Scatchard plot for the data in Figure 4.1 is shown in Figure 4.4. The solid line obtained from linear regression gave a slope of $-4.0 \pm 0.6 \times 10^7$ M^{-1} and an intercept of 9.2 ± 0.5. According to equation 6, the intrinsic binding constant of the monoclonal mouse anti-BSA is $4.0 \pm 0.6 \times 10^7$ M^{-1}. This result is about 10 times lower than that previously reported for a rabbit polyclonal anti-BSA (3.7×10^8 M^{-1}) using a fluorescence polarization method.[13] Labeling is most likely an important factor for the difference since these authors also reported a 40% decrease in binding constant to 2.1×10^8 M^{-1} for anti-BSA when labeled antigen (2.7 dansyl residues per BSA*) is used instead of unlabeled antigen. In contrast, the BSA* used in this work was labeled with fluorescein with an average of 11.2 fluorescein residues per BSA molecule (as specified by Sigma). A near 10-fold decrease of affinity is possible. Other factors that may contribute to the difference in affinity include the use of different types of labels and a different source of antibody (the anti-BSA used in Reference 13 was a rabbit polyclonal anti-BSA).

The average number of binding sites per molecule of anti-BSA used in this study can be determined from the intercept of the Scatchard plot according to equation 6, giving 1.0 ± 0.2. This value suggests the dominant form of all complexes in the concentration range studied is the one-to-one complex, IgG-BSA*. This species can be assigned to complex 1 since it is the more dominant of the two complexes observed in the electropherograms.

Complex 2 is a minor species which becomes more apparent in mixtures with antibody present in excess. Since the migration of the species is from anode to cathode, its appearance at an earlier time than that of IgG-BSA* in electrophoretic separations indicates a more electropositive character. Since IgG was observed to be more electropositive than BSA (shown in chapter 2), the more electropositive character of complex 2 relative to complex 1 (IgG-BSA) indicates it could be formed by two or more antibodies bound to a BSA* molecule (i.e. Ab_2Ag, Ab_2Ag_2 ...). These types of complexes are plausible since BSA* is a large protein molecule which may have more than one antigenic determinant[1, 14]. Schumaker et al.[15] have introduced a mathematical model for a special case of interactions where both antigen and antibody are bivalent. This model allows the calculation of concentration of all possible complexes from known values of the concentration of antigen and antibody. A detailed discussion of this theory is given in Reference 15. Steengaard[1] (pp.15-16) used the model to predict relative concentrations of different complexes in various mixtures of monoclonal antibody with a macromolecular bivalent antigen. One relevant conclusion was that

Ab_2Ag is the major species for a mixture with the antibody in excess (Ab/Ag = 5). This is consistent with the observed complex 2 in the concentration ratio range used, and also with the observed electropositive character of complex 2. The low saturation value of 330 nM BSA* versus 361 nM Ab may result from the formation of $Ag\text{-}Ab_2$ complex.

4.5 Conclusion

A chip-based capillary electrophoresis method was developed for determination of protein binding interaction. The antigen/antibody association equilibrium constant and binding stoichiometry of systems such as the BSA/anti-BSA system can be quickly determined from non-purified antibody solution. This method potentially can be used as a rapid technique for screening cloned cells that generate the specific antibody to an antigen while at the same time evaluating the antibody's affinity constant. Combining this method with work reported in chapter 6 would make it possible to directly couple CE chips to cell cloning reservoirs for real-time monitoring of the concentration of the specific antibody.

4.6 References

1. Steward, M. W.; Steensgaard, J. "Antibody Affinity: Thermodynamic Aspects And Biological Significance" CRC Press, Boca Raton, Florida, **1983**.
2. Eisen, H. N.; Karush, F. *J. Am. Chem. Soc.* **1949**, 71, 363.
3. Velick, S. F.; Parker, C. W.; Eisen, H. N. *Proc. Natl. Acad. Sci.* **1960**, 46, 1470-1482.
4. Parker, C. W.; Yoo, T. J.; Johnson, M. C.; and Godt, S. M. *Biochemistry* **1967**, 6, 3408-3416.
5. Stone, M. J.; Metzger, H. *J. Biol. Chem.* **1968**, 243, 5049-5055.
6. Steward, M. W.; Petty, R. E. *Immunology* **1972**, 22, 747-756.
7. Heegaard, N. H. H.; Robey, F. A. *Anal. Chem.* **1992**, 64, 2479-2482.
8. Karak, J. C.; Busch, S.; and Poope, H. *J. Chromatogr.* **1992**, 608, 257-264.
9. Chu, Y. H.; Whitesides, G. M. *J. Org. Chem.* **1992**, 57, 3525-3527.
10. Chu, Y. H; Lees, W. J.; Stassinopoulos, A. Walsh, C. *Biochemistry* **1994**, 33, 10616-10621.
11. Nisonoff, A.; Pressman D. *J. Immunology* **1958**, 80, 417-428.
12. Scatchard, G. *Ann. N. Y. Acad. Sci.* **1949**, 51, 660-672.
13. Kierszenbaum, F.; Dandliker, J.; and Dandliker, W. B. *Immunochemistry* **1969**, 6, 125-137.
14. Sela, M.; "The Antigens" Academic Press, N. Y.; **1974**, pp 71.
15. Schumaker V.N.; Green, G.; Wilder, R. *Immunochemistry* **1973**, 10, 521-528.

Chapter 5

Separation and Quantitation in Immunoassays On-Chip [§]

5.1 Introduction

Microfluidic devices etched in glass substrates provide a fluidic network in which chemical reactions, sample injection and separation of reaction products can be achieved.[1-13] Electroosmotic pumping may be used to deliver reagents and samples on-chip[2,5,8-11], and separation of the reaction products is performed using electrophoresis. This method pumps fluid at velocities up to 1 cm/s, while also controlling the direction of fluid flow at capillary intersections, without a need for valves or other moving parts. Electrophoretic effects lead to separation of ions in the applied fields, so that both sample transport, reactions and separations can be integrated within a single manifold of channels on-chip. The demonstration that these types of devices can be applied to commercially important analyses is of considerable significance for further development of this field[11].

Application of capillary electrophoresis (CE) to immunoassays is a newly developing field.[14-25] Immunologically based assays are a commonly used method for selective determination of many chemicals at low concentration. In immunosorbent assays, in which the reagents are adsorbed onto surfaces, there are many fluid handling steps involved. We expect[11] that the unique fluid delivery capabilities of the micro-electrophoresis chip format will provide a novel, important new method of automating immunoassays in a manner which does not involve the conventional robotics used in clinical labs today. The chip format should also provide much more rapid presentation of results for samples in clinical and environmental applications, as was suggested by our preliminary study of on-chip immunoassay.[11a] Since that report, these potential advantages have also been recognized by Koutny et al.[25] One of the first key steps towards this technology is the separation of products and reactants resulting from

---

[§] A version of this chapter has been published as:

Nghia Chiem; D. Jed Harrison, "Microchip-based Capillary Electrophoresis for Immunoassays: Analysis of Monoclonal Antibodies and Theophylline", *Analytical Chemistry*, **1997**, *69*, 373-378.

homogeneous immunoassays. In this paper we present on-chip, clinically relevant, immunological assays for proteins such as immunoglobulin G (IgG) and drugs such as theophylline.

Protein separations, particularly separations of antibodies (Ab) and complexes of antibodies with antigens (Ag), are made difficult by adsorption onto the capillary walls.[15,17,20-23] A number of approaches to reduce adsorption have been attempted, such as the use of zwitterionic buffers in the earliest Ab studies,[14,16] use of high pH and/or ionic strength,[15,18-20] cleavage of the antibodies into fragments to remove the heavy Fc chain[15,17,20,24] and coating of the capillary walls with polymeric agents.[17,23,24] Of these methods we have targeted the use of zwitterionic buffers combined with solution phase, surface active components[22] to produce dynamic coating of the capillary walls. This is considerably simpler than dealing with coating the walls of planar glass chip devices, and offers the potential advantage of being more reproducible. In addition, where polymer coatings tend to suppress electroosmotic flow, it is easier to maintain flow with dynamic coatings.[17,23] Since electroosmotic pumping provides a useful pumping mechanism in our system, it is preferable that it not be quenched.[1-6] The buffer solution we have utilized also provides for mobilization of antibody, antigen and their reaction complex, in contrast to the recently reported methods employed for on-chip cortisol analysis.[25]

5.2 Experimental

5.2.1 Materials and Reagents

Human Immunoglobulin G (H-IgG), bovine serum albumin (BSA), fluorescein labeled bovine serum albumin (BSA*, 11.2:1 average fluorescein to BSA mole ratio), monoclonal anti-BSA in mouse ascites fluid, fluorescein isothiocyanate isomer I (FITC), theophylline, and tricine were from Sigma (St. Louis, Missouri, USA). Fluorescein labeled theophylline and anti-theophylline were part of the Abbott TDx reagent set (from Sigma). Dimethylsulfoxide (DMSO), hydroxylamine, NaOH, NaCl, sodium bicarbonate, were from BDH, while boric acid and sodium azide were from J.T.Baker (all via Fisher Sci., Edmonton, Canada). Tween 20 was from Aldrich (Milwaukee, WI, USA). Human serum was a gift from Bio-Rad (Hercules, CA, USA). All chemicals were reagent grade; doubly distilled water was used for all solutions. Most solutions were filtered with 0.22 μm pore size filters (Millipore); small volumes were filtered with Micropure separators with 0.22 μm pores (Amicon,

Oakville, Canada). Microconcentrators with various molecular weight cut-offs (MWCO) were from Amicon or Filtron (Northborough, MA, USA).

The high ionic strength 50 mM "tricine" buffer was previous described in Chapter 2. Tricine buffer was filter sterilized (0.22 μm filter) and was used within 3 days for sample dilution and separation.

5.2.2 Device Fabrication, Instrumentation and Chip operation.

Device fabrication, the computer controlled power supply and relay arrangement and chip operation has been described previously in the Experimental Section of Chapter 2. Briefly, devices with layout in Figure 2.2 were fabricated in 3" square photomask glass using microlithographic patterning and an HF/HNO_3 etchant. The microchips used in this study were etched to a depth of 13-15 μm. Permanent bonding was done at 440° C for 2 hours. Approximately 10 μL of sample was added to the sample reservoir (#2) and buffer to the other reservoirs. Sample was injected using the double-T injector by applying -1 kV at the injection waste (#3) and ground at the sample (#2) as show in Figure 5.1a. Separation was effected by switching to -6 kV applied at the waste (#4) and ground at the buffer (#1) reservoirs, Figure 5.1b. Laser induced fluorescence detection was used and emission was collected with a photomultiplier tube (PMT). The typical injector to detector distance was 5 cm. The PMT signal was filtered with a 50 Hz low-pass cut off frequency and then recorded on a computer. The A/D board sampling rate was 20 Hz. Peak areas or height were analyzed using software written in Labview (Austin, TX, USA). For anti-BSA assays, the peak heights are reported. For theophylline assays, the peaks were integrated and normalized as discussed later in the Discussion Section.

5.2.3 Labeling of H-IgG

H-IgG was labeled as previously described,[26] with some modifications. Purified H-IgG (3.4 mg) was dissolved in 1 mL of 0.1 M sodium bicarbonate (pH 9.0). While stirring, 50 μL of 1 mg/mL of FITC in DMSO was slowly added in 5 μL aliquots. The mixture was left in the dark at 4° C overnight, then 150 μL of freshly prepared 1 M hydroxylamine (pH 8.0) was added and incubated for 30 min. to stop the reaction. The 1.2 mL solution was concentrated and dialyzed down to 150 μL by spinning a 10,000 MWCO Filtron Macrosep concentrator with a centrifugal force of 7000 at 4 °C.

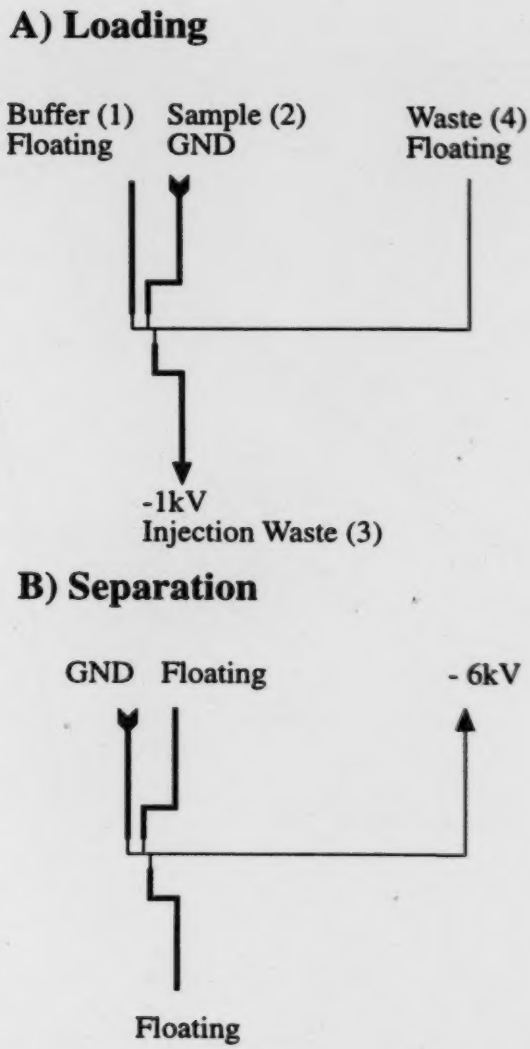

Figure 5.1. Schematic of chip layout showing A) voltages applied for sample loading and B) voltages applied during separation. Arrow heads and tails show the direction and source of fluid flow, respectively. Narrow lines are 58 μm wide channels, wider lines are 240 μm wide channels. Reservoir names and numbering schemes are also given in (A).

Then 1 mL of water was added to the mixture and the dialysis process was repeated twice more. The final concentrated sample was reconstituted to 1 mL with antibody dilution buffer (25 mM Tris-boric acid, 10 mM NaCl (pH 9), 0.0025 % Tween 20 (w/v), 0.0025% sodium azide (w/v)) and stored at 4° C in the dark.

5.2.4 Direct assay for Anti-BSA

Various volumes (0, 6 , 12, 18, 24 µL) of mouse ascites fluid (Sigma, 2.8 mg/mL of monoclonal anti-BSA in 27 mg/mL of total protein) were mixed with 25 µL aliquots of BSA* (1 mg/mL) in microcentrifuge tubes. Tricine buffer was added to each tube to give a total of 500 µL. The samples were incubated for 15 minutes at room temperature, then about 10 µL was introduced into the on-chip sample reservoir for analysis.

5.2.5 Direct anti-theophylline assay

Solution T from the theophylline kit (fluorescein labeled theophylline tracer) was used as received. To adjust the ionic strength, 150 µL of solution S (anti-theophylline) was dialyzed through a 30,000 MWCO Amicon Microcon concentrator to about 10 µL, then reconstituted with 140 µL of tricine buffer and stored at 4° C. (There is about 5% loss of IgG in the dialyzing process.[27]) The antibody was diluted by a factor of 4 with tricine buffer before assays. For direct anti-theophylline assay, 10 µL aliquots of solution T were mixed with 0, 3, 6, 10 and 40 µL portions of the 4x diluted anti-theophylline solution and additional buffer to give a total of 80 µL in microcentrifuge tubes. These mixtures were vortexed for about 10 s then incubated for 15 min. at room temperature before transferring 10 µL to the sample reservoir on-chip for analysis.

5.2.6 Competitive theophylline assay

For competitive theophylline assays, serum theophylline standards from the calibrator kit (0, 2.5, 5.0, 10, 20, 40 µg/mL) were used as received. Samples were made by spiking theophylline into human serum or buffer to give solutions 15 and 20 µg/mL in theophylline. Standard or sample solutions were then diluted 25x in tricine buffer. 10 µL of solution T, 10 µL of the diluted standard or serum samples and 50 µL of tricine buffer were mixed and vortexed for 3 s. 10 µL aliquots of 4x diluted anti-theophylline solution were then added, vortexed for about 10 s, then 10 µL was transferred to the sample reservoir on-chip.

5.3 Results and Discussion

5.3.1 Buffer Composition

Adsorption of proteins leads to poor separations in capillary electrophoresis. The dynamic coating system we tested used the neutral surfactant, Tween 20, to reduce protein adsorption, since it is commonly present in immunological reagent preparations and does not negatively affect the reagents or the immunoreaction.[29] Tricine buffer was selected from Good's listing[30] of biological buffers, as it has a pK_a around 8, which is close to that used in the Abbott TDx theophylline kit discussed below. The ionic strength was adjusted with NaCl, since the presence of 40-100 mM salt has been reported to accelerate complex formation.[19] A value of 26 mM (total ionic strength 40 mM) was chosen in order to minimize Joule heating effects.

Nielsen et al.'s original antibody separation studies utilized tricine as the buffer, with no other additives.[14] However, when only tricine was used within the glass chips, substantial tailing was seen and trace adsorption was evidenced by weak fluorescence from the walls of the channels. Additionally, formation and injection of sample plugs at the double-T injector was poorly reproducible, presumably due to adsorption induced changes in the zeta potential in the sample channel. All of these phenomena were eliminated by the addition of Tween 20 and NaCl to the tricine buffer.

Figure 5.2 illustrates the separation of fluorescently labeled, polyclonal, human IgG and BSA. The IgG peak gave a clean, symmetrical peak with 750-1000 theoretical plates with 6 kV applied (750 V/cm), indicating the buffer/surfactant system selected is reasonably effective in uncoated chips. The BSA peak is well separated from IgG, so that we can anticipate an IgG-BSA complex, as discussed below, will lie between the two peaks in Figure 5.2 and should be resolvable. The large breadth of the BSA main peak and the presence of several other nearby peaks is due to the very heterogeneous character of the commercially labeled BSA. MALDI mass spectrometry showed the labeled BSA had a full width at half maximum of 6,000 Daltons, compared to the 1,000 Dalton width of native BSA from the same commercial source.

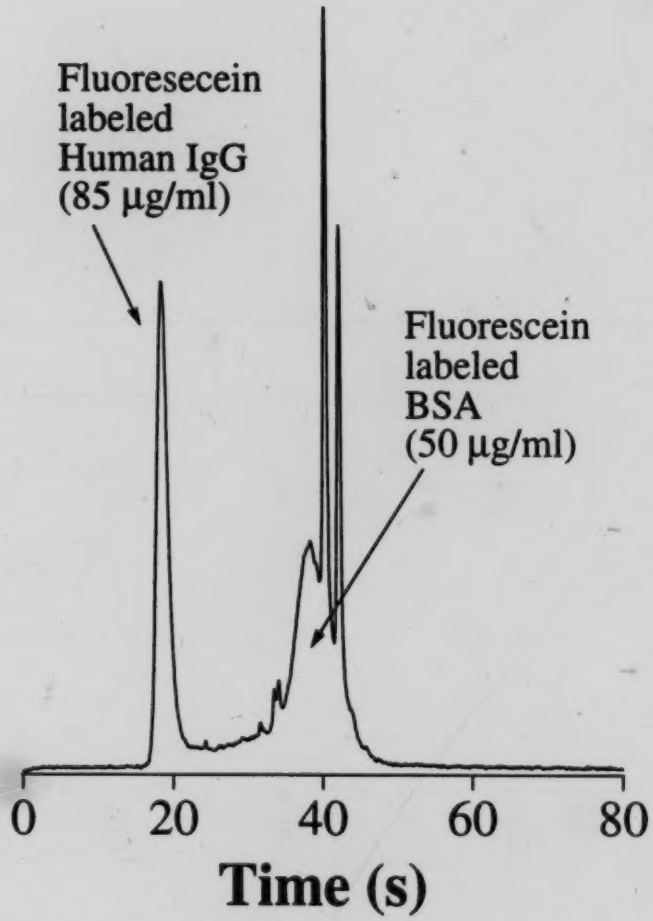

Figure 5.2 Separation of a mixture of fluorescein-labeled Human IgG and bovine serum albumin on a chip. A pH 8.0, 50 mM tricine, 26 mM NaCl, 0.01 % Tween 20 buffer was used, with a 6 kV separation potential between reservoirs 1 and 4.

5.3.2 Protein Assays

On-chip immunoassays are solution phase reactions of an antibody and its target molecule, the antigen (Ag). By labeling either the antigen or the antibody with a fluorescent tag the complex produced will also be labeled.[15-17,20] Capillary electrophoresis can then be used to separate the reactants and products, since the complex will have a different charge to size ratio than either free Ab or Ag. On-chip assays can then be run in a number of modes (immunometric or competitive assays), and used to determine either the antibody or the antigen. Examples of both types of assays will be presented here.

Immunoassay with the moderate molecular weight protein, bovine serum albumin (BSA) was performed in a direct (immunometric) assay mode designed to determine the concentration of anti-BSA produced in mouse ascites fluid. Fluorescein labeled BSA (BSA*) was used as the probe for monoclonal anti-BSA. Reaction of BSA* with anti-BSA results in decreased signal for BSA* and the appearance of an Ab-BSA* complex peak, as seen in Figure 5.3. The complex migrates at a rate between that of labeled IgG and BSA* (c.f. Figure 5.2). While the separation efficiencies observed are not high, it is important that the components are sufficiently well resolved to allow a high quality assay of the anti-BSA.

The increase in complex peak height or area is proportional to the amount of anti-BSA present. Figure 5.4 shows a calibration curve for the assay of BSA antibody present in mouse ascites fluid. The measurement precision was ±3 %, for 4 replicate injections. Assays could be run repetitively for weeks within the same chip with the same precision. Deliberate addition of up to 100 μg/mL polyclonal human IgG showed no complex formation, as illustrated in Figure 5.2, consistent with the known selectivity of most antibody reactions. The monoclonal IgG content of mouse ascites fluid is about 90% of the total IgG present, so the determination of anti-BSA can be successfully performed in the presence of a 10% content of other mouse antibodies.

Ascites fluid is extracted directly from mice during monoclonal antibody harvesting. It is rich in a variety of proteins (27 mg/mL), of which only 10% is IgG. The fact that adequate separations and good, quantitative assays can be obtained over many days in this complex fluid, illustrates the robustness of the microchip-CE system for these assays. This direct, on-chip assay is fast and simple and can potentially be used for rapid screening in hybridoma production of monoclonal antibodies to allow

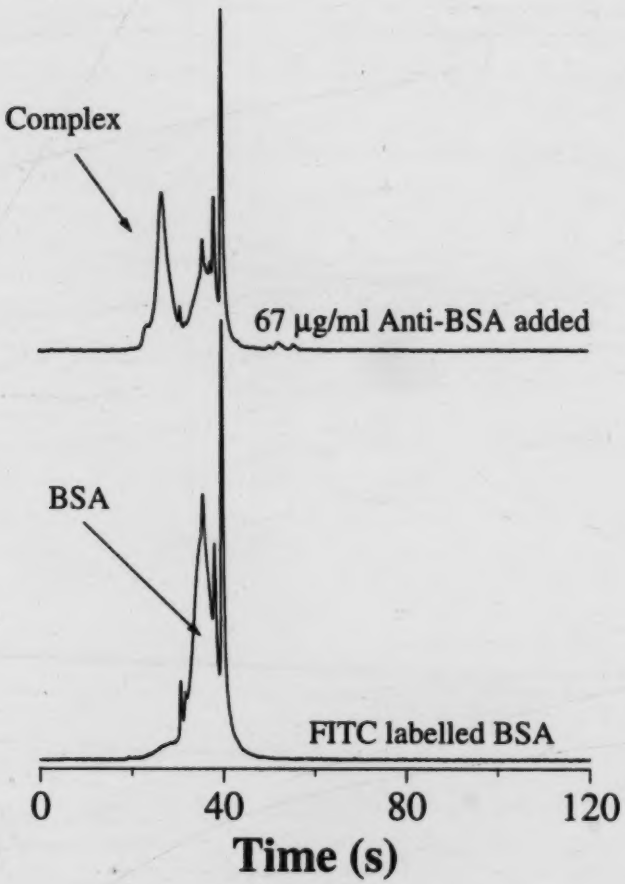

Figure 5.3 On-chip electropherograms of 50 µg/mL of FITC labeled BSA, and of a mixture containing 50 µg/mL labeled BSA and 67 µg/mL of monoclonal anti-BSA in diluted mouse ascites fluid. Buffer and separation conditions were the same as for Figure 5.2.

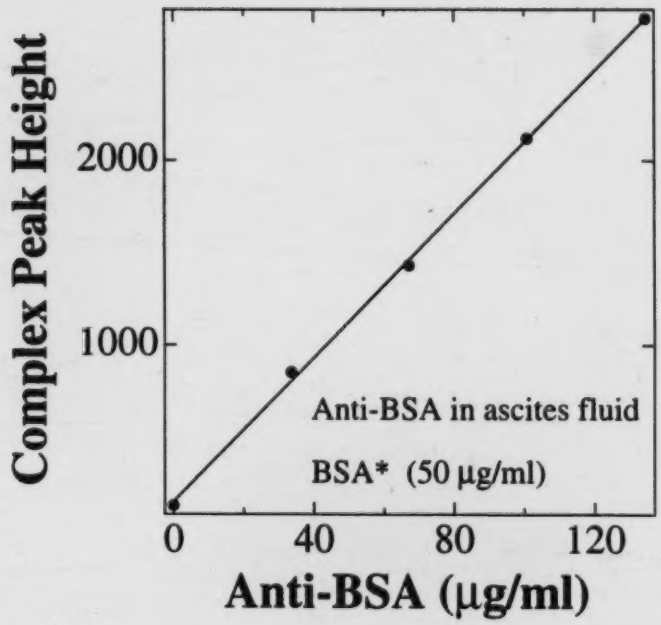

Figure 5.4 Calibration curve for anti-BSA in diluted mouse ascites fluid, showing peak height for the antibody complexed with 50 µg/mL of labeled BSA as a function of antibody concentration. Buffer and separation conditions were the same as for Figure 5.2. Each point is the mean of 4 replicates. Standard deviations were equal to or smaller than the data points in the plots.

selection of suitable antibody-secreting cells. Hybridoma production is normally limited by the screening method[26], so that rapid methods to determine whether a cell line is producing antibody with a useful binding constant for a particular target would be welcomed.

5.3.3 Hapten Assays

A large number of immunoassays target small molecules, known as haptens. A typical example is the analysis of a therapeutic drug for asthma treatment, theophylline (Th).[22] In order to get good separations by CE when using haptens, it is necessary to label the hapten instead of the antibody.[20,22-25] Labeled Th (Th*) is thus mixed with a sample containing unlabeled Th, and the two are allowed to compete for a limited amount of antibody to Th, as illustrated below.

$$Ab + Th^* \Leftrightarrow Ab\text{-}Th^*$$
$$Th + Ab + Th^* \Leftrightarrow Ab\text{-}Th + Ab\text{-}Th^*$$

A competitive assay leads to an increase in signal for the free, labeled Th* as the Th in the sample increases in concentration. There is a corresponding decrease in signal from the Ab-Th* complex. Figures 5.6 and 5.7 show a series of separations performed on-chip, in which varying amounts of Th, Th* and Ab were mixed. The separations occur in less than 1 minute and the complex is well resolved from free Th*. A theoretical plate number of 40,000 was measured for Th* (1000 plates/s, 10.7 plates/V), while the Ab-Th* complex gave about 1000 plates. The migration times for both Th* and the Ab-Th* complex proved to be quite stable in the tricine buffer. Variations in migration times (6 replicates) were within ±0.6 and 0.9% for the complex and free Th*, respectively, over a day, and within ±1 and 1.5%, respectively, over a four day period. This stability illustrates the robustness of the chip when used with the tricine, Tween 20 and salt buffer combination, as extensive exposure to protein can cause large migration time variations if adsorption is not substantially prevented.

Figure 5.5 shows electropherograms of Th* and mixtures of Ab with Th* obtained at 6 kV. Addition of the Ab causes a decrease in the free Th* peak and formation of a new pair of peaks assigned to Ab and Th* complexes.[14] In order to perform a competitive assay it is necessary to know the ratio of Ab and Th* which should be combined. The required ratio may differ from the 1:1 volume ratio used in the TDx instrument, owing to the different buffer conditions and measurement methods we have used. (Below, the Ab and Th* solution volumes are expressed in terms of the stock

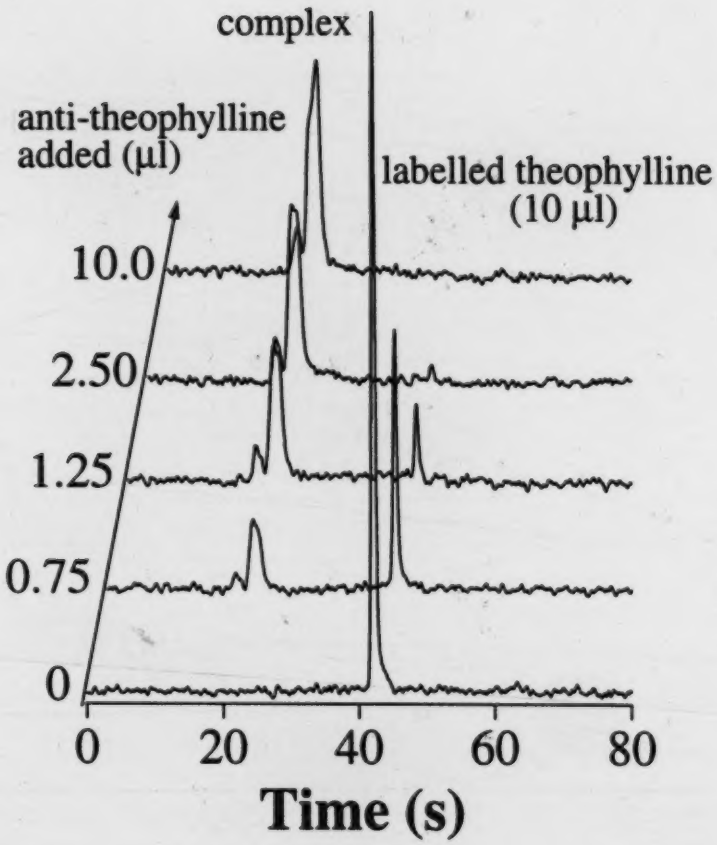

Figure 5.5 Series of on-chip electropherograms for 10 µL of labeled theophylline with added antibody solution, showing titration of Th* with the antibody. Buffer and separation conditions were the same as for Figure 5.2.

solutions of the Abbott reagent kit. Actual concentrations are not available from Abbott.) Figure 5.5 shows the results of titration of 10 μL of Th* tracer solution with Ab. No free Th* is seen when 10 μL of Ab solution is used, while only 2.5 μL of Ab solution is required to reduce the free Th* peak to about 5% of its original area. These results indicate the equilibrium binding constant in the tricine/Tween 20 buffer is not decreased relative to that seen in the Abbott buffer system. This result contrasts favourably with the decreased binding constant reported for the theophylline assay when SDS is used in micellar electrokinetic capillary chromatography.[22]

A competitive assay for Th was performed by mixing unlabeled Th with Ab and Th*. Separations for a series of theophylline standard solutions are shown in Figure 5.6, in which the Ab and Th* reagent kit stock solutions were mixed at a 1.5:10 volume ratio. The area of the two complex peaks can be summed to obtain the amount of complex, while the amount of free Th* may be determined from its peak area. The peak areas can then be normalized to the total amount of fluorescent Th injected with each standard, determined by adding the areas for all the peaks. This procedure was made possible by our ability to mobilize both the free Th* and its complex with the antibody, and obviates the need for an additional internal standard.[23,25]

Figure 5.7 shows a calibration curve obtained with a set of calibrator kit standards, and Ab and Th* reagent kit stock solutions mixed at a 2.5:10 volume ratio. A slightly higher Ab:Th* ratio was used in Figure 5.7 relative to Figure 5.6, which reduced the free Th* signal to near zero in the absence of added Th and improved the sensitivity at low Th concentrations. A plot of normalized peak area for Th* versus log[theophylline] was linear (slope = 0.386, intercept = 0.091), and allowed calculation of the solid line shown in the figure. The lower axis of Figure 5.7 shows the original concentrations of Th in the serum standards, while the upper axis shows the actual concentrations in the measurement, following the buffer dilution steps. The calibration curve covers the important clinical range of 10-20 μg/mL for serum samples.

Spiked human serum samples were run at 15 and 20 μg/mL (4 replicates). Use of the calibration curve to estimate their Th concentrations gave values of 16.2 ± 1.6 and 21.7 ± 2.7 μg/mL, respectively. To evaluate the role of the serum matrix, a 20 μg/mL Th sample was prepared in buffer. The serum-based standard curve provided an estimate of 20.1 ± 1.6 μg/mL for Th in the spiked buffer solution. These results demonstrate the calibrated device is accurate. The standard deviation measured from 12 replicate runs was ±5 %, over both single and 4 day periods, confirming the robust response of the device. In addition, there is no apparent bias of the result introduced by

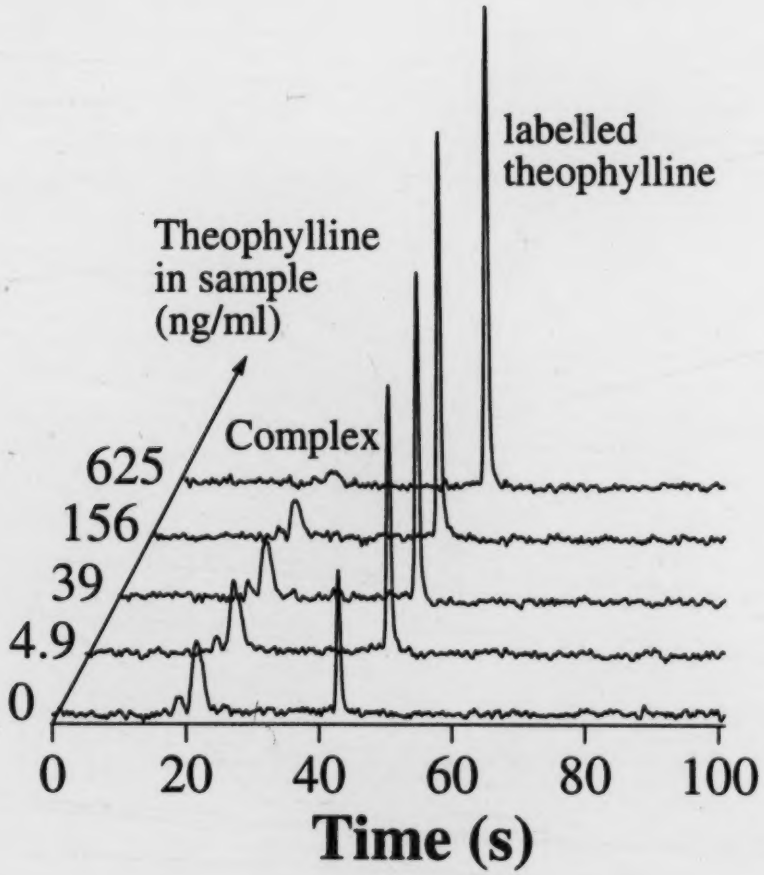

Figure 5.6 Series of on-chip electropherograms for a competitive theophylline assay using 10 μL of labeled theophylline, 1.5 μL of stock anti-theophylline and increasing amounts of unlabeled Theophylline. Buffer and separation conditions were the same as for Figure 5.2.

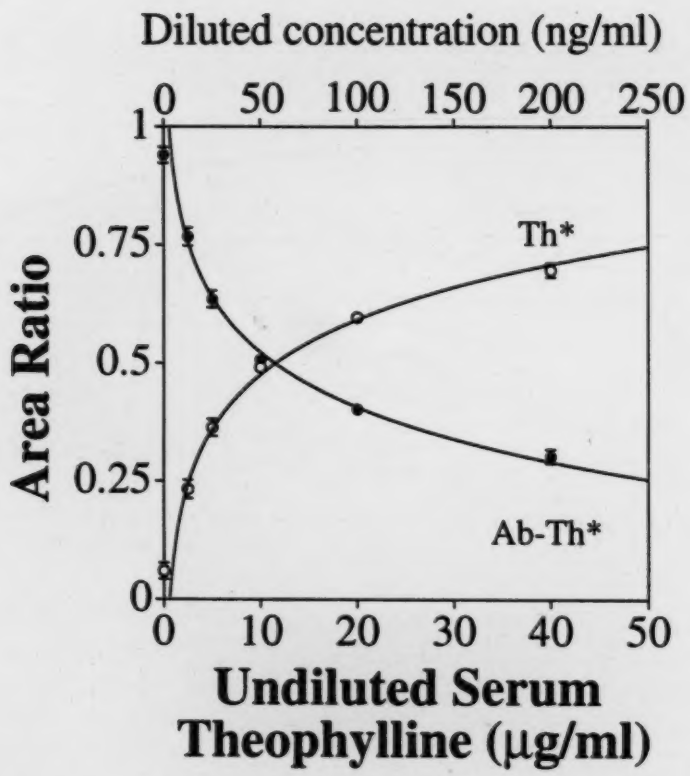

Figure 5.7. Calibration curve of normalized peak area (see text for procedure) versus concentration of Th in serum standards. Competitive assay used mixtures of 10 μL of labeled theophylline, 2.5 μL of stock anti-theophylline and increasing amounts of unlabeled Th. Lower axis shows Th concentrations in serum standards before dilution, upper axis shows actual concentrations during on-chip separation. Buffer and separation conditions were the same as for Figure 5.2. Each point is the mean of 4 replicates. Error bars show the standard deviations, where they were larger than the data points.

the serum matrix, so that serum based standards should not be required.

In order to determine the absolute threshold for detection of theophylline, we diluted a 2.5:10 μL mixture of Ab and Th* until the complex peak height had an S/N of 4.6, close to the detection limit of 3. Unlabeled Th was then mixed with Th* and Ab at this concentration until the S/N value for the free Th* peak increased to 7 from its initial value of 4. We have used a change of 3 in S/N as an estimate of the Th detection threshold. Defining the threshold in this way gave a value of 1.25 ng/mL, or 6.9 nM, in the diluted sample.

5.4 Conclusions

A key element in utilizing electrokinetically driven microfluidic devices for immunoassays is demonstration that separations of homogeneous immunological reaction products can be performed on-chip. The work presented here shows such separations can be performed on chip from a range of analytes with molecular weights between a few hundred and about 150,000 Daltons. When combined with our previous on-chip results,[11] those of Koutny et al.[25], and those of many other authors for conventional capillaries,[14-24] it becomes clear that such separations will be readily achieved on-chip. The particular examples selected here also illustrate potential application areas in clinical analysis and the biotechnological production of proteins.

One of the difficult issues in CE separations of immunological reagents is associated with protein adsorption. Our results show we can obtain good, robust performance within microchips simply by using an appropriate buffer system, even with challenging sample matrices such as human serum or mouse ascites fluid. The buffer allowed us to mobilize and observe both the labeled antigen and the antibody-antigen complexes. The ability to see both components will provide for a higher level of precision, and should obviate the need for additional internal standards. The ability to use antibodies without modification, and to work at near neutral pH values, means that reagent kits presently in use can be directly adapted to the chips. The fact that coatings can be avoided may reduce the manufacturing cost of future devices substantially.

5.5 References

1. Harrison, D. J.; Manz, A.; Fan, Z.; Lüdi, H.; Widmer, H. M. *Anal. Chem.* **1992**, *64*, 1926-1932.
2. Manz, A.; Fettinger, J. C.; Verpoorte, E.; Lüdi, H.; Widmer, H. M.; Harrison, D. J. *Trends Anal. Chem.* **1991**, *10*, 144-149.
3. Seiler, K.; Harrison, D. J.; Manz, A. *Anal. Chem.* **1993**, *65*, 1481-1488.
4. Effenhauser, C. S.; Manz, A.; Widmer, H.M. *Anal. Chem.* **1993**, *65*, 2637-2642.
5. Harrison, D. J.; Fluri, K.; Seiler, K.; Fan, Z.; Effenhauser, C. S.; Manz, A. *Science* **1993**, *261*, 895.
6. Fan, Z.; Harrison, D. J. *Anal. Chem.* **1994**, *66*, 177-184.
7. Jacobson, S. C.; Hergenröder, R.; Koutny, L. B.; Warmack, R. J.; Ramsey, J. M. *Anal. Chem.* **1994**, *66*, 1107-1113.
8. Harrison, D. J.; Fan, Z.; Fluri, K.; Seiler, K. *Technical Digest*, Hilton Head Sensor and Actuator Workshop, June 13-16, 1994, 21-24.
9. Jacobson, S. C.; Koutny, L. B.; Hergenröder, R.; Moore, A. W.; Ramsey, J. M. *Anal. Chem.* **1994**, *66*, 3472-3476.
10. Seiler, K.; Fan, Z. F.; Fluri, K.; Harrison, D.J. *Anal. Chem.* **1994**, *66*, 3485-3491.
11. a) Harrison, D. J.; Fluri, K.; Chiem, N.; Tang, T.; Fan, Z. *Technical Digest, Transducers 95*, 8th Intl. Conf. Solid-State Sensors Actuat., Stockholm, June 25-29, 1995, pp 752-755, b) Harrison, D. J.; Chiem, N. *Technical Digest, Solid State Sensor Actuator Workshop*, Hilton Head Island, SC, June 3-6, 1996, pp 5-8.
12. Jacobson, S. C.; Moore, A. W.; Ramsey, J. M. *Anal. Chem.* **1995**, *67*, 2059-2063.
13. Liang, Z.; Chiem, N.; Ocvirk, G.; Tang, T.; Fluri, K. Harrison, D.J. *Anal. Chem.* **1996**, *68*, 1040-1046.
14. a) Nielsen, R. G.; Rickard, E. C.; Santa, P. F.; Sharknas, D. A.; Sittampalam, G. S. *J. Chromatogr.* **1991**, 539, 177-185. b) The two peaks may be Ab-Th* and Ab-Th*$_2$, as suggested by reference 14a, although a change in peak height ratios as the amount of Th increased would then be expected. Alternatively, the Abbot reagent kit may contain more than one form of antibody for Th.

15. Schultz, N. M.; Kennedy, R. T. *Anal. Chem.* **1993**, 65, 3161-3165.
16. Arentoft, A. M.; Frøkiaer, H.; Michaelsen, S; Sorensen, H.; Sorensen, S. *J. Chromatogr. A* **1993**, 652, 189-198.
17. Shimura, K.; Karger, B. L. *Anal. Chem.* **1994**, 66, 9-15.
18. Rosenzweig, Z.; Yeung E. S. *Anal. Chem.* **1994**, 66, 1771-1776.
19. Reif, O.-W.; Lausch, R.; Scheper, T.; Freitag, R. *Anal. Chem.* **1994**, 66, 4027-4033.
20. Chen, F.-T. A.; Pentoney, S. L. *J.Chromatogr. A* **1994**, 680, 425-430.
21. Chen, F.-T. A. *J. Chromatogr. A* **1994**, 680, 419-423.
22. Steinmann, L.; Caslavska, J.; Thormann W. *Electrophoresis* **1995**, 16, 1912-1916.
23. Schultz, N. M.; Huang, L.; Kennedy, R. T. *Anal. Chem.* **1995**, 67, 924-929.
24. Schmalzing, D.; Nashabeh, W.; Yao, X.-W.; Mhatre, R.; Regnier, F. E.; Afeyan, N. B.; Fuchs M. *Anal. Chem.* **1995**, 67, 606-612.
25. Koutny, L. B.; Schmalzing D.; Taylor, T. A.; Fuchs M. *Anal. Chem.* **1996**, 68, 18-22.
26. Harlow, E.; Lane, D. Eds. *Antibodies: A Laboratory Manual*; Cold Spring Harbor Laboratory: Cold Spring Harbor, N.Y. 1988; pp 174-243 and 354-355.
27. *Amicon Instruction Manual*; Amicon, Oakville, Ontario, Canada.
28. a) Albin, M.; Weinberger, R.; Sapp, E.; Moring, S. *Anal. Chem.* **1991**, *63*, 417-422, b) Zare, R.N.; Gassmann, E. Eur. Pat. Appl. EP 216600, **1987**, c) Cheng, Y.F.; Dovichi, N.J. *Science* **1988**, *242*, 562-564.
29. Engval, E.; Perlmann, P. *J. Immunology* **1972**, *109*, 129-135.
30. Good, N. E.; Winget, G. D.; Winter, W.; Connolly T. N.; Izawa, S.; Singh, R. M. M. *Biochem.*, **1966**, 5, 467

Chapter 6

Integration of Sample Processing, Separation and Detection On-Chip[§]

6.1 Introduction

Micromachining technology has provided a means of fabricating miniaturized, three dimensional structures capable of performing clinically relevant analyses.[1-5] This technology offers promise in developing miniaturized instrumentation with a high level of automation and rapid analysis times.[2,5-8] Passive devices, in which sample flow is driven by some external means have been used for treatment of blood or serum,[5,9] measurement of sperm motility,[9,10] coagulation-based immunoassay[9,11] and as miniature containers for performing the polymerase chain reaction to amplify DNA.[5,9,12,13] Most of the successful active devices, in which fluid flow and delivery is driven on-chip, have been based on electrokinetic effects.[2-4,6-8,14] In these devices electroosmotic flow has been used to drive fluid flow in complex networks of fluid channels, providing pumping and valving action without the need for moving parts. On-chip chemical reactions followed by separation using electrophoretic effects have been shown.[15-17] Applications of microchip based capillary electrophoresis (CE) devices to some clinically relevant samples has been shown,[4,8,17-20] but the integration of several sample preparation steps together to create a lab-on-a-chip for clinical measurements has only just begun.[21]

Application of CE to immunoassays is a newly developing field showing considerable promise,[22-24] and appears appropriate for translation to the microchip CE format.[4,8,18] The CE immunoassay method utilizes a homogeneous phase immunoreaction, which is frequently very rapid due to good mass transfer kinetics, followed by a separation step to isolate and analyze the reactants and products. The separation is also very rapid, especially when performed on-chip, due to the very short separation distances. To our knowledge, the reaction of immunoreagents on-chip,

---

[§] A version of this chapter has been submitted for publication as:

Nghia Chiem, D. Jed Harrison, "Microchip Systems for Immunoassay: An Integrated Immunoreactor with Electrophoretic Separation for Serum Theophylline Determination", *Clinical Chemistry*, **1997**.

followed by on-chip separation, which represents an increased level of automation of the CE immunoassay has not been demonstrated. In this report we demonstrate that on-chip mixing of diluted serum samples with a labeled tracer compound and a selective antibody can be followed by separation and analysis of the components. This result, shown for the drug theophylline, provides confirmation that the integration of several steps to create a lab-on-a-chip for a real, clinical analysis is indeed feasible. We expect that the unique fluid delivery capabilities of the microchip electrophoresis format will provide a novel, important new method for automating immunoassays for use at the point-of-care in the clinical environment.[4,8,25]

6.2 Experimental

6.2.1 Materials and reagents

Borofloat glass was from Paragon Optical (Reading, PA). Theophylline and tricine were from Sigma (St. Louis, MO, USA). Fluorescein labeled theophylline and anti-theophylline were part of the Abbott TDx reagent set (from Sigma). NaOH, NaCl were from BDH (all via Fisher Sci., Edmonton, Canada) . Tween 20 was from Aldrich (Milwaukee, WI, USA). Human serum was a gift from Bio-Rad (Hercules, CA, USA). All chemicals were reagent grade; doubly distilled water was used for all solutions. Most solutions were filtered with 0.22 μm pore size filters (Millipore); small volumes were filtered with Micropure separators with 0.22 μm pores (Amicon, Oakville, Canada). Microconcentrators with various molecular weight cut-offs (MWCO) were also from Amicon.

The "tricine" buffer contained 50 mM tricine adjusted with sodium hydroxide to pH 8.0, 0.01% w/v Tween 20, and 26 mM NaCl as described in Chapter 2. Tricine buffer was filter sterilized (0.22 μm filter) and was used within 3 days for sample dilution and separation.

6.2.2 Device fabrication

Devices were fabricated in 7.6 x 7.6 cm square Borofloat glass using microlithographic patterning technique and an HF/HNO_3 etchant as previously described in Chapter 2. The chip layout is shown in Figure 6.1. The solution reservoirs are numbered from 1 to 7 for identification. The line thickness represents the relative width of the channels, with other dimensions given in Table 6.1. To allow for easy calculation

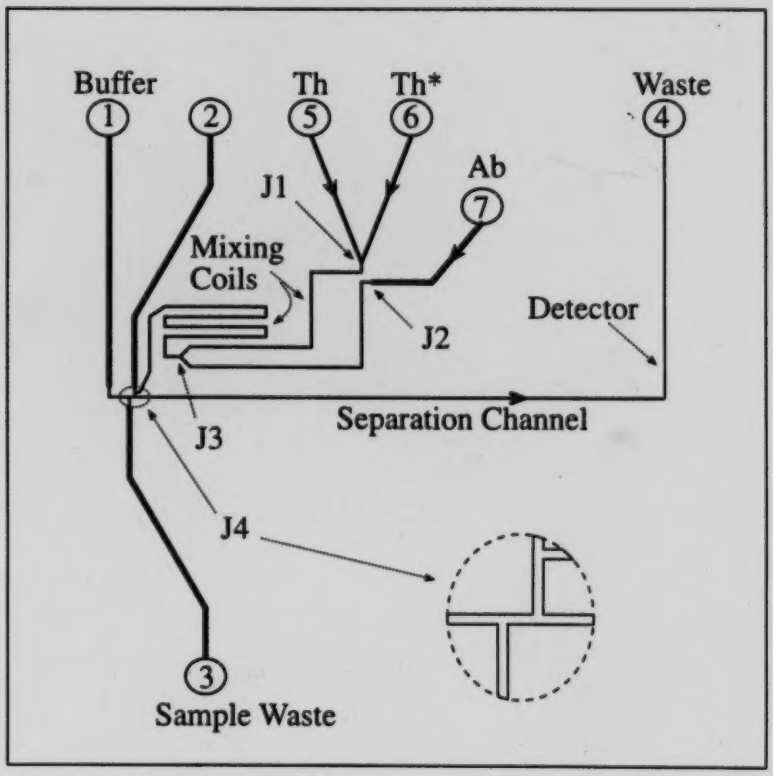

Figure 6.1. Device layout for competitive immunoassay with integrated sample mixing, reaction and separation, showing numbering scheme for solution reservoirs and junctions. Differing line thicknesses indicate relative channel widths; actual dimensions are given in Table 6.1. The segment joining J1 to J3 was used for mixing of antigen (Th) and tracer (Th*) solutions. The segment J3 to J4 was used to mix the antibody (Ab) with the antigen and tracer. The double T injector is shown in the inset. The drawing is not exactly to scale.

Table 6.1: Dimensions* of channels of the chip layout in Figure 6.1.

Segment Connecting	To	Width (μm)	Actual Length (mm)	Equivalent Length (mm)
Reservoir 5	Junction (J1)	116	13.46	5.69
Reservoir 6	Junction (J1)	116	13.46	5.69
Junction (J1)	Junction (J3)	52	26.50	26.50
Reservoir 7	Junction (J2)	236	13.49	2.74
Junction (J2)	Junction (J3)	52	26.50	26.50
Junction (J3)	Junction (J4)	52	81.63	81.63
Junction (J4)	Reservoir 4	52	81.11	81.11
Reservoir 1	Junction (J4)	236	26.00	5.28
Junction (J4)	Reservoir 3	236	36.34	7.38

*Device etched 13 μm deep. Cross section of channels is approximatley trapezoidal, with the largest width reported in column 3. The actual lengths of the channel segments are given in column 4 and their corresponding lengths in terms of a channel 52 μm wide are given in column 5.

of electric field strengths in each channel, the lengths of all channel segments are also given in Table 6.1 and expressed in terms of an equivalent length of a channel 52 μm wide.[26] Channel segments from reservoirs 5 and 6 meet at junction J1. When the solutions flowed in the directions indicated by the arrows, the segment between J1 and junction J3 served as a mixer for the two solutions from reservoirs 5 and 6. The mixture from J1-J3 was then mixed with the solution from reservoir 7 in segment J3-J4. The inset magnification shows the double-T injector[27] region, with a center to center length between the two arms of the T of about 100 μm, and a volume of ~ 100 pL.

6.2.3 Instrumentation

Some modifications were made to the computer controlled power supply and relay arrangement described previously[4,16] and in Chapter 2. Only a single 30 kV power supply (Spellman model CZE 1000R , Plainview, NY) and two 30 kV, Kilovac double throw relays were used to operate the chip, using the scheme indicated in Figure 6.2. Laser induced fluorescence with excitation at 488 nm was used. Emission was measured with a 25 x, 0.35 N.A. microscope objective, an 800 μm pinhole, an Omega Optical 508-533 bandpass filter and a photomultiplier tube (PMT) as previously described in Chapter 2.

6.2.4 Competitive immunoassay and chip operation

For competitive theophylline assays, serum theophylline (Th) standards from the TDx calibrator kit (0, 2.5, 5.0, 10, 20, 40 μg/mL) were used as received. Samples were made by spiking theophylline into human serum to give solutions 10, 12.5 and 15 μg/mL in theophylline. Standard or sample solutions were then diluted 50x in tricine buffer. Solution T containing the fluorescein labeled theophylline (Th*) tracer was diluted with the tricine buffer in a 1:1 ratio (V/V). Solution S containing antitheophylline (Ab) was dialyzed and reconstituted in the tricine buffer as previously described,[4] then 2.5 μL of this solution was further diluted with tricine buffer to 40 μL before use.

10 μL of diluted theophylline sample or standard, Tracer Th*, and anti-theophylline solution were added to reservoirs 5, 6 and 7, respectively as indicated in Figure 6.1. Tricine buffer was added to all other reservoirs. Figure 6.3a illustrates the injection scheme. Sample reservoirs (5, 6, 7) were connected to ground while sample waste (3) was connected to a negative high voltage (-3 to -6 kV).

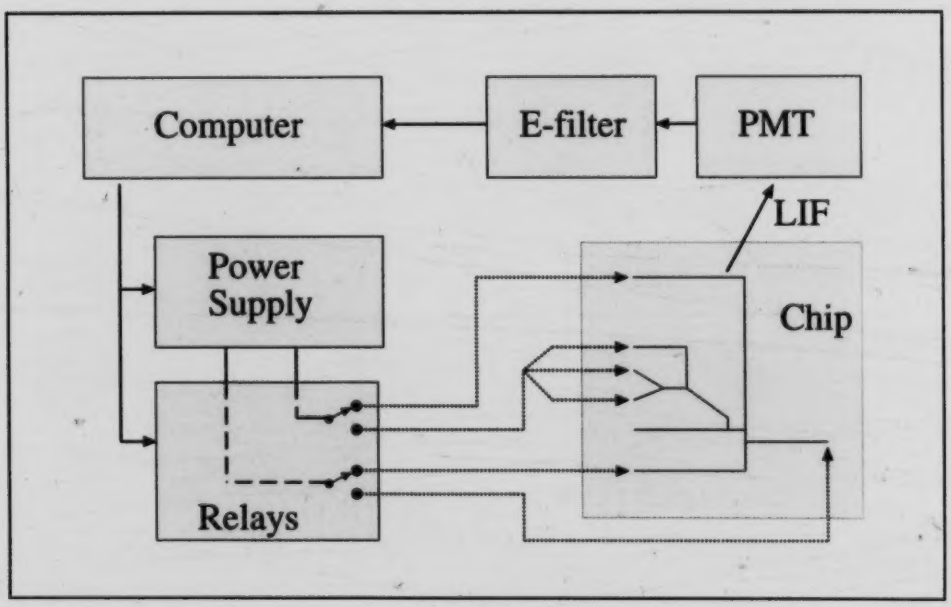

Figure 6.2. Instrument setup showing relays and voltage connections to the chip reservoirs. Only a single power supply and two double throw relays were used to toggle between different reservoirs. Laser induced fluorescence (LIF) and microscope collection optics were used to detect fluorescent species directly on-chip.

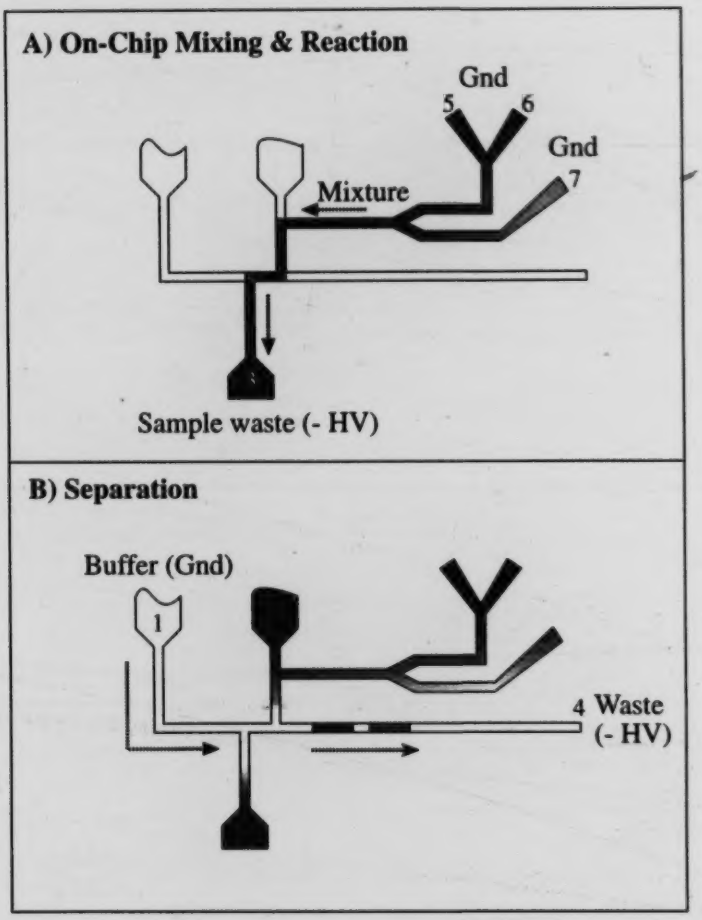

Figure 6.3. Schematic diagram showing on-chip mixing, reaction and separation. A) Solutions of Th, Th*, and Ab in reservoirs 5, 6 and 7, respectively, were electroosmotically pumped along the shaded area by applying electrical ground to these reservoirs and -3 to -6 kV at sample waste (reservoir 3). This forms a plug of the mixture at the double T. B) Separation of the reagents and products was effected by switching ground to reservoir 1 and -6 kV to the separation waste (reservoir 4).

The samples were electroosmotically pumped in the direction indicated by the arrows, using the applied voltage. On-chip mixing of the solution streams and reaction of reagents took place in the mixing coils. The channel segment between junctions J1 and J3 was used to mix the antigens (theophylline and tracer) while the segment between J3 and J4 was used to mix the antigens with the antibody. The mixed solution passed through the double T injector, thereby forming a plug of mixed sample and Ab about 100 μm in length (~ 100 pL).

Figure 6.3b illustrates the separation step. Both relays were switched so that the separation buffer (1) and waste reservoirs (4) were at ground and -6 kV, respectively, while the other reservoirs were disconnected. The reactants and products within the injected plug were separated along the separation channel and typically detected at 56 mm downstream. During separation, sample mixtures were stationary in the mixing coils. Typical separation times were one minute, but the period the solution sat in the mixing coils could be varied. During sample exchange, only the sample solution in reservoir 5 was replaced. The levels of reagents and buffer in other reservoirs were replenished with the appropriate solution when required.

We have estimated the detection limit (DL) for Th by determining the Th concentration needed to increase the normalized Th* area to a value 3 standard deviations in noise background larger than the value obtained in a sample with no Th. The estimate of DL was obtained by linear extrapolation of the results for a 20 ng/mL Th sample, which corresponds to a concentration of 5 ng/mL in the separation channel given a 4-fold dilution factor on-chip.

6.3 Results and Discussion

The mixing manifold illustrated in Figure 6.1 and 6.3 was designed to premix sample and Th* tracer in a 1:1 ratio, then mix the resulting solution with Ab, also in a 1:1 ratio. The intention was to apply the same potential to each reservoir and let the geometry of the channels control the mixing ratios. The efficacy of the diffusion based mixer, the speed of the immunoreaction on-chip, and the performance of the chip for assays of theophylline in serum samples is outlined below.

6.3.1 Mixing dilution ratio.

The volume flow rate of solution at each of the junction points in the mixing manifolds was designed to be equal. The two channel segments between reservoirs 5 and 6 and junction J1 were designed to have equal resistivities and equal cross-sectional areas at the junction, in order to give 1:1 mixing.[26] To obtain 1:1 mixing at junction J3, the segment between reservoir 7 and J3 was designed to have a resistivity equal to the combined resistance of the channels between reservoirs 5 and 6 and junction J3. The cross-sectional areas of the two mixing channels at J3 were again equal. Figure 6.4 shows electropherograms resulting from on-chip dilution of Th* at the J3 mixing point. In Figure 6.4a, reservoirs 5, 6 and 7 all contained the same Th* solution, while in Figure 6.4b reservoir 7 contained buffer instead. The latter configuration should give a 50% dilution of the Th*. Mixing was effected with -6 kV applied to sample waste reservoir 3 to create a sample plug at the double T junction, while separation was performed with -6 kV applied between reservoirs 4 and 1, as described in Figure 6.3 and the experimental section. In Figure 6.4a the area under the Th* peak was 490 ± 9 mV•s (mean and SD for 4 replicates (n)), while in Figure 6.4b dilution resulted in an area of 236 ± 4 (n = 7). This corresponds to a Th* solution:buffer ratio of 48.2 ± 1.2 %.

Comparison of On-and-Off Chip mixing

Mixing both on- and off-chip was also compared. With sample present in reservoir 5, and buffer in reservoirs 6 and 7, a 4-fold dilution of Th* was expected when it reached the double T injection port at J4. A Th* sample diluted on-chip with buffer gave a peak area of 729 ± 29 (n =3). When the same Th* solution, diluted 4-fold off-chip, was introduced through reservoir 2 to the double T injector so that there was no dilution on-chip, it gave a value of 707 ± 42 (n =5). The ratio of the dilution achieved on-chip to that off-chip was thus 103 ± 7 %. Since the second mixer gave a dilution of 48.2%, this meant the first mixer favored reservoir 5, giving a mixing ratio of reservoirs 5 to 6 of 53.4 ± 4 %. In this study we used a simplified potential delivery system, with a single fixed voltage applied to each of the delivery reservoirs, but greater control of mixing is clearly possible if the potentials on each of those reservoirs is varied.[3,14,26] Consequently, slight differences in mixing ratio between design and result can be readily compensated.

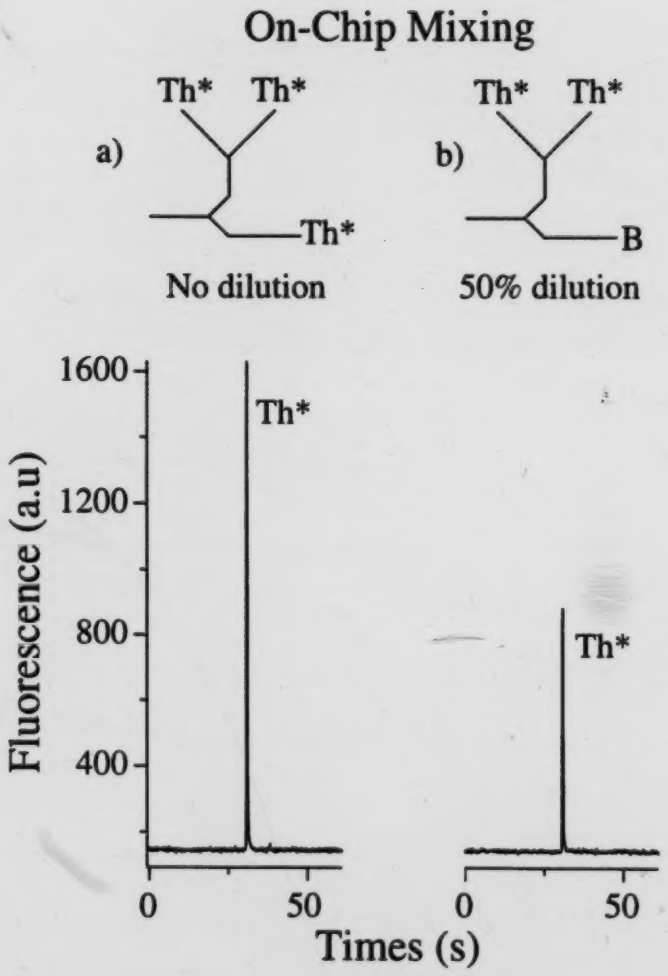

Figure 6.4. Electropherograms showing on-chip dilution of fluorescein-labeled theophylline (Th*) as detailed in the text. On the left, Th* was present in reservoirs 5, 6 and 7 and was loaded into the double T injector at -3 kV. On the right, the Th* solution in reservoir 7 was replaced with buffer, leading to a 1:1 dilution of the Th* at the double T injector during loading. For separation and detection, a pH 8.0, tricine buffer was used, with 6 kV between reservoirs 1 and 4.

6.3.2 Diffusional Mixing Design Issues

The immunoreagents must be uniformly mixed with the sample before analysis of the reaction products takes place. Dispersion of the reactants must be driven by diffusion, given that the flow conditions on-chip gave low Reynolds numbers.[28] To this end, we designed narrow, long mixing coils of channels to allow the species to have sufficient time to uniformly disperse across the channels.

6.3.2.1 Residence Time

The residence time of Th or antibody is defined here as the time the molecules spend in the mixing coil before they are injected for separation. For continuously flowing streams, residence time of a species can be determined from the length of the mixing coil and the flow velocity in the channel.

The velocity of a molecule, v, can then be determined from[29]

$$v = \mu E \qquad [1]$$

where μ is the overall mobility of the species and E is the electric field in the channel segment of interest. From the separation data for a mixture of Th* and anti-theophylline, the mobilities obtained for Th* and the IgG-Th* complex were 2.84 and 4.45 $x10^{-4}$ cm^2/Vs respectively. Determination of electric field in the mixing coils is complicated by the branches of connecting channels but can be estimated from Ohm's law for resistivity.[26]

The resistance R of a channel segment can be expressed as

$$R = \frac{\rho}{A} l \qquad [2]$$

where ρ is the resistivity coefficient, A is the cross section area and l is the length of the channel. For a channel with the same ρ and A, R is directly proportional to l. We assumed a constant resistivity coefficient in all the channels since they contain the same buffer. Determination of equivalent length to channels of the same cross section area was described earlier and listed in Table 6.1. The relative total resistance and voltage drop across a channel segment can be determined following the combination rules applied for resistors in series and parallel where

$$R_{series} \propto l_{series} = l_1 + l_2 \quad [3]$$

$$R_{parallel} \propto l_{parallel} = \frac{l_3 \times l_4}{l_3 + l_4} \quad [4]$$

for equivalent length l_{series} of two segments l_1 and l_2 in series and equivalent $l_{parallel}$ of two segment l_3 and l_4 in parallel, the equivalent total length $l_{equiv.total}$ of a combination of series and parallel channels is given by

$$R_{total} \propto l_{equiv.total} = l_{series} + l_{parallel} \quad [5]$$

and the voltage drop across a channel fragment (V_{seg}) of length l_{seg} is a fraction of the total voltage applied (V_{total}) and is given by

$$V_{seg} = \frac{l_{seg}}{l_{equiv.total}} V_{total} \quad [6]$$

For the 6 kV injection voltage we typically used, the calculated fraction of the voltage drop across the mixing coil J3-J4 was 0.785 or 4.709 kV, giving E = 577 V/cm. The potential between junctions J1 and J3 was 0.762 kV giving 28.8 V/cm.

The calculated velocity for Th* in the 26.5 mm premixing coil J1-J3 was 0.82 mm/s and under continuous flowing condition, its residence time was 32 s. In mixing coil J3-J4, the Th* velocity would be 1.64 mm/s, requiring 50 s to travel the 81.6 mm to the injection port. The IgG-Th* complex migrated at a rate of 2.57 mm/s, giving a 32 s residence time in the J3-J4 mixing coil. Previous studies indicate the free Ab will migrate at a similar rate, although likely somewhat faster.[4,22-24]

6.3.2.2 Diffusional Dispersion

Knowing the time each species spends in the mixing channel, we can estimate the time and channel length required for diffusional dispersion downstream of the junctions. Crank provides a solution to the initial-boundary value problem of diffusion for a finite system, where a species is initially confined to half the width of a channel and then is allowed to diffuse across the full channel[30]

$$C(x,t) = \frac{1}{2} C_o \sum_{n=-\infty}^{\infty} \left\{ erf\left(\frac{h + 2nw - x}{2\sqrt{(Dt)}} \right) + erf\left(\frac{h - 2nw + x}{2\sqrt{(Dt)}} \right) \right\} \qquad [7]$$

Here x is the location across the channel of width w (52 μm), t is the diffusion time, $C(x,t)$ is the concentration at any given x and t, C_o is the initial concentration before diffusion (t = 0), n is an integer, h is the portion of the channel width that the species was initially confined to, and D is the diffusion coefficient. This expression was numerically evaluated using a program written in HiQ script language (National Instruments, Austin, TX), with summation taken over the first 7 terms (other terms were < 0.0025% of the total sum).

Diffusion of IgG molecules initially confined to half the mixing channel's width was calculated using Equation 7, giving the results shown in Figure 6.5a. Due to its small diffusion coefficient of 4.0 X 10^{-7} cm^2/s,[31] IgG requires a long time to become uniformly dispersed across the 52 μm wide mixing channel. With 6 kV applied, the 81.6 mm long mixing coil J3-J4 (51 nL capacity) allowed sufficient mixing to give only a 1% variation in concentration across the channel under continuous flow conditions (32 s residence time). (It should be noted that this calculation does not take into account the effect of immunoreaction on the diffusion process, which would tend to speed the time of mixing by increasing the concentration gradient across the channel.)

A similar analysis can be applied to theophylline dispersion as shown in Figure 6.5b. Lacking the diffusion coefficient for Th or Th*, we have used a value reported[6] for fluorescein of D = 3.3 X 10^{-6} cm^2/s, which should be similar to that of fluorescein labeled Th*. Calculation shows that small molecules such as theophylline or fluorescein will be uniformly dispersed across a 52 μm wide channel (a 1% concentration variation across the channel) in about 4 seconds. For the first mixer between J1-J3, with a velocity of 0.82 mm/s, this requires a length of 3.3 mm. Consequently, the 26.5 mm length between J1 and J3 (16 nL capacity) allowed for more than adequate premixing of the antigens before they met with the antibody solution at J3. For the second mixer from J3 to J4, the velocity of 1.64 mm/s means a 6.7 mm length is required. Since the dispersion of Th and Th* is much faster than that of IgG, this suggests the second mixer may be unnecessarily long.

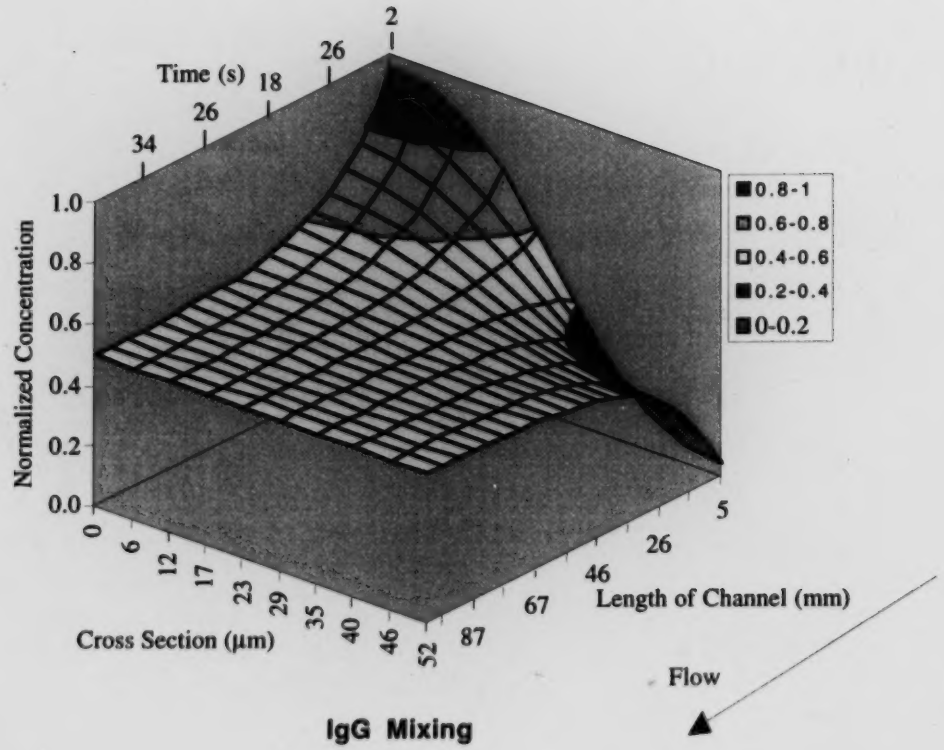

Figure 6.5a. Plot of normalized concentration of IgG as it diffuses across a 52 μm wide channel, initially entering from the right side of the figure, occupying one half of the channel. Equations 1 and 7, with $D = 4.0 \times 10^{-7}$ cm^2/s and a linear velocity of 2.57 mm/s, were used to calculate the diffusion profiles downstream of intersection J3.

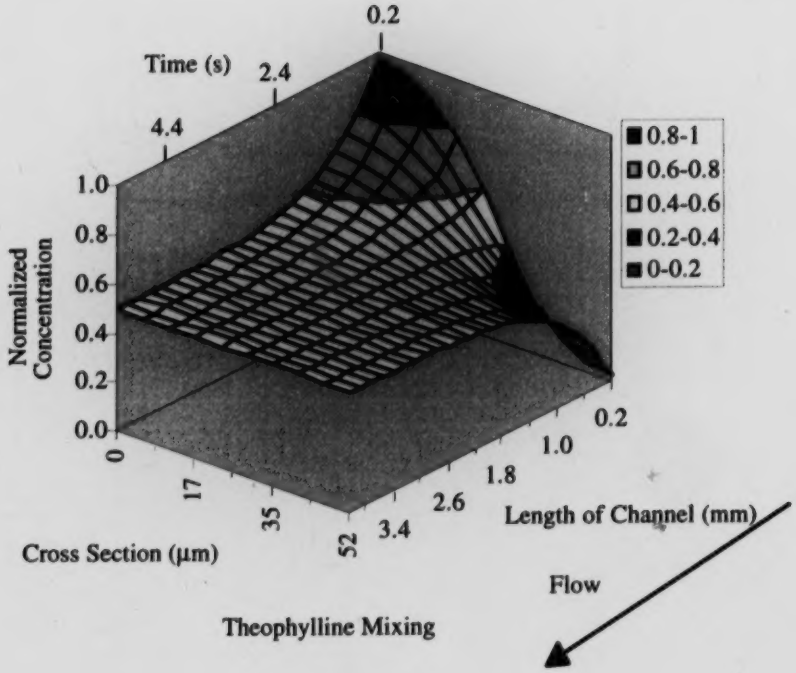

Figure 6.5b. Plot of normalized concentration of theophylline as it diffuses across a 52 µm wide channel, initially entering from the right side of the figure, occupying one half of the channel. Equations 1 and 7, with $D = 3.3 \times 10^{-6}$ cm^2/s and a linear velocity of 0.82 mm/s, were used to calculate the diffusion profiles downstream of intersection J1.

6.3.3 Immunoreactions On-Chip

Figure 6.6 shows electropherograms obtained for on-chip competitive immunoassays of serum theophylline. Mixing was performed at -6 kV under continuous flow conditions to give about 32 s reaction times, followed by separation at -6 kV. The lower trace, showing Th* as a single fluorescence peak at about 30 s, was obtained by injection of Th* solution through reservoir 6 and buffer through reservoirs 5 and 7. The central electropherogram was obtained following on-chip mixing of a diluted blank theophylline (0 μg/mL) serum sample in reservoir 5 with tracer Th* from 6, then with anti-theophylline from 7. The Th* was completely bound to anti-theophylline to form complexes, which were detected as a new pair of partially resolved peaks at about 18 s as previously described.[4] Competitive assays were achieved by replacing the blank sample in reservoir 5 with diluted serum theophylline solution. In forming complexes, theophylline in the sample competes with tracer Th* for a limited amount of the antibody in the mixture:

$$\text{Th} + \text{Ab} + \text{Th}^* \Leftrightarrow \text{Ab-Th} + \text{Ab-Th}^* \qquad [8]$$

The competition leads to an increase in signal for free tracer Th* and a decrease in the Ab-Th* complex as shown in the upper electropherogram. The separation was completed in less than 1 minute, the bound Th*-antibody complexes were well resolved from the free Th* and the peak areas were easily quantitated (*vide infra*).

The extent of immunoreaction prior to the analysis step is clearly critical to quantitative analysis. The chip can be operated in continuous flow mode during the reaction stage. However, it is also possible to increase reaction times by using it as a stop-flow mixer, allowing incubation in the mixing coil while there is no flow in the mixer. The volume ratio of the second mixer to that of the injector port (51 vs 0.15 nL) means there will be enough reacted sample available. Figure 6.7 shows the effect of cumulative mixing time on the distribution between free and bound Th* in a series of competitive assays with serum theophylline standards at 21° C. Remaining unreacted Th*, normalized to the total fluorescent Th* and injected as previously described,[4] is plotted as a function of total mixing time. The results show that the competitive immunoreaction is nearly complete in the first 30 s of continuous flow mixing. A slight continued decrease in free Th* with increased mixing time at low Th concentration suggests that the reaction continues at a slow rate for an extended period.

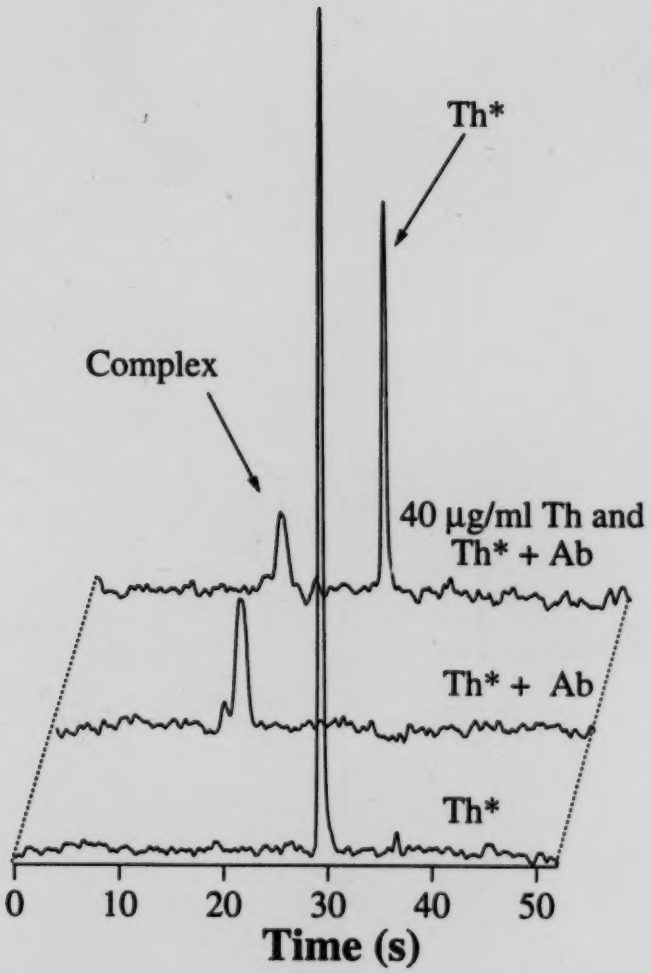

Figure 6.6. Electropherograms of the competitive theophylline assay with on-chip mixing of reagents. Lower trace with buffer in reservoir 5, Th* in 6 and buffer in 7; middle trace with buffer in 5, Th* in 6 and Ab in 7; upper trace with a 40 µg/mL theophylline sample (prior to off-chip 50x dilution) in reservoir 5, Th* in 6 and Ab in 7. Buffer and separation conditions were the same as for Figure 6.4.

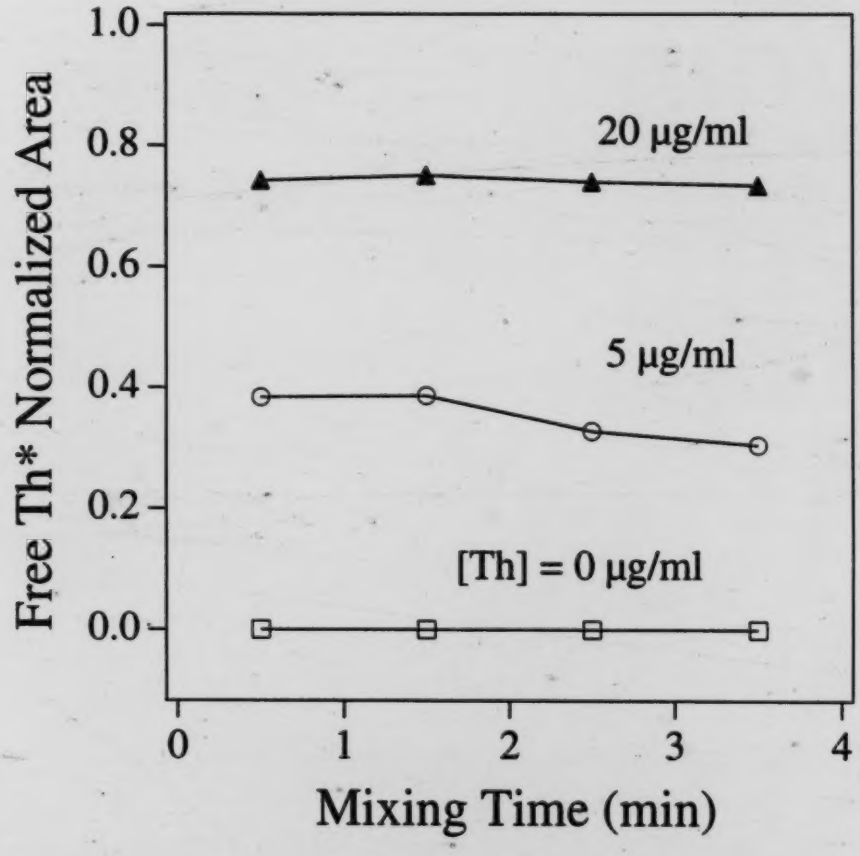

Figure 6.7. Stop-flow study of the effect of mixing time on the amount of free, unreacted Th* in the presence of Ab and the indicated amounts of unlabeled Th (concentrations reported as the value prior to 50x dilution off-chip). The mixed Ab, Th* and Th solutions were allowed to sit in the channel segment between J3 and J4 for varying periods. The shortest mixing time corresponds to the minimum possible residence time, given the velocity of flow with -6 kV applied to the sample waste reservoir.

Earlier reports indicate the Abbot TDx system, based on a fluorescence polarization immunoassay (FPIA) with these same reagents, allows 15 minutes incubation at room temperature or 3 minutes incubation at 35° C.[32] Control of the reaction time should lead to reproducible results, even if complete reaction has not occurred, although raising the temperature of the chip is equally feasible.

6.3.4 Competitive Theophylline Assays On-Chip

6.3.4.1 Calibration

Figure 6.8 shows a calibration curve obtained from a series of separations, in which varying concentrations of diluted serum theophylline standards were mixed on-chip with Tracer Th* and anti-theophylline solutions. The chip was operated in stop-flow mode, allowing reaction times of 32, 90, 150, and 210 s. A plot of normalized peak area for Th* (averaged over all reaction times) versus log[theophylline] was linear (slope = 0.54 ± 0.03, intercept = 0.003 ± 0.04), and allowed calculation of the solid line shown in Figure 6.8. The lower axis of Figure 6.8 shows the original concentrations of Th in the serum standards, while the upper axis shows the concentrations of the standards at the stage they were added to reservoir 5. (Dilution of standards and serum sample is a standard step with these reagents in the Abbot TDx FPIA assay, and so was adopted in the present procedure to ensure viable comparison.) The calibration curve covers the important clinical range of 10-20 μg/mL for serum samples. It is similar to those obtained with on-chip analysis of off-chip mixed samples or with the FPIA method.

6.3.4.1 Accuracy and Precision

The recovery of theophylline from spiked human serum samples run over a two day period was determined using calibration curves obtained with the theophylline standards run on a single day. Human serum samples with theophylline at 10, 12.5, and 15 μg/mL were found to have 9.4 ± 1.0, 12.9 ± 1.8 and 17 ± 2 μg/mL, respectively, (mean and SD over 4 replicate injections) when the peak areas from the four different reaction times were averaged. The precision of the recovery results obtained with on-chip mixing is poorer than those we obtained with off-chip mixing. This discrepancy appears to arise from averaging data with several different reaction times. When samples and standards for calibration curves were analyzed at any one of the fixed mixing times, the precision of the recovery improved by 40 % over that obtained from the time averaged analysis (i.e. 16.0 ± 1.2 μg/mL for 15 μg/mL sample).

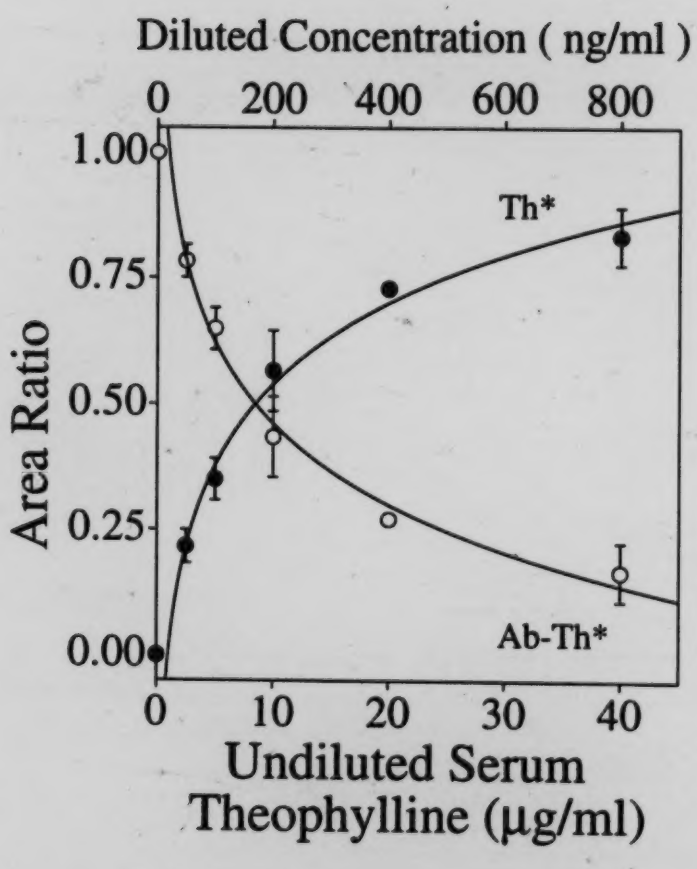

Figure 6.8 Calibration curve of normalized peak area for (•) free Th* and (o) Ab-Th* complex vs concentration of Th in 50x diluted serum standards (upper axis). Lower axis shows Th concentrations as they were in serum standards before 50x dilution off-chip. Buffer and separation conditions were the same as for Figure 6.4. Each point is the mean of 4 replicates. Error bars show the standard deviations where they were larger than the data points. Solid lines are fits to a log function; see text.

This improvement leads to a precision for on-chip mixing that is similar to what we obtained with off-chip mixing.[4] Careful monitoring of the mixing time in both standards and sample testing is required to achieve this, but is not overly difficult given the computer control used to run the chips.

6.3.4.3 Detection Limit of Theophylline

The absolute detection limit (DL) for a solution within the chip's separation channel was determined to be 1.1 ng/mL, using the method described in the Experimental Section. This is consistent with the value of 1.25 ng/mL we reported previously[4] for off-chip mixing with separation on-chip. Since the present chip performs a 4-fold dilution, the minimum concentration that can be placed in sample reservoir 5 is 4.3 ng/mL. Given the 50x dilution step performed before the samples and standards are introduced to the chip, the on-chip reaction and separation system provides a DL of 0.22 μg/mL for undiluted serum. This value is similar to the 0.4 μg/mL reported for theophylline assay by FPIA,[33] serving to illustrate that detection limits are not sacrificed by performing the on-chip immunoassay. (Since all of these analyses are run in diluted serum samples, it is clear that detection limits can be modified by varying the extent of dilution.)

6.4 Conclusion

This study has illustrated that integration of several sample processing steps with capillary electrophoretic based separation of solution components is feasible. Performing reagent mixing with diluted serum samples, immunological reaction and separation together on one monolithic device makes it clear that entire groups of laboratory steps used in clinical analyses can be integrated. The performance of the device is comparable to conventional instrumentation, so that no sacrifice is made by integrating. It is clear that the ability to work with blood or serum samples directly within the chips would be another important development. Nevertheless, our results serve to demonstrate the rapid analysis times possible and the level of automation that can be achieved within the chip. It is reasonable to conclude that such devices could form the basis of an automated sample treatment system that would be located at the point-of-care in the clinical and hospital environment, able to provide rapid reporting of critical analytes in emergency situations.

6.5 References

1. Shoji, S.; Esashi, M.; Matsuo, T. *Sensors and Actuators* . **1988**, 14, 101-107.
2. Manz, A.; Fettinger, J.C.; Verpoorte, E.; Lüdi, H.; Widmer, H.M.; Harrison, D.J. *Trends Anal Chem* . **1991**, 10, 144-149.
3. Harrison, D.J.; Fluri, K.; Seiler, K.; Fan, Z.; Effenhauser, C.S.; Manz, A. *Science* **1993**, 261, 895-897.
4. Chiem, N.; Harrison, D.J. *Anal. Chem.* **1997**, 69, 373-378.
5. Cheng, J.; Fortina, P.; Surrey, S., Kricka, L.J., Wilding, P. *Mol. Diagn.* **1996**, 1, 183-200.
6. Harrison, D.J.; Manz, A.; Fan, Z.; Lüdi, H.; Widmer, H.M. *Anal Chem* **1992**, 64, 1926-1932.
7. Manz, A; Harrison, D.J.; Verpoorte, E.; Widmer, H.M. In: Brown, P.R.; Grushka, E. eds. Advances in chromatography. New York: Marcel Dekker, **1993**, 1-66.
8. Koutny, L.B.; Schmaizing, D.; Taylor, T.A.; Fuchs, M. *Anal. Chem.* **1996**, 68, 18-22.
9. Kricka L.J, Wilding P. *Pure & Appl Chem* . **1996**, 68, 1831-1836.
10. Kricka L.J.; Faro, I.; Heyner, S.; Garside, W.T.; Fitzpatrick, G.; Wilding, P. *Clin. Chem.* **1995**, 41, 1358-1359.
11. Song, M.I.; Iwata, K.; Yamada, M.; Yokoyama, K.; Takeuchi, T.; Tamlya, E.; Karube, I. *Anal. Chem.* **1994**, 66, 778-781.
12. Wilding, P.; Shoffner, M.A.; Kricka, L.J. *Clin. Chem.* **1994**, 40, 1815-1818.
13. Northrup, M.A.; Ching, M.T.; White, R.M.; Watson, R.T. *Technical Digest, Transducers 1993* , Proc. 7th int. conf. on solid-state sensors and actuators, New York: Institute of Electrical and Electronic Engineers, 1193, 924-926.
14. Jacobson, S.C.; Hergenröder, R.; Koutny, L.B.; Warmack, R.J.; Ramsey, J.M. *Anal. Chem.* **1994**, 66, 1107-1113.
15. Jacobson, S.C.; Hergenröder, R.; Moore, A.W.; Ramsey, J.M. *Anal. Chem.* **1994**, 66, 4127-4132.
16. Fluri, K.; Fitzpatrick, G.; Chiem, N.; Harrison, D.J. *Anal. Chem.* **1996**, 68, 4285-4290.
17. Jacobson, S.C.; Ramsey, J.M. *Anal. Chem.* **1996**, 68, 720-723.

18. von Heeren, F.; Verpoorte, E.; Manz, A.; Thormann, W. *Anal. Chem.* **1996**, 68, 2044-2053.
19. Colyer, C.; Mangru, S.D.; Harrison, D.J. *J. Chromatogr. A* 1997; submitted.
20. Li, P.C.H.; Harrison, D.J. *Anal. Chem.* **1997**, 69, 1564-1568.
21. Woolley, A.T.; Hadley, D.; Landre, P.; deMello, A.J.; Mathies, R.A.; Northrup, M.A. *Anal. Chem.* **1996**, 68, 4081-4086.
22. Nielsen, R.G.; Rickard, E.C.; Santa, P.F.; Sharknas, D.A.; Sittampalam, G.S. *J. Chromatogr. A* **1991**, 539, 177-185.
23. Chen, F-TA.; Pentoney, S.L. *J. Chromatogr. A* **1994**, 680, 425-430.
24. Schultz, N.M.; Huang, L.; Kennedy, R.T. *Anal. Chem.* **1995**, 67, 924-929.
25. Dirks, J.L. *AACN Clin. Issues.* **1996**, 7, 249-259.
26. Seiler, K.; Fan, Z.H.; Fluri, K.; Harrison, D.J. *Anal. Chem.* **1994**, 66, 3485-3491.
27. Effenhauser, C.S.; Manz, A.; Widmer, H.M. *Anal. Chem.* **1993**, 65, 2637-2642.
28. Branebjerg, J.; Fabius, B.; Gravesen, P. In: van den Berg, A.; Bergveld, P. eds. Micro total analysis systems. Netherlands: Kluwer Academic Publishers, 1995:141-51.
29. Jorgenson, J.W.; Lukacs, K.D. *Anal. Chem.* **1981**, 53, 1298-1302.
30. Crank, J. The mathematics of diffusion 2nd ed. Oxford: Clarendon Press. **1975**, 14-16.
31. Sober, H.A., ed. Handbook of biochemistry. Selected data for molecular biology, 2nd ed. Cleveland, Ohio: CRC Press. 1970, C-11.
32. Jolley, M.E.; Stroupe, S.D.; Schwenzer, K.S.; Wang, C.J.; Lu-Steffes, M.; Hill, H.D; Popelka, S.R.; Holen, J.T.; Kelso, D.M. *Clin. Chem.* **1981**, 27, 1575-1579.
33. Loomis, K.F.; Frye, R.M. *Am. J. Clin. Pathol.* **1983**, 80, 686-691.

Chapter 7

Conclusions

As stated in Chapter 1, one of the objectives of this work is to demonstrate the feasibility of developing microfabricated devices for immunoassays. This objective was achieved and the details have been given in Chapters 2 to 6. The purpose of this Chapter is to summarize some of the main conclusions gained from this work. Also presented are directions for future development of an automated assay system for point-of-care testing (POCT).

7.1 Summary

In summary, microlithographic and etching techniques were used to fabricate networks of microchannels in small devices used for immunoassays. The channels made it possible to handle very small amounts of sample and reagent solutions, typically in the nano- to picoliter range. Computers, relays and high voltage sources were used to control fluid flow. Fluid delivery and manipulation was effected by capillary electroosmosis, while efficient separation was achieved by capillary electrophoresis. Laser induced fluorescence was used for detecting low analyte concentrations.

Separation, detection and quantitation were the key aspects used to evaluate immunoassay performance of the microfabricated devices. In Chapters 2 through 5, a simple design of microchannels was used to address these aspects of performance.

Separation performance was evaluated by comparing flow profiles and separation efficiency with current theories. Separation efficiencies with submicron plate heights close to the theoretical limit were achieved. The separations were rapid, typically within less than a minute. While rapid separation is a desired characteristic, short separation time limits the resolution of the analytes. Adjusting of ionic strength proved to be an effective means to control electroosmotic flow and separation time, allowing the desired separation speed and resolution. These results show that on-chip separation efficiencies are dependent on separation distance, electric field, electroosmotic flow and the type of analyte(s) used and are consistent with results obtained from fused silica capillaries in conventional CE.

The optimized laser induced fluorescence detection system gave on-chip detection limits in the low picomolar range for small molecules such as fluorescein and labeled

amino acids, and in the high picomolar range for large protein molecules such as BSA. These detection levels are satisfactory for many immunoassays such as those for drug monitoring. Detection of lower concentrations are limited in part by the background fluorescence of the glass substrates .

One of the difficult issues in the CE separation of immunological reagents is protein adsorption. Our results show we can obtain good, robust performance within microchips simply by using an appropriate buffer system, even with challenging sample matrices such as human serum or mouse ascites fluid. The buffer allowed us to mobilize and observe both the labeled antigen and the antibody-antigen complexes. The ability to see both components provides for a high level of precision, and should obviate the need for additional internal standards. The ability to use antibodies without modification, and to work at near neutral pH values, means that reagent kits presently in use can be directly adapted to the chips.

In Chapter 6, devices with a more complex design of microchannels were studied for automated immunoassay systems. The results show that integration of several sample processing steps with capillary electrophoretic based separation of solution components is feasible. Performing reagent mixing with diluted serum samples, immunological reaction and separation together on one monolithic device makes it clear that entire groups of laboratory steps used in clinical analyses can be integrated. The performance of the device is comparable to conventional instrumentation, so that no sacrifice is made by integrating. These results serve to demonstrate the level of automation that can be achieved within the chip. It is reasonable to conclude that such devices could form the basis of a compact automated immunoassay system that would be located at the point-of-care in the clinical and hospital environment, able to provide rapid reporting of critical analytes in emergency situations.

7.2 Future Directions

The work presented in this thesis shows that microfabricated devices hold great promise as a simple, compact and automated immunoassay system suitable for point-of-care testing (POCT). However, POCT instruments are also used by nonlaboratory personnel; therefore, several technical features still need to be developed. Some of these features are discussed below.

POCT systems need be self contained and portable[1]. The size of the instruments should be in the range from a small hand-held device to a larger instrument which can

be wheeled around on a cart. In our present setup, the power supplies, relay controlling unit and the detection system were chosen because they were flexible and readily available commercially. However, these units are still relatively large and unsuitable for POCT. Smaller power supplies, more compact diode lasers, or light emitting diodes and detectors such as avalanche photodiodes, photodiode arrays or charge coupled devices (CCD) are available as alternate units for developing a miniature system. However, packaging of all these components into a small functional system is still required.

Complete automation including quality control is also a requirement for POCT systems because multidisciplinary users will be operating the instrument. In addition, a system designed for POCT must be easy to operate so that users would require a minimal amount of training. Computer software should be developed for complete analysis, from testing requests to final result reporting. A complete test menu should be provided with user-friendly instructions for all users, including non-specialists. Software should also be designed to automate electronic data processing, interpretation and result reporting to the point where it is usable and understandable to non-specialists. Automated data processing includes storing and retreiving raw data, calibrating against standards results stored in computer.

Quality control is one of the most important aspects of laboratory testing. Traditional quality control in the lab is most effective for monitoring systematic errors; however, with POCT in alternate sites, random errors which are more related to operator error than to a test system failure, are more likely to occur. These errors include inaccurate timing, reagent or system exposure to inappropriate environmental conditions, reagent contamination, poor equipment maintenance, outdated or deteriorated reagents, reagent miscalibration, omission of a reagent or use of a reagent in the wrong order and incorrect specimen or reagent sampling or dispensing[1]. Automated procedures should be designed to guard against these potential errors. Without appropriate quality control, test results would become unreliable.

---

[1] Anderson, D. J.; Kricka, L. J.; Skogerboe, K. J.; et al. *Anal. Chem.* **1997**, *69*, 165R-229R